

FABRICATION AND MODIFICATION OF BIOLOGICAL MATERIALS UTILIZING
SHEAR FLOW SYSTEM

By

Shaowen Ji

A DISSERTATION

Submitted to
Michigan State University
in partial fulfillment of the requirements
for the degree of

Chemical Engineering - Doctor of Philosophy

2013

ABSTRACT

FABRICATION AND MODIFICATION OF BIOLOGICAL MATERIALS UTILIZING SHEAR FLOW SYSTEM

By

Shaowen Ji

Efficient mixing and reaction can promote the fabrication and modification processes to obtain the products with desired properties. A modified Taylor-Couette nanomixer, which can generate extreme turbulent shear flow environment, was introduced to facilitate the production of biodegradable polymer particles and biorenewable materials. We developed a simple and fast single emulsion technique to fabricate hollow polymer particles by turbulent viscous fluid flow. The process involves the one-step emulsification of a polylactic acid-ethyl acetate solution in the water-glycerol medium under shear and the solidification of polylactic acid particles by the diffusion of ethyl acetate to plenty of water. Turbulent regime and processing temperature were found as key factors to dynamic control the production of polymer particles from solid nanospheres to hollow microspheres. This method allows the easy control of polymer particle shape and size. Successful incorporations of hydrophilic iron oxide nanoparticles and a small peptide were introduced here as representative examples of its practical applications in the efficient encapsulation of hydrophilic materials in the hydrophobic polymer matrix for different demands.

We also reported a fast and highly efficient nanoscale hybrid pretreatment method of lignocellulosic biomass. Corn stover was pretreated in this nanomixer at a reduced temperature for two minutes with alkaline condition. Composition analysis showed the significant removal of both lignin and hemicellulose after the hybrid pretreatment.

Microscopy images revealed the severe disruption of corn stover structure and exposure of cellulose microfibrils from the cell wall. Effective fractionation and structure disruption can be achieved by this method. In order to make the production economically feasible, cationic polyelectrolyte was first introduced as the additive in this pretreatment of corn stover. At room temperature and fast processing conditions (about 2 minutes), lignin was found to redistribute on the inner and outer surfaces of the cell wall as lignin aggregate droplets instead of being extracted. Free nano-/microfibrils in the residues were also observed. The yields of enzymatic hydrolysis were enhanced for the pretreated corn stover with the aid of polyelectrolyte. We speculate that lignin was effectively modified, which opened up the cell wall structure during the short pretreatment process and prevented non-productive binding of enzymes in the enzyme hydrolysis reaction. This can improve cellulose accessibility and digestibility, indicating that polyelectrolyte is a promising alternative to modify the biomass surface and reduce the use of expensive enzymes.

Copyright by
SHAOWEN JI
2013

Dedicated to my beloved parents, father Ping Ji and mother Ling Hu, for their tender care and unconditional support. Without their knowledge, wisdom, and guidance, I would not have the goals that I have to strive and try to be the best to reach them!

ACKNOWLEDGMENTS

Working on the Ph.D. has been wonderful and often overwhelming. It would not have been possible to complete this journey without the help and support of the kind people around me. I am indebted to many people for making my Ph.D. an unforgettable experience, to only some of whom it is possible to give particular mention here.

First of all, I am deeply grateful to my advisor, Dr. Ilsoon Lee. My Ph.D. program and this thesis would not be possible without his help, support and patience, not to mention his good advice and ideas. It has been a pleasure to me to work with him throughout my Ph.D. Furthermore, I would like to thank my committee member Dr. K Jayaraman for sharing insightful comments on my work. Also like to thank my committee member Dr. David Hodge for supporting me and having motivating discussions on both the course of my project and future career. I would also like to thank my committee member Dr. Wei Liao for all his contributions of time and ideas to make my Ph.D. experience productive and stimulating. I also appreciate the help from Dr. Worden for letting me use the facilities in Protein Expression Laboratory.

I would also like to thank PRIMIX Corporation, Japan for providing our lab with the nanomixer which led me complete my course of program work. I am most grateful to Dr. Jue Lu from Metna Corporation, Lansing for supporting and mentoring me in the final part of my research. I would also like to thank specialists, Carol, Abby, Alicia, Melinda,

Dr. Flegler and Dr. Fan at the Center of Advanced Microscopy for training and helping me to getting excellent SEM, TEM and CLSM images.

In addition, I have been very privileged to get to know and work with many other great people who became friends over the last several years. I would like to thank my group members, Dr. Devesh Srivastava, Dr. Sumit Mehrotra, Wei Wang, Ankush Gokhale and Oishi Sanyal for the work we did together as well as the invaluable help and support from them. I would also extend my thanks to Rui Lin, Yangmu Liu, Lee Alexander, Tongjun Liu, Nathan Parker, Markus Downey, Per Askeland, Ying Liu, Bhushan Awate, Xianfeng Ma, Hyun Ju Cho, Xian Jiang, Rui Li, Alvaro Orjuela, Dena Shahriari for their generous assistance and support.

Last but not the least, I also would like to thank all my other dear friends who put up with me through the whole Ph.D. process and helped me with personal challenges, in particular Chang Liu, Jie Li, Wenjuan Ma, Jinglei Xiang, Ke Zhang, Fei Chen, Zhongping Gao, Chenling Huang, Yanjun Liu, Yujia Lu, Meijuan Lu.

Finally, I would like to thank my mom and dad for their infinite support throughout everything.

TABLE OF CONTENTS

LIST OF TABLES.....	xii
LIST OF FIGURES.....	xiii
Chapter 1	
Introduction.....	1
1.1 Overview of mixing system with Nanomixer	2
1.2 Fabrication of polymer particles by emulsion technique	3
1.3 Encapsulation of hydrophilic materials by single emulsion technique	4
1.4 Biomass pretreatment facilitated by shear field	4
1.5 Effect of cationic polyelectrolyte on the pretreatment	5
Chapter2	
Transitional Behavior of Polymeric Hollow Microsphere Formation in Turbulent Shear Flow by Emulsion Diffusion Method	6
2.1 INTRODUCTION.....	7
2.2 BACKGROUNDS	9
2.2.1 Emulsion processing.....	10
2.2.3 Emulsion polymerization.....	14
2.2.4 Block copolymer Self-Assembly.....	16
2.2.5 Templating process.....	20
2.2.6 Other methods.....	29
2.3 MATERIAL AND METHODS	30
2.3.1 Material.....	30
2.3.2 Preparation of PLA particles	30
2.3.3 Hydrodynamic Particle Size	31
2.3.4 Droplet and Particle Morphology	31
2.4 EMULSION IN TURBULENT FLUID FLOW	32
2.5 RESULTS AND DISCUSSION	34
2.5.1 Determining the major stage of hollow particles formation.....	34
2.5.2 Theoretical analysis of the effect of viscosity on the formation of open hollow structure.....	38
2.5.3 Effect of mixing temperature in the process of open hollow shape formation.....	43
2.6 Conclusion.....	46
Chapter3	
Encapsulation of Hydrophilic Materials into Hydrophobic Polymer by Emulsion Solvent Removal Technique	47
3.1 INTRODUCTION.....	48
3.2 BACKGROUNDS	50
3.2.1 Emulsion solvent removal technique.....	51
3.2.2 Phase separation and coacervation	53
3.2.3 Spray drying	54
3.2.4 Introduction of Nisin	54

3.2.5 Magnetic NPs	57
3.3 MATERIAL AND METHODS	57
3.3.1 Material.....	57
3.3.2 Preparation of hydrophilic magnetic NPs.....	58
3.3.3 PLA/nisin particles production.....	58
3.3.4 PLA/magnetic NPs preparation	59
3.3.5 Shear and temperature resistance test on the preformed nisin solution.....	59
3.3.6 Nisin encapsulation quantification	60
3.3.7 Zeta potential analysis for particle surface charge	60
3.3.8 Particle morphology characterization.....	60
3.4 RESULTS AND DISCUSSION	61
3.4.1 Preliminary tests on shear and temperature resistance of nisin	61
3.4.2 Nisin distribution in the PLA particles	63
3.4.3 Surface characterization of composite particles	65
3.4.4 Morphological observation of composite particles	66
3.4.5 Quantification of nisin encapsulation	68
3.4.6 Dynamic control of nisin encapsulation	69
3.4.7 Observations of magnetic NPs encapsulation	70
3.5 CONCLUSION	73

Chapter4

Fractionation of Corn Stover by a Novel Nanoshear Hybrid Alkaline Pretreatment	74
4.1 INTRODUCTION.....	75
4.2 BACKGROUNDS	77
4.2.1 Lignocellulosic biomass	77
4.2.1.1 Cellulose	77
4.2.1.2 Hemicellulose	78
4.2.1.3 Lignin.....	79
4.2.2 Pretreatment of lignocellulosic biomass.....	79
4.2.2.1 Alkaline Pretreatment	80
4.2.2.2 Acid Pretreatment	81
4.2.2.3 Ammonia Fiber/Freeze Explosion (AFEX).....	82
4.3 MATERIAL AND METHODS	83
4.3.1 Material.....	83
4.3.2 Corn stover pretreatment	84
4.3.3 Enzymatic hydrolysis	84
4.3.4 Composition analysis.....	85
4.3.5 Sugar analysis	85
4.3.6 Microscope observation by Scanning Electron Microscope (SEM)	85
4.4 RESULTS AND DISCUSSION	86
4.4.1 Analysis of compositional change	86
4.4.2 Proposed mechanism	88
4.4.3 Microscopy observations on morphological changes.....	89
4.4.4 Hybrid pretreatment effect on enzymatic hydrolysis	92
4.5 CONCLUSION	93

Chapter5	
Impact of Cationic Polyelectrolyte on the Nanoshear Hybrid Alkaline Pretreatment of Corn Stover: Morphology and Saccharification Study	94
5.1 INTRODUCTION.....	95
5.2 BACKGROUNDS	97
5.2.1 Effect of surfactants on the pretreatment of lignocellulosic biomass.....	97
5.2.2 Effect of inorganic salts on the pretreatment of lignocellulosic biomass.....	99
5.2.3 Effect of cationic polyelectrolytes on the enzymatic hydrolysis of lignocellulosic biomass.....	100
5.3 MATERIAL AND METHODS	101
5.3.1 Material.....	101
5.3.2 Sample pretreatment	102
5.3.3 Enzymatic hydrolysis	103
5.3.4 Composition analysis.....	103
5.3.5 Sugar analysis	104
5.3.6 Surface morphology of pretreated samples	104
5.3.7 Inner structure of pretreated samples.....	104
5.3.8 Confocal Laser Scanning Microscope (CLSM)	105
5.3.9 X-ray photoelectron spectroscopy (XPS)	105
5.4 RESULTS AND DISCUSSION	105
5.4.1 Chemical compositions change	105
5.4.2 Microscopic morphology observation of pretreated corn stover.....	108
5.4.3 Verification of droplets deposited on the surface	109
5.4.4 Surface content analysis by X-ray photoelectron spectroscopy (XPS)	111
5.4.5 Visualization of cell wall by TEM	113
5.4.6 Effect of the polyelectrolyte on sugar yields	115
5.5 CONCLUSION	118
Chapter6	
Future Work	119
REFERENCES	123

LIST OF TABLES

Table 5. 1 Lignin surface coverage of pretreated corn stover analyzed by XPS	113
--	-----

LIST OF FIGURES

- Figure 1. 1 Scheme of chamber geometry and principle of nanomixer. For interpretation of the references to color in this and all other figures, the reader is referred to the electronic version of this dissertation. 3
- Figure 2. 1 Schematic representation of the emulsion solvent-evaporation/ extraction preparation method of hollow PLA microcapsules. Reproduced with permission from [37]. 12
- Figure 2. 2 Transitional behavior of polymeric hollow microsphere formation in turbulent shear flow by emulsion diffusion method. Reproduced with permission from [40]. 12
- Figure 2. 3 Schematic formation mechanism of hollow microspheres via the phase-inversion method. Reproduced with permission from [41]. 13
- Figure 2. 4 Schematic of two-stage voided latex particle process. Reproduced with permission from [47]. 15
- Figure 2. 5 Illustration of vesicle formation from supramolecular block copolymers. Reproduced with permission from [55]. 17
- Figure 2. 6 Schematic diagram for hollow capsule production by exploiting colloidal templating and self-assembly methods [67]. 22
- Figure 2. 7 Schematic illustration of the formation of cage-like a) and multiple multihollow structure b) microspheres. Reproduced with permission from [66]. 23
- Figure 2. 8 Formation mechanism of monodispersed hollow polymer particles by seeded polymerization for the dispersion of (toluene/DVB)-swollen PS particles prepared utilizing the dynamic swelling method. Adapted from [70]. 25
- Figure 2. 9 Schema of stepwise colloid particle coating with polyelectrolytes. The grey and black molecules represent polycations and polyanions respectively. Reproduced with permission from [76]. 26
- Figure 2. 10 Schematic illustration of the formation of polyelectrolyte capsules on an ‘air’ core. a) The Tween/Span mixture is used to form air microbubbles; b-d) Microbubbles are stabilized by the electrostatic assembly of PAH/PSS multilayers. The photograph shows air-containing polyelectrolyte capsules in aqueous solution after centrifugation. Reproduced with permission from [86]. 28
- Figure 2. 11 SEM images of PLA particles formed at 40% (a), 50% (b), and 60% (c) v/v of glycerol at the apparent shear rate of 12500 s^{-1} for 1 minute and PLA concentration of 15 mg/ml in the dispersed phase when the temperature of the internal vessel was increased to 78°C . Multiple emulsion like droplet (W/O/W) containing PLA before

diffusion step, where acridine orange as fluorescent species was dissolved in the aqueous phase (W) (bright region) (d). Dark region shows the ethyl acetate phase containing PLA (O). TEM images of PLA particles collected by vacuum filtration (e) and dialysis (f), respectively. 35

Figure 2. 12 Proposed mechanism of the formation of open-hollow polymer particles. Gradually changing grayer color represents the condensation of polymer in the drop. Surfactant PF68 is displayed as centered hydrophobic short chain (red) tailed by two hydrophilic long chains (blue). 37

Figure 2. 13 (a) The mean polymer particle diameter at mixing shear rate of 12500 s^{-1} and mixing time of 1 minute. Glycerol was added at different volume fractions at room temperature ($25 \text{ }^\circ\text{C}$). (b) The influence of viscosity on the three parameters, eddy diameter, stable droplet diameter in inertial turbulent regime, d_{KH} and stable droplet diameter in viscous turbulent regime, d_{KV} . Also plotted is the mean particle diameter. .. 39

Figure 2. 14 Schematic illustration of the transitional behavior of droplet formation, single polymeric emulsion droplets in inertial turbulent regime (a,b) where droplet size $>$ eddy size, and multiple emulsion droplets in viscous turbulent regime (c,d) where droplet size $<$ eddy size. Smaller eddies break up bigger polymer-containing droplets in dynamic condition (a). When mixing is stopped, droplets are stabilized (b). Smaller emulsion droplets are caught in a larger eddy, dynamically self-assembling or coalescing inside the eddy (c) and forming a multiple emulsion like droplet (W/O/W) when mixing stops (d). 42

Figure 2. 15 SEM images of PLA particles to show the effect of PLA concentrations on the shell wall thickness of formed open hollow particles, 5mg/ml (a, thinner) and 30mg/ml (b, thicker), compared with Figure 2.11 (b, 15 mg/ml). 43

Figure 2. 16 SEM images of PLA particles formed at emulsification temperatures of $25 \text{ }^\circ\text{C}$ (a), $65 \text{ }^\circ\text{C}$ (b), $40 \text{ }^\circ\text{C}$ (c), and $55 \text{ }^\circ\text{C}$ (d), respectively. SEM image of nanospherical polystyrene particles formed at mixing shear rate of 12500 s^{-1} for 1 minute (e). 45

Figure 3. 1 Morphology of microparticles: A) reservoir system; B) matrix system. (Redrawn with permission from Ghosh [120]) 51

Figure 3. 2 Schematic representation of the coacervation process. a) Core materials are dispersed in the solution of coating materials; b) phase separation of coacervate from solution; c) deposition of coacervate on the core materials; d) coalescence of coacervate to form continuous shell. (Reproduced with permission from [120]) 53

Figure 3. 3 Primary structure of nisin. (Reproduced with permission from [138]) 56

Figure 3. 4 Inhibition ratios of different sample nisin solutions for four subtypes of listeria monocytogenes. The inhibition ratio was defined as (OD630 reading difference from control group) / (OD630 reading of control group). 62

Figure 3. 5 CLSM images of composite particle surface and cross-sectional view.	63
Figure 3. 6 Zeta potential of plain PLA and polymeric composite particles at different nisin loadings of 0.025 (S1), 0.075 (S2), 0.125 (S3), 0.175 (S4), and 0.225 (S5) mg/ml in the water phase solution.....	65
Figure 3. 7 SEM images of final polymeric composite particles with nisin loadings of 0.05 (A), 0.25 (B), 0.5 (C), 0.75 (D) mg/ml in the water phase solution.	66
Figure 3. 8 Encapsulated nisin amount of different polymeric composite particles. S1, S2, and S3 represent the particles with nisin loadings of 1.5, 2.0, 3.0 mg/ml.	68
Figure 3. 9 The effect of alternating emulsification temperatures between ~60 °C and room temperature (25 °C) on the encapsulated nisin amount. HT0, HT2, and HT4 represent that the emulsification process was performed by alternating temperatures 0 time, 2 times, and 4 times and the ending emulsification temperatures were at ~60 °C. RT1 and RT3 represent that the emulsification was performed by alternating temperatures 1 time and 3 times, and the ending emulsification temperatures were at room temperature.	69
Figure 3. 10 SEM images of PLA/magnetic NPs composite particles at low (A) and high (B) magnification.	70
Figure 3. 11 TEM images of PLA/magnetic NPs composite particles at the cross-sectional view. A) a representative hollow structure composite particle; B) part of particle shell wall at high magnification.	72
Figure 4. 1 Structure of repeating unit of a cellulose chain in the lignocellulosic biomass.	78
Figure 4. 2 Structure of partial xylans from softwood chain.	78
Figure 4. 3 Structure of building units of lignin in the lignocellulosic biomass.....	79
Figure 4. 4 Scheme of pretreatment on lignocellulosic materials. (Reproduced with permission from [169])	80
Figure 4. 5 Major chemical components of untreated and pretreated corn stover at different NaOH concentrations. All samples were analyzed at least triplicates with standard deviation (\pm SD) calculated.	87
Figure 4. 6 SEM images of corn stover pretreated at 8% (A and B) and 20% (C and D) (w/v) NaOH solutions and shear rate of 12500 s^{-1} in 2 min. A) and C) are taken at low magnification; B) and D) are at relatively high magnification.	90

Figure 4. 7 Cellulose and hemicellulose conversion of corn stover pretreated with 0.4% and 4% (w/v) NaOH. The enzyme loading is 20 FPU/g cellulose and incubation temperature is 50 ± 1 °C. 93

Figure 5. 1 Percentage of major chemical components in untreated and pretreated corn stover. A) Untreated CS: Corn Stover without pretreatment; Pretreated CS 1: Corn Stover pretreated with 0.4% (w/v) NaOH; Pretreated CS 2: Corn Stover pretreated with 4% (w/v) NaOH. B) Pretreated CS w/ 1_1: Corn Stover pretreated with 0.4% (w/v) NaOH and 10mM PDAC; Pretreated CS w/ 1_2: Corn Stover pretreated with 0.4% (w/v) NaOH and 60mM PDAC; Pretreated CS w/ 2_1: Corn Stover pretreated with 4% (w/v) NaOH and 10mM PDAC; Pretreated CS w/ 2_2: Corn Stover pretreated with 4% (w/v) NaOH and 60mM PDAC. 106

Figure 5. 2 SEM image of untreated and pretreated corn stover. A) Untreated corn stover; B) Corn stover pretreated with 4% (w/v) NaOH; C) Corn stover pretreated with 4% (w/v) NaOH and 10 mM PDAC; D) Corn stover pretreated with 4% (w/v) NaOH and 60 mM PDAC. 109

Figure 5. 3 CLSM image of untreated and pretreated corn stover. A) Untreated corn stover; B) Corn stover pretreated with 4% (w/v) NaOH; C) Corn stover pretreated with 4% (w/v) NaOH and 10 mM PDAC; D) Corn stover pretreated with 4% (w/v) NaOH and 60 mM PDAC. 110

Figure 5. 4 TEM images of sectional view of untreated and pretreated corn stover which were stained with KMnO_4 . A) Untreated corn stover; B) Corn stover pretreated with 4% (w/v) NaOH; C) Corn stover pretreated with 4% (w/v) NaOH and 10 mM PDAC; D) Corn stover pretreated with 4% (w/v) NaOH and 60 mM PDAC. 114

Figure 5. 5 Sugar conversions of 0.4% (w/v) NaOH and 10 mM PDADMAC pretreated corn stover. The substrate loading is 2% (w/v) and enzyme loading is 20 FPU/g glucan. 116

Chapter 1

Introduction

1.1 Overview of mixing system with Nanomixer

Efficient mixing and reaction can promote the fabrication and modification processes to obtain the products with desired properties and considerably improve the process performance. A modified Taylor-Couette mixer, also called nanomixer, which can generate extremely high shear turbulent fluid flow environment, was introduced to facilitate the production of biodegradable polymer (or composite) particles and biorenewable materials. To simplify the estimate of turbulent fluid flow in this nanomixer, Taylor-Couette mixer was used to describe the geometrical characteristics [1]. As illustrated in Figure 1.1, it consists of a pair of concentric cylinders with rotating inner perforated turbine and stationary outer tank with turbine rotating at peripheral speeds from 0 to 50 m/s which can generate high shear stress on the processing materials and achieve extremely high Re (upto several million) [1].

The mixing is carried out in this modified Taylor-Couette fluid flow which occurs in the annular space between the two cylinders [2]. Based on the definition of Re for fluids and the type of forces mainly responsible for drop breakup, regimes in turbulent flow can be defined as turbulent viscous and turbulent inertial regime. When the process fluid is spinning at the same speed as the turbine, it is pressed strongly against the inside of vessel wall. The perforated cylinder wheel with many holes in the circumferential wall allows the whirling process fluid to spurt out through the holes due to the centrifugal force. The process fluid is divided into two flows along the inside wall. The upward flow smashes against the top and is going downward, while the downward flow smashes against the bottom and is going upward. These two flows return to the inside of the spinning thin film with numerous small turbulent eddies. Then the process is repeated

within the nanomixer. The processing temperature of emulsification can be controlled by flowing heating or cooling fluid around the mixing chamber. Under turbulent conditions, the drops of one fluid mixing in a second continuous phase could break upon the action of viscous or inertial turbulent stress [3, 4]. The stress that will dominate is determined by the size of the smallest turbulent eddies that are formed in the fluid flow.

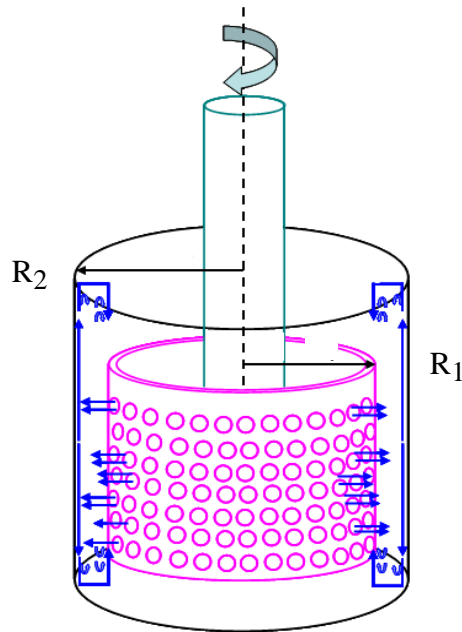


Figure 1. 1 Scheme of chamber geometry and principle of nanomixer. For interpretation of the references to color in this and all other figures, the reader is referred to the electronic version of this dissertation.

1.2 Fabrication of polymer particles by emulsion technique

Polymeric hollow microspheres have attracted growing attention because of their unique properties and extensive applications. In the Chapter 2, we developed a simple and fast single emulsion technique to fabricate hollow polylactic acid (PLA) particles by viscous turbulent fluid flow. The process involves the emulsification of a PLA-ethyl acetate solution in the water-glycerol medium under high viscous turbulent shear flow

where emulsion droplets coalesce into multiple emulsions and the solidification of PLA particles by the diffusion of ethyl acetate to plenty of water. Turbulent regime and processing temperature were found as key factors to the dynamic control of the production of polymer particles from solid nanospheres to hollow microspheres. The addition of glycerol changed the viscosity of the continuous aqueous phase, resulting in the transition of fluid flow from inertial turbulent to viscous turbulent dominant regime and thus PLA particle size and shape from solid nanospheres to hollow microspheres. The emulsification temperature also needs to exceed the glass transition temperature of PLA to form hollow microstructure. This method allows the easy control of polymer particle shape and size.

1.3 Encapsulation of hydrophilic materials by single emulsion technique

The structure of multiple emulsion droplets with useful inner water space has been utilized for encapsulation of hydrophilic materials within hydrophobic polymer matrix. Successful incorporations of hydrophilic nanoparticles such as iron oxide nanoparticles and biomacromolecules such as peptides were introduced in the Chapter 3 as representative examples of its practical applications in the efficient encapsulation of hydrophilic materials by single emulsion technique for different demands.

1.4 Biomass pretreatment facilitated by shear field

We also reported a fast and high efficiency nanoscale hybrid pretreatment method of lignocellulosic biomass in the Chapter 4. Corn stover was pretreated in this nanomixer at a reduced temperature for two minutes with alkaline condition. Composition analysis

showed the significant removal of both lignin and hemicellulose after the nanoshear hybrid alkaline pretreatment. Microscopy images revealed the severe disruption of corn stover structure and exposure of cellulose microfibrils from the cell walls. Effective fractionation and structure disruption can be achieved by this novel pretreatment method. Compared to untreated sample, cellulose and hemicellulose conversion were greatly enhanced.

1.5 Effect of cationic polyelectrolyte on the pretreatment

In order to make the process economically feasible, cationic polyelectrolyte was first introduced as an additive in this pretreatment of corn stover. At room temperature and fast processing conditions (about 2 minutes), lignin was found to redistribute on the inner and outer surfaces of the cell walls as lignin aggregate droplets instead of being extracted. Free nano-/microfibrils in the residues were also observed. The yields of enzymatic hydrolysis were enhanced for the pretreated corn stover with the aid of polyelectrolyte as an additive. We speculate that lignin was effectively modified which opened up the cell wall structure during the short pretreatment process and prevented non-productive binding of enzymes in the enzyme hydrolysis reaction. This can improve cellulose accessibility and digestibility, indicating that polyelectrolyte is a promising alternative to modify the biomass surface and reduce the use of expensive enzymes.

Chapter 2

Transitional Behavior of Polymeric Hollow Microsphere Formation in Turbulent Shear Flow by Emulsion Diffusion Method

**Papers published in *Current Trends in Polymer Science*, vol 15, p 63-75, 2011 and
Polymer, vol 53(1), p 205-212, 2012**

2.1 INTRODUCTION

The fabrication of polymeric particles with unusual and complex structures has greatly developed owing to their unique shapes and properties. There has been extensive research in methods and processes, including emulsion, self-assembly, and phase separation, to develop functional or structured polymeric nano- and micro-particles [5-15]. The particle size and shape can be considered to be closely related to its functionality. Those particles find wide applications in drug delivery, petroleum, paints, cosmetics, and so on. Especially, hollow microspheres or open-shaped particles would be suitable for carriers, chemical protection, and catalysis due to their unique structures [16-19].

Emulsion process is very versatile which has been used to prepare various kinds of particles. Emulsion formation requires the dispersion of one phase into another in the presence of a stabilizing agent, which can be achieved by mechanical agitation based on spontaneous emulsification [20]. These emulsion droplets can be used as templates for further processing to form core-shell structures. Similarly, they have long been used as a micro/nano-reactor chamber for the fabrication of metallic nanoparticles [21-24]. These emulsions can also be used to make solid particles by emulsifying the polymer-containing dispersed phase and then removing the dispersed solvent by diffusion or evaporation, leaving polymer solidified to particles. The process can be tailored to incorporate various functional materials of interest [11, 12, 17, 19]. Double or multiple emulsions are commonly applied to produce final particles with hollow structure [13]. Due to their biocompatibility and complete degradability, poly(D,L-lactide) or poly(D,L-lactide-co-glycolide)-based particles are frequently utilized in the drug delivery systems [10, 14, 18].

Existing spherical polymer particles such as polystyrene (PS) and poly(methyl-methacrylate) (PMMA) have been used to form hollow polymer particles with holes on their surfaces for the potential application in microencapsulation and delivery by Xia et al [25]. Okudo et al. also demonstrated a seeded dispersion polymerization route in the presence of decane droplets to prepare nonspherical polystyrene particles [26]. However, they are both a slow two-step process where polymer particles are prepared in advance and then swollen by or absorb a solvent which is removed by phase separation and evaporation. Recently, Xue et al. have reported a self-assembly diffusion process to synthesize the polyurethane (PU) hollow microspheres with size tunable single holes [27]. The formation of single holes was attributed to the removal of chloroform in methanol. However, they have not shown that biodegradable polymers like PLA can be used for the same process in the paper. Despite much progress has been made in the fabrication of various structured polymeric particles, little has been done in the formation of hollow structure particles in a simple fashion.

In this study, we introduce a facile method to prepare polymeric hollow particles using simple oil in water (O/W) emulsion diffusion process. The hollow particles prepared by this method are of micrometer scale. There are few studies to utilize the turbulent fluid flow to fabricate hollow particles with the single emulsion technique. The process involves an eddy driven dynamic coalescence of emulsion droplets to form multiple emulsions in the viscous turbulent regime. The changes in the size and structure of polymeric particles are controllable by manipulating emulsification conditions, such as viscosity of the continuous phase and temperature. The experiments and analysis reveal the transitional behavior of those particles emulsified in the turbulent regimes. Based on

the presented data below, both PLA nanospheres and hollow microspheres can be fabricated under different conditions, which show the advantages of simple operation and easy control capable of yielding desired particle shapes and properties for widespread use.

2.2 BACKGROUNDS

The control of the morphology of polymer particles is of great interest both from an academic and practical perspective. Recently, hollow polymer microspheres have attracted considerable attention due to their unique properties. These particles have a large surface to volume ratio making the adsorption of active substances more easily, which can be potentially applied as capsules for controlled release drug delivery and catalyst carriers [28, 29]. They also can be used as light-weight fillers for low density property. The void within the hollow particles not only provides useful spacious compartments but also unique light scattering properties [30]. These particles have been widely used in encapsulation, cosmetics, paper coatings, and so on [31]. Their composite with inorganic particles can provide added functionality in hybrid structures, such as magnetic, electronic, and catalytic properties [32, 33]. Progress on preparation methods of hollow polymer microspheres allow the synthesis of polymers with well controlled structure and compositions, obtaining the final particles with desired properties.

The aim of this review is to summarize different fabrication processes of producing hollow polymer microspheres. The fundamental formation mechanism of each method is given firstly and their updated progresses on different polymer materials and applications are pointed out. The advantages and differences of one approach compared to the others are briefly introduced. The understanding of different preparation methods

of hollow structures is useful for future development and application of these materials and their functions.

2.2.1 Emulsion processing

Emulsion processing is one of the traditional methods to fabricate the hollow polymer particles, usually combined with a subsequent solidification, such as phase separation or solvent evaporation. Quintanar-Guerrero et al first developed the emulsion-diffusion method [34]. In this two-step process, polymer containing oil phase is emulsified in the water phase and the organic solvent contained in it is then eliminated by extraction or evaporation. The removal of organic solvent hardens the particle and reduces the particle size.

Double emulsion method is widely applied in the microencapsulation technology, producing liquid microcapsules that contain a liquid or a gas core. Rosca et al produced poly(lactide-co-glycolide) (PLGA) microparticles with different morphologies by double emulsion solvent evaporation method [35]. Hollow and porous microparticles could be generated depending on the formulation conditions. However, multi-core morphology is not able to provide effectively entrapped volume and efficient mass transfer across the polymer shells. Wang and Ma et al reported an emulsion ripening process to obtain single-core W_1/O globules from their multicore precursors in $W_1/O/W_2$ emulsions [36]. Subsequent suspension polymerization ensures the encapsulation of water phase in the biocompatible hollow poly(methyl methacrylate) (PMMA) microcapsules. This method involves many procedures and is costly and time consuming.

A conventional single emulsion process can also prepare hollow polymer particles (Figure 2.1) [37]. Polymer/solvent/oil mixture is emulsified in the nonsolvent phase, where oil acts as the co-solvent having poor solubility for polymer in the mixture. The capsules are formed during the solvent out-diffusion step, leaving the polymer and oil concentrated in the droplets. The polymer continuously solidifies as a shell at the interface between the dispersed and continuous phase. Subsequent removal of the oil by freeze-drying results in the formation of the polymer shell in the appropriate morphology. The size and membrane thickness of capsules by the emulsion-diffusion method depends on the concentration of oil, polymer, and stabilizer and the volume of the solvent [38]. The solidification of the polymer shell is not only obtained by diffusing the solvent, but also by removing or freezing the water [38]. Chevalier et al showed the geometric relationship between the primary emulsion and the final nanocapsule size [39]. The formulation and processing parameters of the primary emulsion, such as the oil-to-polymer ratio and the mixing shear rate, can influence the properties of nanocapsules. Recently our group demonstrated a facile emulsion diffusion process to fabricate poly(lactic acid) (PLA) hollow microspheres driven by viscous turbulent fluid flow, as shown in Figure 2.2. Based on one-step emulsification, turbulent regime and emulsification temperature have been used to control the shape and size of polymeric particles from nanospheres to hollow microspheres [40]. In the drug delivery technology, single emulsion process usually obtains hollow polymer particles containing oil in the core which are suitable for encapsulating hydrophobic drugs. It is possible to prepare water containing polymer particles by double or multiple emulsion method where

hydrophilic molecules can be carried. Generally the hollow particles formed from double or multiple emulsions are larger in size than those from single emulsions.

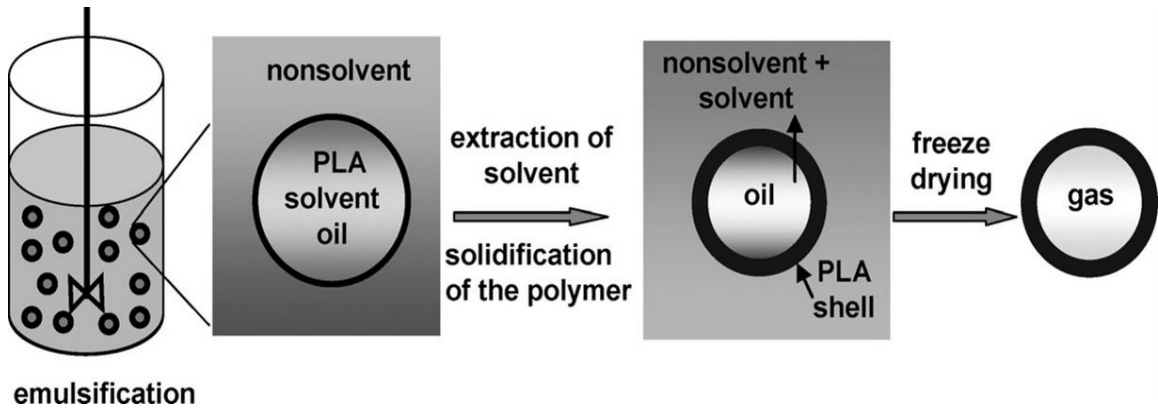


Figure 2. 1 Schematic representation of the emulsion solvent-evaporation/ extraction preparation method of hollow PLA microcapsules. Reproduced with permission from [37].

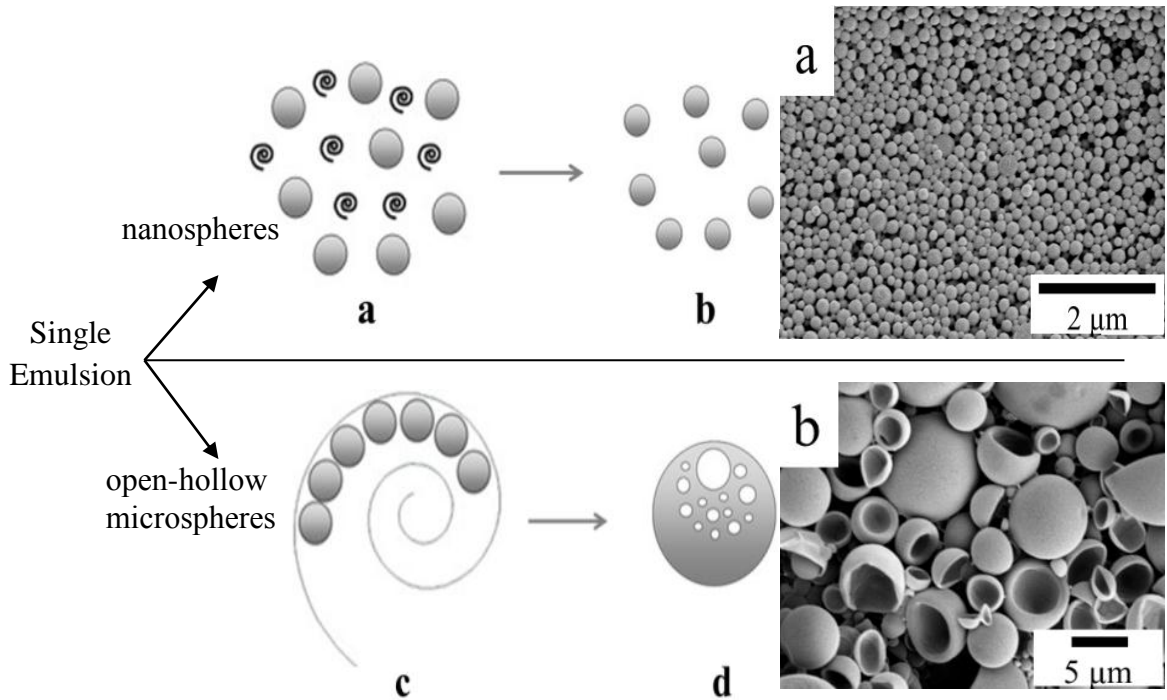


Figure 2. 2 Transitional behavior of polymeric hollow microsphere formation in turbulent shear flow by emulsion diffusion method. Reproduced with permission from [40].

Phase inversion is another approach to fabricate hollow polymer microspheres. The one-step single emulsification process is directly related to multiple emulsions formation

during phase inversion [41] (Figure 2.3). You and Wu et al grafted hydrophobic chlorinated polypropylene with hydrophilic methyl methacrylate, butyl acrylate, and acrylic acid parts [42]. The solvent containing the modified polymer was diluted by water which induced the phase inversion beyond the critical point and then formed the hollow structure after evaporation. They took advantages of the semimiscibility of butanone with water and the carboxyl group content to entrap the water-butanone compartments in the hydrophobic emulsion droplets as well as lead to the complete phase separation and generation of both inner and outer sphere interfaces.

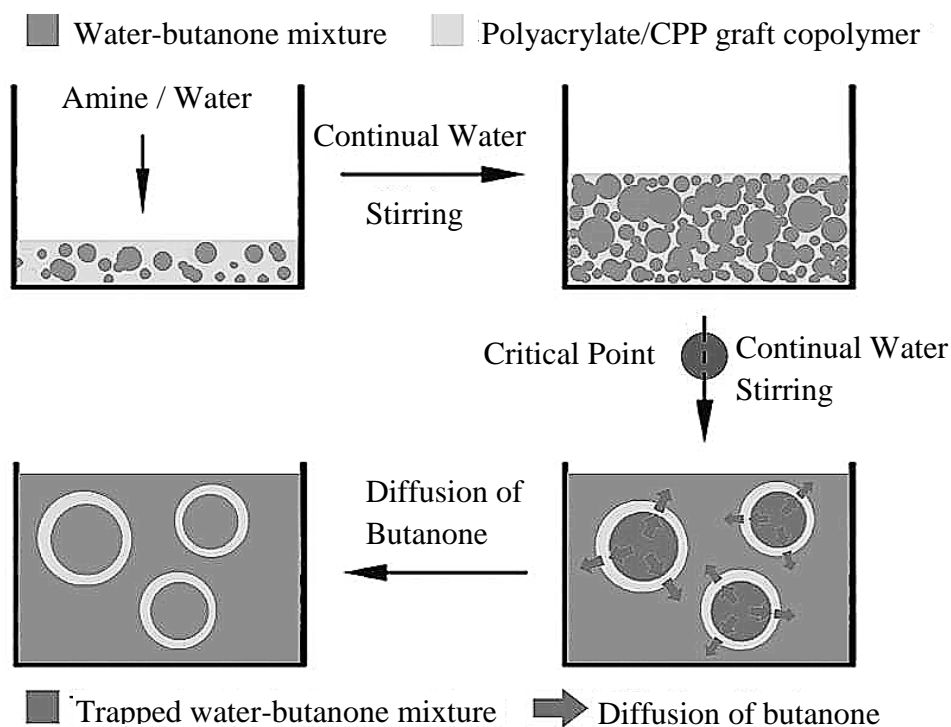


Figure 2. 3 Schematic formation mechanism of hollow microspheres via the phase-inversion method. Reproduced with permission from [41].

Conventional emulsification techniques, such as magnetic stirring, sonication, and homogenization, cannot provide a good control over the size and size distribution of hollow particles. The membrane emulsification is used to prepare monodisperse

emulsions by passing premixed emulsion droplets through the pores of the glass fiber membrane [43, 44]. Combined co-solvent single emulsification with membrane extraction, narrowly dispersed hollow polylactide microcapsules with sizes 0.35-5 μm were prepared from a polylactide/dichloromethane/dodecane solution in alcohol-water mixtures.

2.2.3 Emulsion polymerization

In general, the polymer shell surrounding the core can be formed either by precipitation of a preformed polymer at the top of emulsion droplets or polymerization occurring at the interface between the dispersed and continuous phase. The latter usually includes conventional emulsion polymerization, inverse emulsion polymerization, miniemulsion polymerization, dispersion polymerization, and microemulsion polymerization [45]. Due to the possible production of polymers with unique properties and the environmental advantages with waterborne products, the emulsion polymerization has been used to prepare a variety of commercial polymers. The earliest work of fabricating hollow polymer particles was developed by Kowalski and co-workers at The Rohm and Hass Company [46]. They prepared the core-shell polymer particles by sequential emulsion polymerization. The core containing carboxylic acid groups was then swollen and extracted by a volatile base, forming microvoids in the particles. Followed by this concept, McDonald et al encapsulated a nonsolvent hydrocarbon within an emulsion polymerization which induced the phase separation of the polymer with the dispersed mixture during polymerization due to the immiscibility between the formed polymer and hydrocarbon [47] (Figure 2.4). The encapsulated hydrocarbon was then removed by vacuum or steam to generate the inner void structure. No high shear stress

was required to control the particle size which was considered mainly related to the surfactant or a nucleating latex seed concentration.

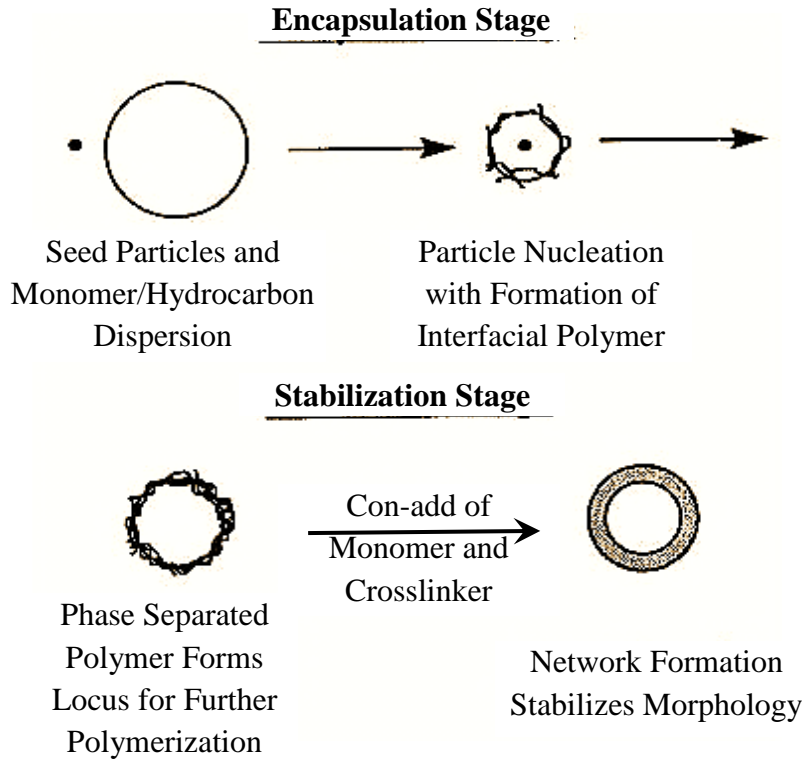


Figure 2. 4 Schematic of two-stage voided latex particle process. Reproduced with permission from [47].

The similar process can also be applied to prepare core-shell structured particles. The core polymer and the surrounding secondary polymer layer are synthesized by the sequential conventional emulsion polymerization. The core materials are degraded or extracted to leave the hollow spheres. Zheng et al consecutively condensed bi- and tri-functional organosilicon onto the poly(dimethylsiloxane) (PDMS) microemulsions [48]. The linear PDMS chains in the core were removed by tetrahydrofuran (THF), forming hollow polysiloxane microcapsules. Similarly, pH-sensitive hollow poly(N,N'-methylene bisacrylamide-co-methacrylic acid) (P(MBAAm-co-MAA)) microspheres with defined size below 200 nm and shell thickness in the range of 8-26 nm were prepared by a

distillation precipitation polymerization, which can be used as the controlled release carrier [49].

Miniemulsion polymerization has been widely applied in the nano/microencapsulation. One of its advantages is the direct encapsulation while forming the polymeric capsules. γ -ray radiation was used to induce the miniemulsion polymerization of styrene and at the same time N-vinyl pyrrolidone (NVP) was reacted by graft copolymerization onto polystyrene (PS) [50]. The graft reaction between PS and PVP increases the hydrophilicity of the polymer and reduces the interfacial tension, which facilitates the formation of PS nanocapsules with phase separated dodecane as the liquid core. Shirin-Abadi et al encapsulated hexadecane (HD) in the PMMA nanocapsules via miniemulsion polymerization as one example of the hydrophobic agents [51]. With the aid of theoretical calculations by using DSC, DLS, and microscopy, processing parameters, such as HD:MMA ratio and the usage of the cross-linking agents, were considered to mainly affect the encapsulation process. Combining with the templating technique, emulsion polymerization can be extended to produce core-shell hybrid particles generating the hollow structure after the removal of the inorganic core. The details will be discussed in the later section.

2.2.4 Block copolymer Self-Assembly

Self-assembling features have been found in amphiphilic block and graft copolymers, which open up an efficient way to form polymeric micelles with a variety of novel morphologies and functions [52]. Block copolymers act as surfactants when dispersed in the solution. The shape of self-assembled hollow structures is determined by the size of hydrophobic moiety to the hydrophilic part. The aggregation of block

copolymers is triggered by minimizing energetically unfavorable contact between the insoluble blocks and the selective solvent [53]. Aggregates with a spherical morphology usually consist of an insoluble core and a soluble corona. Polymeric micelles have good stability and toughness and can be tailored to suite physical, chemical, and biological requirements by varying experimental parameters, such as the block copolymer composition, block length, chemical structure, solvent composition, copolymer concentration, etc [53, 54].

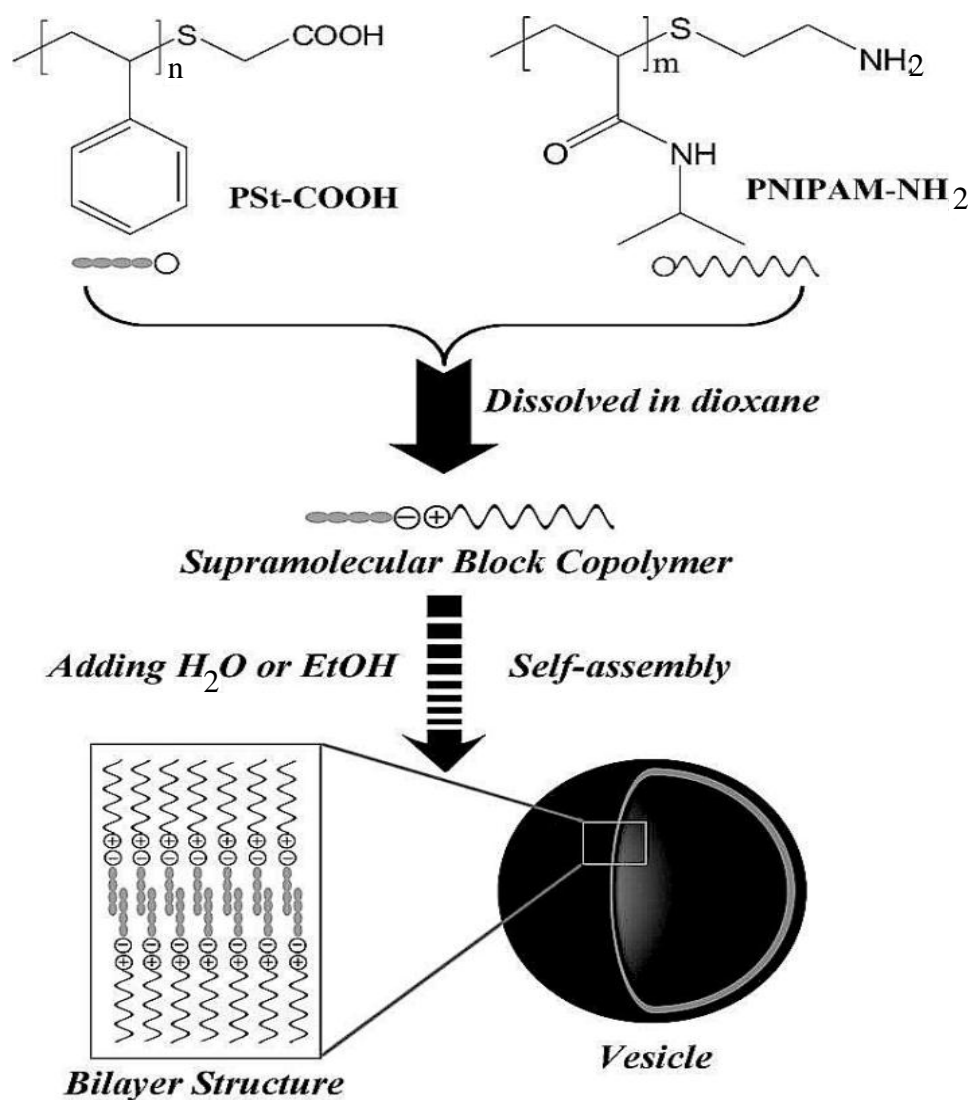


Figure 2. 5 Illustration of vesicle formation from supramolecular block copolymers. Reproduced with permission from [55].

Eisenberg et al first showed the dependence of block copolymer morphologies on the molecular architecture, e.g. block lengths [52]. The formation of polystyrene-b-poly(acrylic acid) (PS-b-PAA) micelles is strongly dependent on the ratio of PAA and PS block lengths. When the PAA content is decreased, the morphology changes from spherical micelle-like to rod-like aggregates, or even further to vesicular. The solvent can also influence the morphology of those block copolymers which is related to the polymer-solvent interaction [56]. When tetrahydrofuran (THF) is used as solvent, both micelles and vesicles are obtained, whereas only spherical micelles exist under N,N-dimethylformamide (DMF). A lot of work has been reported on the regular amphiphilic block copolymers, such as polystyrene-block-poly(4-vinylpyridine) (PS-b-P4VP) [57], poly(ethylene oxide)-block-poly(n-butyl acrylate) (PEO-b-PnBA [54], poly(ethylene oxide)-block-poly(ethyl ethylene) (PEO-b-PEE) [58], poly(butadiene)-block-poly(ethylene oxide) (PBD-b-PEO) [59]. Discher et al integrated the hydrolysable and non-cross-linkable diblock, poly(ethylene oxide)-poly(lactic acid) (PEO-PLA), into bilayer vesicles of PEO-PBD copolymer to offer the controlled destabilization property to the solid polymer shell and facilitate the encapsulant release as degradable delivery agents [60]. Amphiphilic copolymers with complex structure can broaden their potential applications. In order to mimic the natural membranes with oriented proteins, artificial membrane which is asymmetric vesicular structure, was build up by ABC triblock copolymer, poly(ethylene oxide)-poly(dimethyl siloxane)-poly(methyl oxazoline) (PEO-PDMS-PMOXA), in the aqueous solution [61].

In the assembly strategies, coil polymer chains are commonly used as building blocks. However, the stiff rod-like block can also affect the macromolecular packing and

facilitate the vesicle formation. The first work of vesicle formation by a multiblock copolymer was reported by Holder et al [62]. Amphiphilic poly(methylphenylsilane)-poly(ethylene oxide) (PMPS-PEO) copolymer was synthesized and vesicles were well formed in the water with narrow size distribution. PMPS chains in the vesicle walls were orientated perpendicular to the air/water interface and packed as rod-like layer which promoted the formation of a hollow spherical structure. Jenekhe and Chen also reported the self-assembly of synthetic rod-coil diblock copolymer, poly(phenylquinoline)-block-polystyrene (PPQ-b-PS) in a selective solvent, trifluoroacetic acid (TFA), which is good for PPQ under different solvent compositions and solution drying rates. The hollow microcavities observed from large micron size spherical aggregates show the potential applications in encapsulating the fullerene molecules or generating ordered microporous materials [63]. Li et al also extended this idea onto two amphiphilic liquid crystal block copolymers consisting of a side-on nematic polymer block and a PEG block with different hydrophilic/hydrophobic ratios. Polymer vesicles were obtained from block copolymers at large hydrophilic/hydrophobic ratios [64]. A mixing of rod-like homopolymer polyimide (PI) and coil-like homopolymer poly(4-vinyl pyridine) (PVPy) in their common solvent chloroform produced the hollow spherical aggregates within nano-scale, which was proposed that grafts with enough stiffness are necessary for the formation of hollow structure even in the nonselective solvents [65].

Besides the structural difference among the covalently connected segments, secondary interactions between the polymer tectons, such as charge interactions, H-bondings, dipolar interactions, etc., can also control the intermolecular conformation. Jiang group have studied a series of building block polymers and successfully prepared

hollow spheres with different homopolymer pairs via inter-polymer H-bonding, such as PVPy and hydroxyl-containing PS in a selective solvent, PVPy and carboxy-ended PI in their common solvent, and PVPy and carboxy-terminated poly(amic acid) ester (PAE) [65, 66]. Qian and Wu connected hydrophilic poly(N-isopropylacrylamide) with amino end groups (PNIPAM-NH₂) and hydrophobic PS with carboxylic end groups (PSt-COOH) through the ionic interaction. These amphiphilic supramolecular block copolymers formed spherical vesicles in the dioxane/H₂O system. Increasing temperature induced the transformation of worm-like vesicles to spherical vesicles in the dioxane/ethanol system [55] (Figure 2.5).

2.2.5 Templating process

Templating method is a simple process which includes the synthesis of the polymer shell on the dispersed template and the removal of the template core particle [67](Figure 2.6). PS latexes, emulsion droplets, inorganic colloids, or gas bubbles are commonly used as templates. Polymer particles prepared by this method are usually monodispersed. The process of fabricating hollow polymer microspheres by osmotic swelling method is originally from Kowalski et al as described above, which produces the submicron-sized hollow particles with water and ionized polymer inside [46]. Okubo group has proposed the stepwise alkali/acid and alkali/cooling treatments on the carboxyl-containing latex particles for forming the multihollow structure [68-70]. In the alkali/acid treatment, poly(styrene-butyl acrylate-methacrylic acid) (P(S-BA-MAA)) was prepared as the seed particle by emulsion copolymerization and carboxylic acid groups in the core PS particle were neutralized and swollen under alkaline condition. Entrapped

water coalesced to form bigger one, resulting in the hollow structure during the acid treatment. It has been shown that the initial pH value, temperature, and time in the post-treatment processes have great effect on the particle morphology. In order to simplify the polymerization process and lower the impact of BA on the glass transition temperature, strength, and rigidity of polymer latex particles, Kan et al further synthesized the porous P(S-MAA) particles via batch soap-free emulsion polymerization, followed by stepwise alkali/acid post-treatment. MAA amount was considered as a crucial factor to control the size and morphology of prepared latex particles [71].

Recently, sulfonated polystyrene (SP) particles have attracted much attention as the template. Wang and Ge et al successfully prepared multihollow PMMA particles by one-step radiation emulsion polymerization, the structure of which was determined by the initial location of SP template particles before emulsification [72]. When SP particles located in the water phase, pickering emulsion was formed giving the cage-like hollow structure. If dissolved in the monomer phase, SP particles were entrapped in the multiple emulsions and multihollow structure would be generated (Figure 2.7).

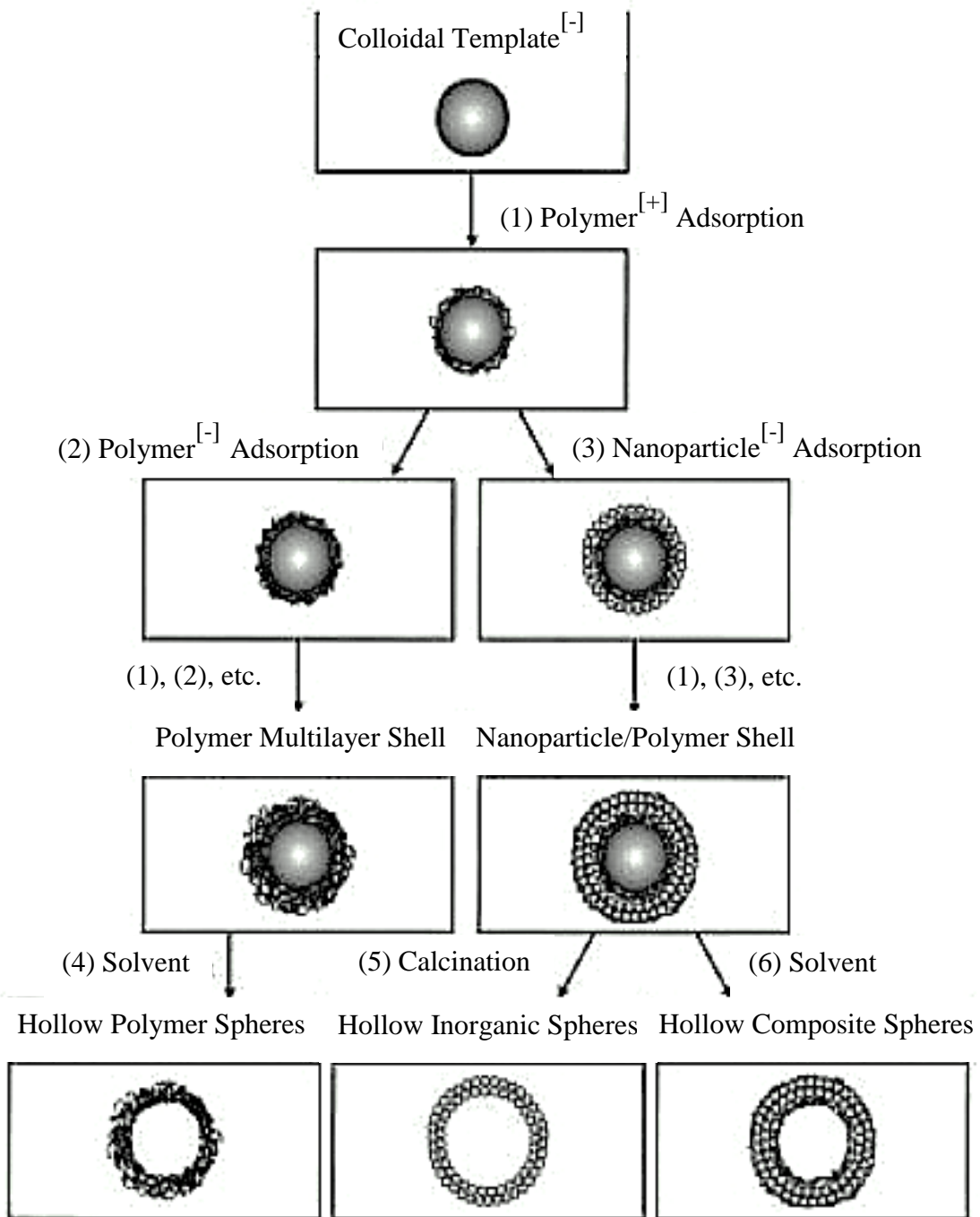


Figure 2. 6 Schematic diagram for hollow capsule production by exploiting colloidal templating and self-assembly methods [67].

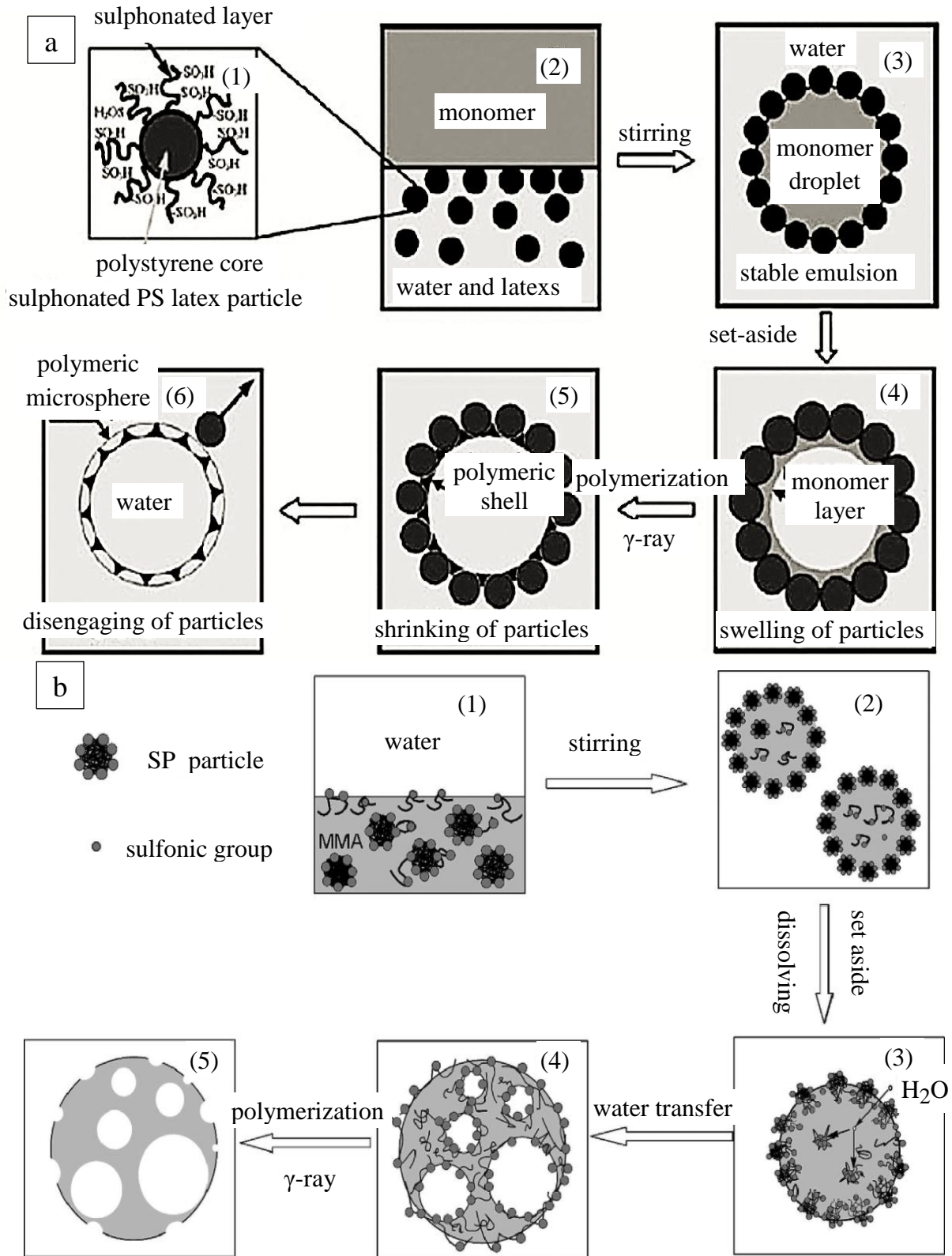


Figure 2. 7 Schematic illustration of the formation of cage-like a) where $-\text{SO}_3\text{H}$ groups were dissolved in the water solution and multiple multi-hollow structure b) microspheres. Reproduced with permission from [72].

Okubo group also developed a seeded emulsion polymerization method, named the “dynamic swelling method” (DSM) [73, 74]. PS particles were used as the seed and swollen by toluene with dissolved divinylbenzene (DVB) monomers. PDVB was polymerized and precipitated near the interface, forming a cross-linked PDVB shell. Dissolving PS built up the uniform inner shell against the PDVB shell after the evaporation of toluene under reflux (Figure 2.8). Processing parameters, such as DVB content [33], polymerization temperature [75], addition of emulsifiers, and PS molecular weight [76], were investigated to control the size and morphology of prepared polymer particles. Xia et al applied the similar concept to form hollow PS and PMMA particles with controllable holes on their surfaces for the potential application in the microencapsulation [77]. They utilized the toluene volume shrinkage from liquid to solid phase to generate a void inside the swollen PS solid particles. A hole was formed after the evaporation of toluene.

Recently decane droplets were used instead of swelling solvents in the seeded dispersion polymerization to prepare monodispersed dimple and hemispherical PS particles [26]. Processing temperature, stirring rate, and medium composition were studied to explain the formation mechanism. Absorption of decane droplets into PS particles was carried out by heating spherical PS particles beyond the glass transition temperature of PS in the aqueous medium. During the cooling process, PS particles phase separated with decane and formed nonspherical structure after its removal.

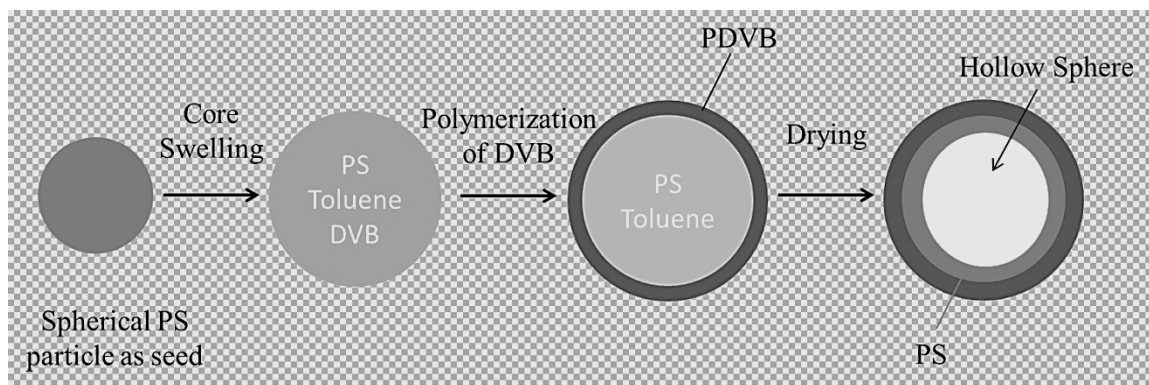


Figure 2. 8 Formation mechanism of monodispersed hollow polymer particles by seeded polymerization for the dispersion of (toluene/DVB)-swollen PS particles prepared utilizing the dynamic swelling method. Adapted from [70].

Layer-by-layer (LbL) self-assembly is suitable for controlling polymer shell thickness and compositions [78]. As its name implies, it is based on the consecutive deposition of oppositely charged polyelectrolyte layers onto a charged particle surface (Figure 2.9). The adsorption is mainly dependent on the electrostatic force. Poly(styrene sulfonate) (PSS), poly(allyamine hydrochloride) (PAH), poly(ethyleneimine) (PEI), and poly(diallyldimethylammonium chloride) (PDAC) are usually used as polyanion and polycations [79, 80]. Template particles, such as PS latex particles modified with sulfate, melamine formaldehyde (MF) microparticles, or inorganic particles, can be dissolved by organic solvents or acid solutions after LbL coating. Multilayer capsules can be functionalized by assembling materials of interest. Micrometer sized hollow silica-polymer spheres were obtained by LbL self-assembly of silica nanoparticles and PDAC layers [81]. The shell thickness can be easily tuned by the adsorption layers, while the template particles can affect the size and shape of final hollow spheres. Similarly, Li and coworkers have built a PEI/PAA-gold hollow nanocomposite capsule system by LbL self-assembly process which is sensitive to near infrared laser light applied in the drug

delivery [82]. The pH responsive behavior of PSS/PAH capsules was studied by Dejugnat and Sukhorukov [83]. Swelling and shrinking of the capsules could be achieved under basic and acidic solutions respectively, which serve as a trigger to control the permeability of the polymer capsules. Hollow polyelectrolyte shells can be used on biological templates, not only for protecting biological interiors but also for mimicking their structures. PSS/PAH layers have been grown on human erythrocytes [84]. After decomposing template proteins, prepared polyelectrolyte shells are considered as the replicas of the original cells. Further deposition of lipids allows the control of the permeability of small polar molecules.

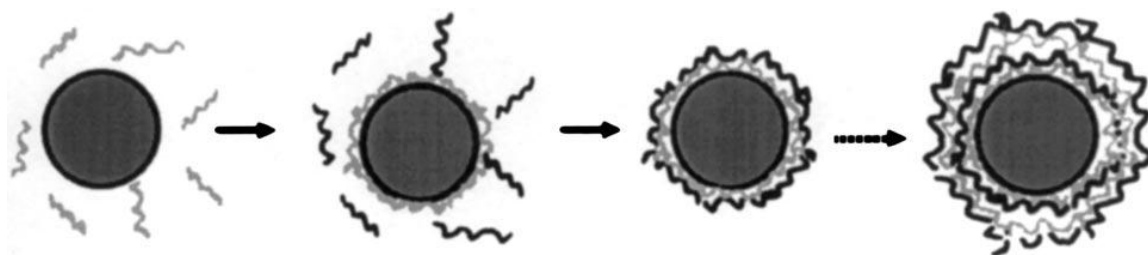


Figure 2. 9 Schema of stepwise colloid particle coating with polyelectrolytes. The grey and black molecules represent polycations and polyanions respectively. Reproduced with permission from [76].

Besides the liquid droplets or solid particles, microbubbles have been used as templates for lipid bilayers and polymer films. Microbubbles covered with a lipid bilayer are expected to be used as ultrasound contrast agents [85]. Shchukin et al and Winterhalter et al described the polyelectrolyte microcapsules with a gaseous interior by LbL self-assembly [86, 87] (Figure 2.10). Air microdispersion was performed by ultrasound generator. PAH/PSS multilayers were adsorbed at the water/air interface. The size of resulting capsules is in a wide size distribution (1-20 μm). Recently a new preparation method of PAH/PSS microcapsules with microbubble templates in the size of

approximate 5 μm has been reported by Daiguji et al [88]. No surfactants were required in this process. By controlling the pH of Na_2CO_3 solution, CO_2 microbubbles covered with R-NHCOO^- and R-NH_3^+ were assembled by a PAH layer and finally deposited a PSS layer.

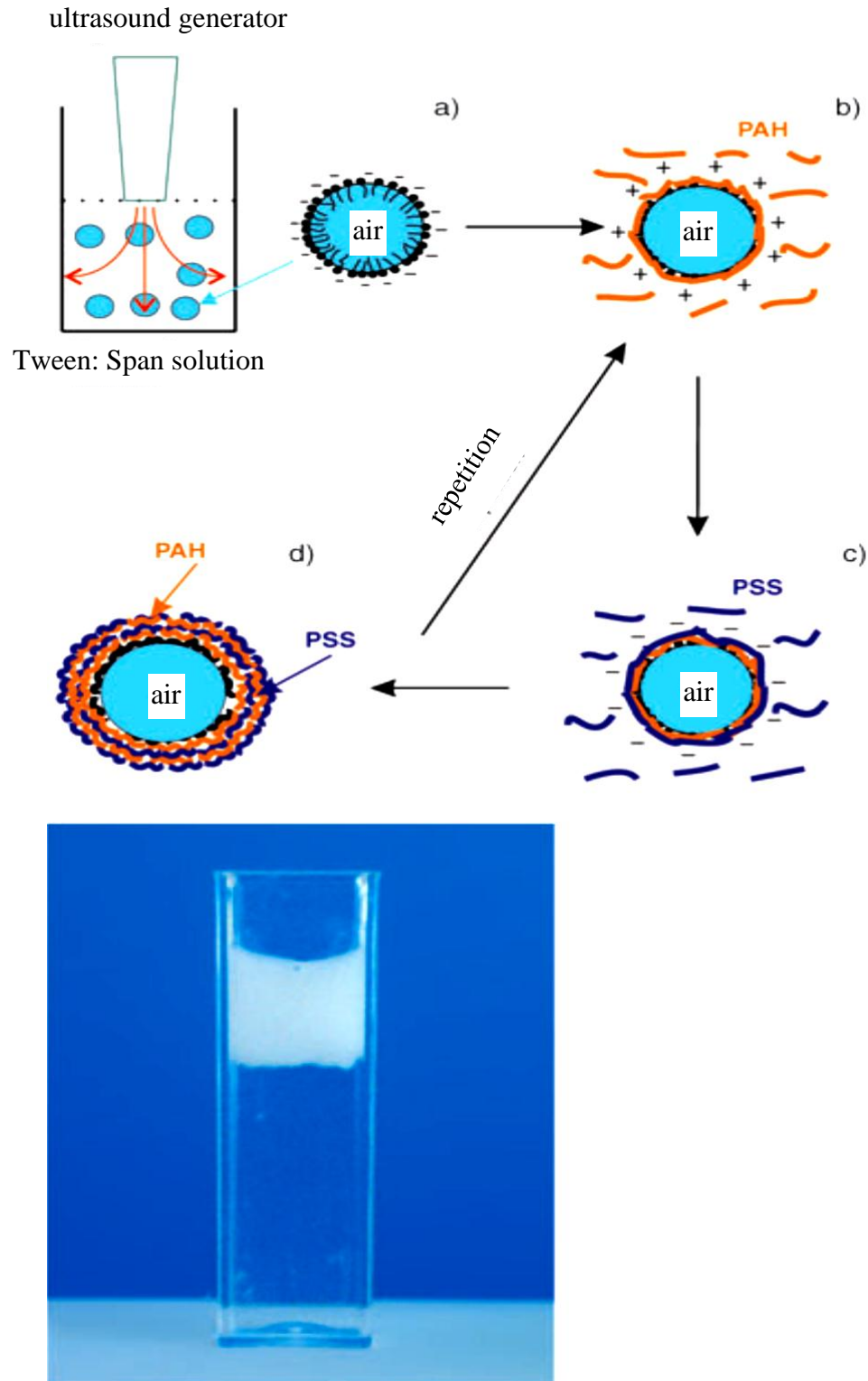


Figure 2. 10 Schematic illustration of the formation of polyelectrolyte capsules on an 'air' core. a) The Tween/Span mixture is used to form air microbubbles; b-d) Microbubbles are stabilized by the electrostatic assembly of PAH/PSS multilayers. The photograph shows air-containing polyelectrolyte capsules in aqueous solution after centrifugation. Reproduced with permission from [86].

2.2.6 Other methods

Many other fabrication methods have been developed for hollow polymer particles. Spray drying technology is a simple and efficient process to obtain products in narrow size distribution [89]. It is based on accumulating solute at the sprayed droplet surface which diffuses relatively slowly than the solvent during the drying process, resulting in forming the solid shell. Spray drying process was applied to produce PLGA microcapsules encapsulating the volatile solid, ammonium carbonate, for use as ultrasound contrast agents [30].

Microfluidics has attracted attention in recent years offering low cost and easy use for controlling fluid flow. The droplet size can be highly controlled and the particles are monodispersed since droplets solidify during the emulsion preparation [90]. Biodegradable PLLA capsules with a narrow size distribution were prepared by optimizing the flow rate of the continuous phase and PLLA molecular weight in the microfluidics system [91].

A new method to prepare particulate polymeric carriers in nano- and micro-meter size has been studied, named electrohydrodynamic atomization (EHDA). No templating or the use of surfactants are required making the process more efficient. A liquid is slowly injected through a capillary which is applied certain voltage and injected flow rate. The liquid emits from the cone vertex and breaks up into fine droplets [92, 93]. The primary droplets are monodispersed and their size is controlled by either spray rate or the electrical conductivity of the liquid.

2.3 MATERIAL AND METHODS

2.3.1 Material

Poly(D,L-lactic acid) (PLA, $M_w=51,000$ Da, $T_g= 52.5$ °C) was purchased from LakeShore Biomaterials (California, USA). Polystyrene ($M_w=50,000$ Da, $T_g= 90$ °C) was gained from Polyscience, Inc. (Pennsylvania, USA). The poloxamer Pluronic F68 (PF68) (average $M_w=8,400$ Da) was obtained from Sigma Aldrich. It is a low foaming and non-ionic surfactant consisting of block polymers in which central polyoxypropylene oxide (PPO) flanked by two polyoxyethylene oxide (PEO) tails. Ethyl acetate (EtOAc) and glycerol were from J.T. BAKER and used as received. Acridine orange, water soluble dye, was given by Center for Advanced Microscopy in Michigan State University with an excitation maximum at 502 nm and an emission maximum at 525 nm (green). All the chemicals used were analytical grade without further purification. All aqueous solutions in the processes were prepared with deionized (DI) water supplied by a Barnstead nanopure Diamond-UV purification unit equipped with a UV source and final 0.2 μ m filter at 18.2 M Ω purity. Dialysis tubing was purchased from Fisher Scientific Inc. (Pennsylvania, USA) with cut-off molecular weight of 12,000 and pore diameter of 4.8 nm.

2.3.2 Preparation of PLA particles

EtOAc and water were used as dispersed solvent and dispersion medium, respectively. They were mutually saturated to avoid any surface irregularities of droplets by sudden inter-diffusion during emulsification. PLA solutions were prepared by dissolving PLA at different concentrations (5 mg/ml, 15 mg/ml, and 30 mg/ml) into

water-saturated EtOAc. EtOAc-saturated aqueous solution was added with PF68 and then mixed with different volume fractions of glycerol, bringing the final concentration of PF68 to 15 mg/ml. The volume ratio of dispersed organic solution (O) to aqueous dispersion medium (W) was kept to be 1:3, regardless of the addition of polymer and glycerol. 20 ml organic solution was emulsified with 60 ml aqueous continuous phase using a modified high shear Taylor-Couette type nanomixer (Model 56-50) from the PRIMIX Corporation, Japan at an apparent shear rate of 12500 s^{-1} (i.e., peripheral speed rate 50 m/s) in 1 min. The O/W emulsion was then added to 300 ml of pure DI water under 600 rpm stirring in a beaker to induce the diffusion of EtOAc into water. After overnight diffusion, the colloidal dispersion was thus transferred to glass vial and stored at 4 °C for future use. Mixing temperature in the nanomixer-chamber was controlled by circulating cooling water around the outer cylinder wall. Different temperatures were applied to the emulsification process at the same formulation and composition.

2.3.3 Hydrodynamic Particle Size

The hydrodynamic particle size was determined at room temperature by Dynamic Light Scattering (DLS) Analyzer (90Plus) from BrookHaven instruments using highly diluted samples. Average of mean diameter was calculated by at least three measurements of each sample.

2.3.4 Droplet and Particle Morphology

Scanning Electron Microscope (SEM) was used to estimate the mean particle size as well as coefficient of variation for particle size. SEM used for high resolution imaging was JEOL 6400 at Center for Advanced Microscopy in Michigan State University, at

working distance of 8 mm and accelerating voltage of 6 KV. PLA particles were collected onto 0.1 μ m filter membrane and washed by plenty of pure DI water under vacuum. Dried particles along with membrane were then covered with gold coating facilitating their conductivity under electron microscope. Part of the colloidal dispersion was placed in a sealed dialysis membrane and gently stirred in the pure DI water at room temperature overnight. PLA particles were purified by allowing diffusion of glycerol and excess PF68 molecules through the selectively permeable membrane. Transmission electron microscopy (TEM) was done on PLA nanoparticles using JEOL 2200FS 60 kV field emission TEM. Copper grids coated with carbon were used to support PLA particles. A Nikon Eclipse E400 microscope was used to image fluorescent droplet solution stained by acridine orange within aqueous phase showing strong contrast with organic phase.

2.4 EMULSION IN TURBULENT FLUID FLOW

The emulsification of the polymer solution includes the deformation, breakup, and coalescence of large drops by the applied shear stress against the interfacial tension. We used a high shear rate nanomixer to emulsify PLA-containing ethyl acetate in the aqueous continuous phase. As mentioned in Chapter 1, Taylor-Couette fluid flow was applied to estimate the turbulent flow behavior in our system. Under turbulent conditions, the drops of one fluid mixing in a second continuous phase could break upon the action of viscous or inertial turbulent stress [3, 4]. The stress that will dominate is determined by the size of the smallest turbulent eddies that are formed in the flow [94-96] .

Theory developed by Kolmogorov was used to define the turbulence inside the nanomixer [4]. In a turbulent flow, the flow breaks down into eddies and each eddy

breaks down further into smaller eddies until the size of smallest possible eddy is attained. The size of the smallest eddies, λ , is given by so called “Kolmogorov Scale” which is approximated by equation 1

$$\lambda \approx \varepsilon^{-1/4} \eta_c^{3/4} \rho_c^{-3/4} \dots\dots\dots(2.1)$$

Where η_c is viscosity (Pa s^{-1}), ρ_c is density of the fluid or continuous phase (kg m^{-3}) and ε is the rate of energy dissipation ($\text{m}^2 \text{s}^{-3}$).

Kolmogorov-Hinze theory gave an estimate of maximum stable drop (d_{KH}) [95] for dispersed phase having density similar to that of water. The maximum stable diameter of the dispersed phase, d_{KH} , in inertial turbulent regime is given by equation 2

$$d_{KH} = A_1 \varepsilon^{-2/5} \sigma^{3/5} \rho_c^{-3/5} \dots\dots\dots(2.2)$$

Where A_1 is a constant of proportionality of the order of unity and σ is interfacial tension (N m^{-1}).

The drop breakup in viscous turbulent regime occurs when a drop is caught inside an eddy and the viscous turbulent stress inside the eddy causes it to break into smaller droplets. The maximum stable drop diameter [95] d_{KV} , is given by equation 3

$$d_{KV} = A_2 \varepsilon^{-1/2} \eta_c^{-1/2} \rho_c^{-1/2} \sigma \dots\dots\dots(2.3)$$

Where $A_2 \sim 4$, is a numerical constant.

Hence, the above mentioned equations can be used to estimate the diameter of emulsion droplets. This theory is valid if the viscosity of continuous phase is greater than

that of dispersed phase. If $\lambda < d_{KH}$, then the emulsification is in inertial regime. Whereas if $d_{KV} < \lambda$, the emulsification occurs in the viscous turbulent regime.

Rate of energy dissipation per unit mass characterizes the hydrodynamic condition during emulsification. For Taylor-Couette kind of geometry and at high Reynolds number, the rate of energy dissipation can be estimated by a simple approximation [97] as given by equation 4

$$\varepsilon = (\Delta U)^3 / \Delta r \dots \dots \dots (2.4)$$

Where ΔU is velocity difference across distance Δr . Δr is difference between inner and outer radii of cylinders.

2.5 RESULTS AND DISCUSSION

2.5.1 Determining the major stage of hollow particles formation

As shown in Figure 2.11, microscopic observations identified the transitional behavior of particle formation between regular spherical nanospheres and open-hollow microstructures as a function of continuous phase viscosity. SEM images of these typical PLA nanospheres (~100 nm) prepared from the aqueous continuous phase at 40 % v/v of glycerol (a) or less (0-40 % v/v) (images not shown here, but very similar to (a)), and novel open-hollow PLA microparticles (~5 μ m) fabricated at 50 % v/v of glycerol or more (b,c) are shown. This experimental process to fabricate open hollow polymer particles is simple and efficient. To understand whether this structure was formed during emulsification or after solvent removal, we applied water soluble dye into the aqueous continuous phase to facilitate our observation of the phase behavior during emulsification. One drop of emulsion solution was taken onto the glass slide immediately after

emulsification. Green light was emitted from the sample where the aqueous phase existed as shown in Figure 2.11(d). Droplets-in-drop structure (W/O/W) was found in the solution which is similar to multiple emulsion drops.

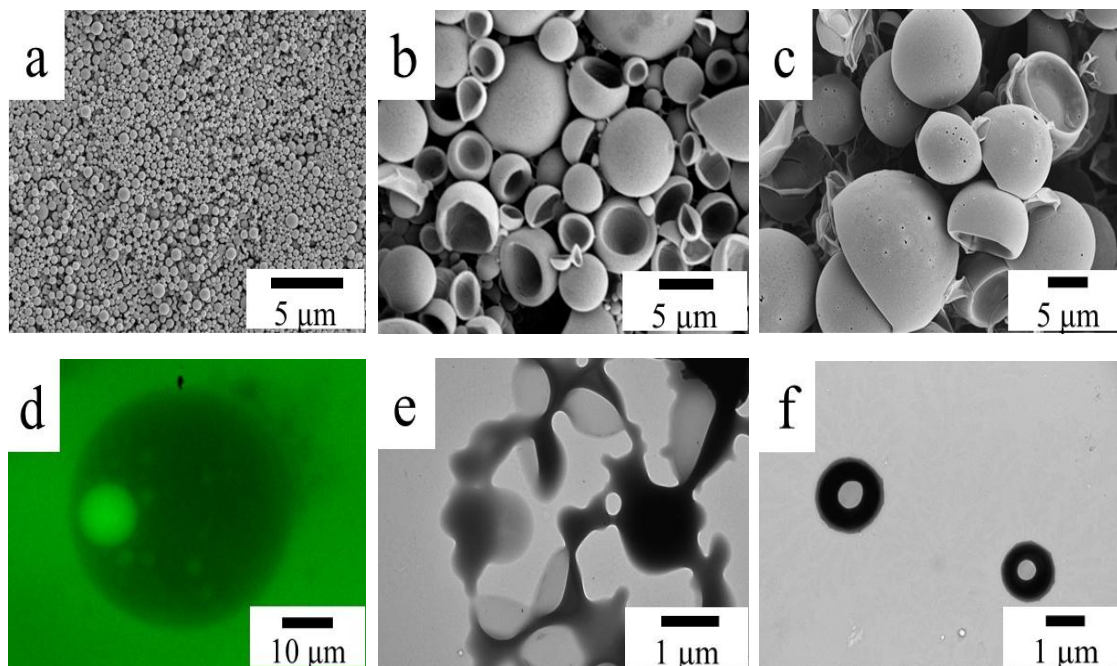


Figure 2. 11 SEM images of PLA particles formed at 40% (a), 50% (b), and 60% (c) v/v of glycerol at the apparent shear rate of 12500 s^{-1} for 1 minute and PLA concentration of 15 mg/ml in the dispersed phase when the temperature of the internal vessel was increased to $78 \text{ }^\circ\text{C}$. Multiple emulsion like droplet (W/O/W) containing PLA before diffusion step, where acridine orange as fluorescent species was dissolved in the aqueous phase (W) (bright region) (d). Dark region shows the ethyl acetate phase containing PLA (O).TEM images of PLA particles collected by vacuum filtration (e) and dialysis (f), respectively.

One-step emulsification is commonly known to prepare single emulsion drops (O/W), which usually leads to the formation of solid spheres after diffusion, as shown in Figure 2.11(a). It has only been reported that multiple emulsions produced by one-step process are a “mesophase” between O/W and W/O emulsions and can be obtained when the system approaches phase inversion [98, 99]. The final particles are formed from multiple emulsion droplets after solidification by removing the solvent. Enclosed droplets

in emulsion drops have been shown to undergo escape events, where inner droplets move to the interface and remain for a sufficient time [100, 101]. Escape occurs when the surrounding interface layer is lack of sufficient stabilization. It has been reported that particles with irregular shapes may be produced due to the sudden diffusion of ethyl acetate from the droplets into the dispersing phase while there will be a diffusion of water into the polymer droplets [102]. A mechanistic investigation has been done to study the diffusion process which is considered as the important step to obtain the nanocapsule structure [18, 27, 103].

We should mention that the thinner part of polymer shell could be within tens of nanometer, especially the side where inner water droplets are close to the interfacial boundary as seen in Figure 2.11(d). Therefore, it is very soft and easy to crack under high vacuum [15]. Figure 2.11(e,f) are TEM images of PLA particles collected as solids under vacuum filtration (e) and in the solution by dialysis (f). Compared with vacuum filtration, dialysis is a slow and mild process for removing glycerol and segments of surfactants from particle solution. Hollow structures are observed among PLA particles formed by the dialysis method (f), whereas most of those by vacuum filtration formed open-hollow structures (e).

Based on the previous studies [98-103] and our experimental observations, the proposed mechanism of droplet solidification to open hollow particles is presented in Figure 2.12. Under certain operating condition (e.g., high viscous solution \equiv viscous turbulent regime), W/O/W multiple emulsion droplets are formed (a). Due to insufficient surfactants inside the drops, inner water droplets may be easily coalescing to form a shell-like emulsion structure (b). After the addition of plenty of water, ethyl acetate is

diffused out to the aqueous phase and water can be diffused into the inner phase through less dense interfacial layer on the other side (c). PLA polymer is gradually deposited onto the interface with the removal of ethyl acetate, where the empty space left is replaced by water. Under harsh conditions (e.g., high vacuum), the entrapped water droplet moves to any part of interfacial boundary and the layer may become thin enough to rupture, leading to water escape. As a result, a hole is formed with the opening on the particle surface (d). PLA is keeping solidified associated with the volume shrinkage. Finally, the open hollow structure is formed (e).

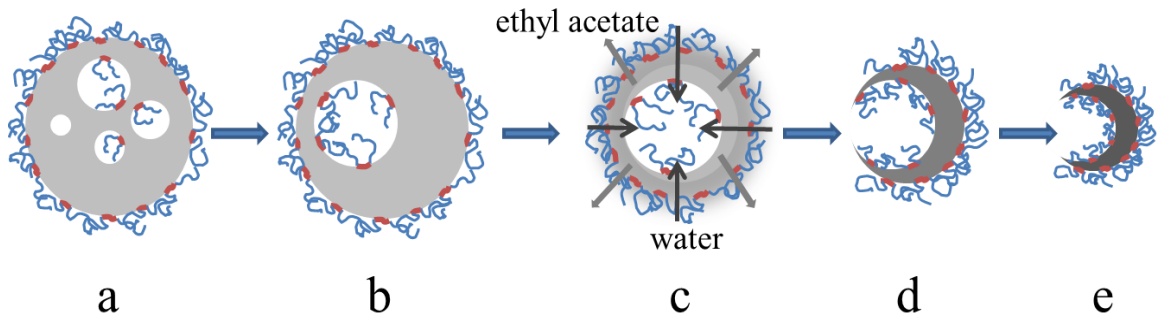


Figure 2. 12 Proposed mechanism of the formation of open-hollow polymer particles. Gradually changing grayer color represents the condensation of polymer in the drop. Surfactant PF68 is displayed as centered hydrophobic short chain (red) tailed by two hydrophilic long chains (blue).

In other cases (e.g., low viscous solution \equiv inertial turbulent regime), hollow particles were not obtained. The experimental observations pointed out that the formation of the unique particle shape was strongly dependent on the formation of multiple emulsion droplets. However, it should be noted that any standard double emulsion process, forming W/O/W, does not lead to such open hollow structures. The effects of major parameters controlling the unique transitional emulsification process as a function of solution viscosity were investigated by using theoretical analysis below.

2.5.2 Theoretical analysis of the effect of viscosity on the formation of open hollow structure

The emulsification is a complex process where the dispersed emulsion drops undergo deformation, break up, or coalescence in shear fluid flow [94-96]. As discussed above, inertial diameter (d_{KH}) of droplet is independent of the viscosity of the continuous phase whereas eddy diameter (λ) and viscous diameter (d_{KV}) are its functions. Hence we can shift the mixing condition from inertial turbulent regime ($\lambda < d_{KH}$) to viscous turbulent regime ($d_{KV} < \lambda$) by increasing the viscosity of the continuous phase. It is achieved by adding different volume fractions of glycerol along with water in our system, while keeping the same volume ratio of O to W (1:3). The emulsification step was carried out at an apparent shear rate of 12500 s^{-1} for 1 min, and then followed by solvent diffusion. The polymer particle size after diffusion was measured instead of droplet one because of its easier operation. The size was mostly proportional to the size of emulsion droplet when keeping the same diffusion process. Final PLA particle sizes measured at different glycerol volume fractions are plotted in Figure 2.13(a). The particle size remained constant till around 40% v/v glycerol and went up suddenly beyond that point. In the following Figure 2.13(b), all the three estimated theoretical parameters: eddy diameter (λ), inertial droplet diameter (d_{KH}), and viscous droplet diameter (d_{KV}) are plotted along with the measured mean diameter of polymer particles as a function of glycerol volume fractions.

The interfacial tension was calculated by using the theory of interfacial tension for partial miscible liquids where one liquid being mixture of water/glycerol and second liquid being ethyl acetate. For the case of partial miscible liquid, the formulation developed by Girifalco and Good [104] is used and given in equation 5

$$\gamma = \gamma_A + \gamma_B - 2(\gamma_A \gamma_B)^{1/2} \dots\dots\dots(2.5)$$

Where γ is the interfacial tension (N/m), γ_A is the surface tension of liquid A (N/m), γ_B is the surface tension of liquid B (N/m).

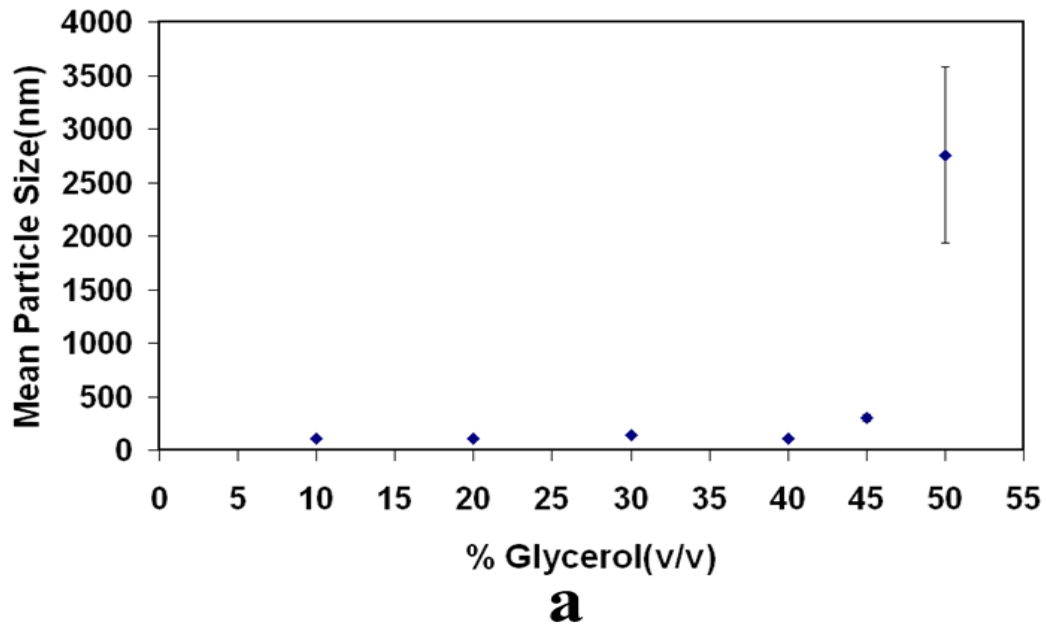
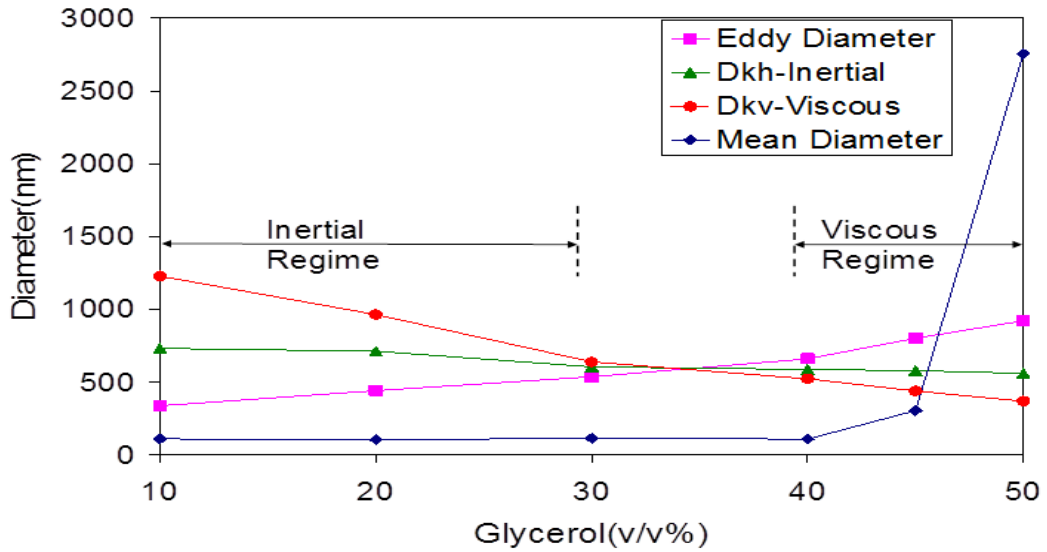


Figure 2. 13 (a) The mean polymer particle diameter at mixing shear rate of 12500 s^{-1} and mixing time of 1 minute. Glycerol was added at different volume fractions at room temperature ($25 \text{ }^\circ\text{C}$). (b) The influence of viscosity on the three parameters, eddy diameter, stable droplet diameter in inertial turbulent regime, d_{KH} and stable droplet diameter in viscous turbulent regime, d_{KV} . Also plotted is the mean particle diameter.

Figure 2.13 (cont'd)



b

For ethyl acetate, the literature value of surface tension at room temperature was used [104]. In the water/glycerol system, the surface tension was used from the plot published by Connor et al [105]. Density and viscosity data were used from the physical properties of glycerol-water solution available in literature [106]. The values obtained were used to calculate λ , d_{KH} , and d_{KV} .

As shown in the Figure 2.13(b), the eddy diameter is less than the d_{KH} for solution with glycerol volume percentage less than about 35%. Hence the mixing is in the inertial turbulent regime. As previously discussed, the emulsion droplet size can be estimated by the equation which is independent of the viscosity. This is confirmed by no observation of a big change in particle sizes after diffusion with increasing viscosity. But beyond 40% v/v of glycerol there was a sudden increase in the particle size with large standard deviation in mean. In addition, particle shape is also affected by the viscosity of the continuous phase. The images of particles obtained at 40% and 50% v/v of glycerol are shown in Figure 2.11(a,b). Particles formed at 40% v/v of glycerol continuous phase

remained nanospherical shape (a), whereas micron-scale open hollow particles were observed at 50% v/v of glycerol system (b).

Figure 2.14 illustrates the transitional behavior of droplet formation during emulsification process, from nano-scale single emulsions (O/W) in the turbulent inertial regime (a,b) to micro-scale multiple emulsions (W/O/W) in the turbulent viscous regime (c,d). In the inertial turbulent flow regime, as discussed previously, the eddy diameter is less than the stable droplet diameter and the larger droplets are located outside the smaller eddies whereas in the viscous turbulent regime the smaller droplets are located inside the larger eddies. As the viscosity is increased there is a shift in the mixing regime from inertial to viscous turbulent fluid flow and the nanodroplets are caught inside the larger eddies. Under the action of shear stress, the droplets are deformed inside and between turbulent eddies. Higher viscosity of the continuous phase increases the viscous stress, and therefore induces droplet deformation and elongation. The collisions and simultaneous coalescences among those droplets engulfed the intervening continuous phase. Successive coalescence of such droplets form the multiple droplets within drop structure [100].

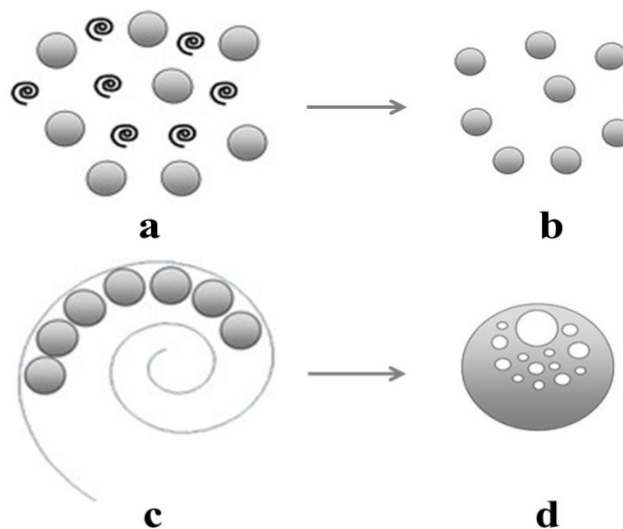


Figure 2. 14 Schematic illustration of the transitional behavior of droplet formation, single polymeric emulsion droplets in inertial turbulent regime (a,b) where droplet size $>$ eddy size, and multiple emulsion droplets in viscous turbulent regime (c,d) where droplet size $<$ eddy size. Smaller eddies break up bigger polymer-containing droplets in dynamic condition (a). When mixing is stopped, droplets are stabilized (b). Smaller emulsion droplets are caught in a larger eddy, dynamically self-assembling or coalescing inside the eddy (c) and forming a multiple emulsion like droplet (W/O/W) when mixing stops (d).

We further investigated the system at 60% v/v of glycerol, as shown in Figure 2.11 (c). Similar trend was observed for particles as in the 50% v/v of glycerol system, showing open hollow structure under viscous turbulent conditions. The size of open or collapsed shells was larger for 60% v/v of glycerol system, which is consistent with the theory that at higher viscosity the size of eddies increased thus increasing the size of emulsion droplets.

In Figures 2.11(b) and 2.15(a,b), it can be seen that increasing the polymer concentration (5 mg/ml (Fig. 2.15a), 15 mg/ml (Fig. 2.11b), and 30 mg/ml (Fig. 2.15b)) in the dispersed phase has little effect on particle size, but leads to thicker shell wall of open hollow particles. This can be predicted since the mixing conditions were kept almost the same and the emulsification should produce droplets with similar sizes which form the final particles with similar sizes as well.

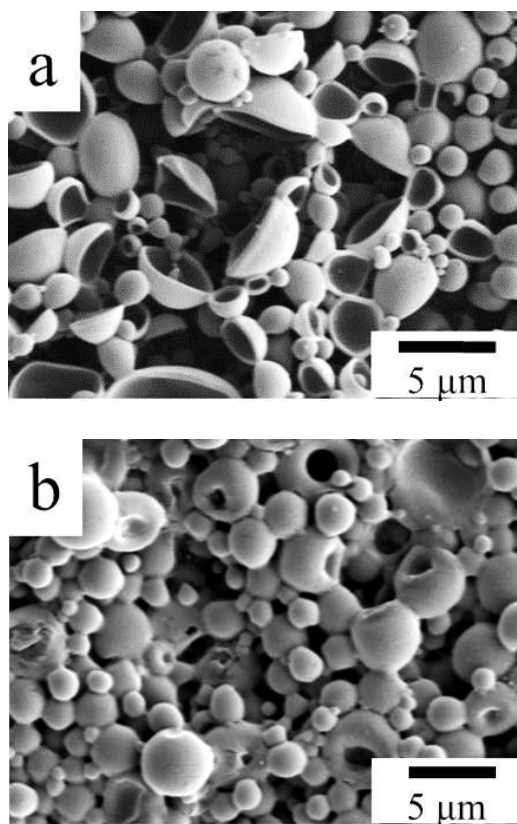


Figure 2. 15 SEM images of PLA particles to show the effect of PLA concentrations on the shell wall thickness of formed open hollow particles, 5mg/ml (a, thinner) and 30mg/ml (b, thicker), compared with Figure 2.11 (b, 15 mg/ml).

2.5.3 Effect of mixing temperature in the process of open hollow shape formation

Mixing at high shear rate led to the rise in temperature within the nanomixer chamber. The nanomixer has a cooling jacket, where the cooling water can be circulated during emulsification. The same temperature at different mixing conditions could be achieved by adjusting the temperature or flow rate of cooling water. To determine whether temperature is one of the controlling factors for the formation of hollow structure, emulsification was conducted at room temperature (25 °C) and 65 °C in the 50% v/v glycerol system. Since the boiling point of ethyl acetate is around 78 °C, higher temperature has not been tested in order to avoid the evaporation of ethyl acetate from

droplets. The particles formed at room temperature were mostly nano-spherical structure shown in Figure 2.16(a). However, those particles prepared at emulsification temperature of 65 °C showed large hollow shape with broad size distribution (see Figure 2.16(b)). Hence the emulsification temperature is indicated to be an important parameter capable of controlling the particular shape. It is known that surfactant lipophilicity increases with increasing temperature due to the dehydration of PEO chains. Due to the rearrangement of surfactant structure, the formulation favors a zero interfacial curvature which makes drops more deformable under shear [107].

Two more emulsification temperatures (40 °C and 55 °C) in between 25 °C and 65 °C were tested to observe the transitional behavior of the particle shape. Figure 2.16(c) shows that after diffusion nanospheres were obtained from the emulsification at 40 °C. Open hollow structure could still be observed when emulsification was carried out at 55 °C, as seen in Figure 2.16(d). The glass transition temperature of PLA used in this experiment is around 52.5 °C as reported by the manufacturer. Above this temperature, PLA is easily deformed, which may enhance the probability of coalescence among them inside the larger turbulent eddies and inclusion of intervening water phase within as discussed above. This was confirmed when polystyrene with glass transition temperature of 90 °C was applied instead of PLA during emulsification while the other experimental conditions were kept the same. The emulsification temperature was lower than the glass transition temperature of polystyrene. No open-hollow shaped particles were formed as shown in Figure 2.16(e).

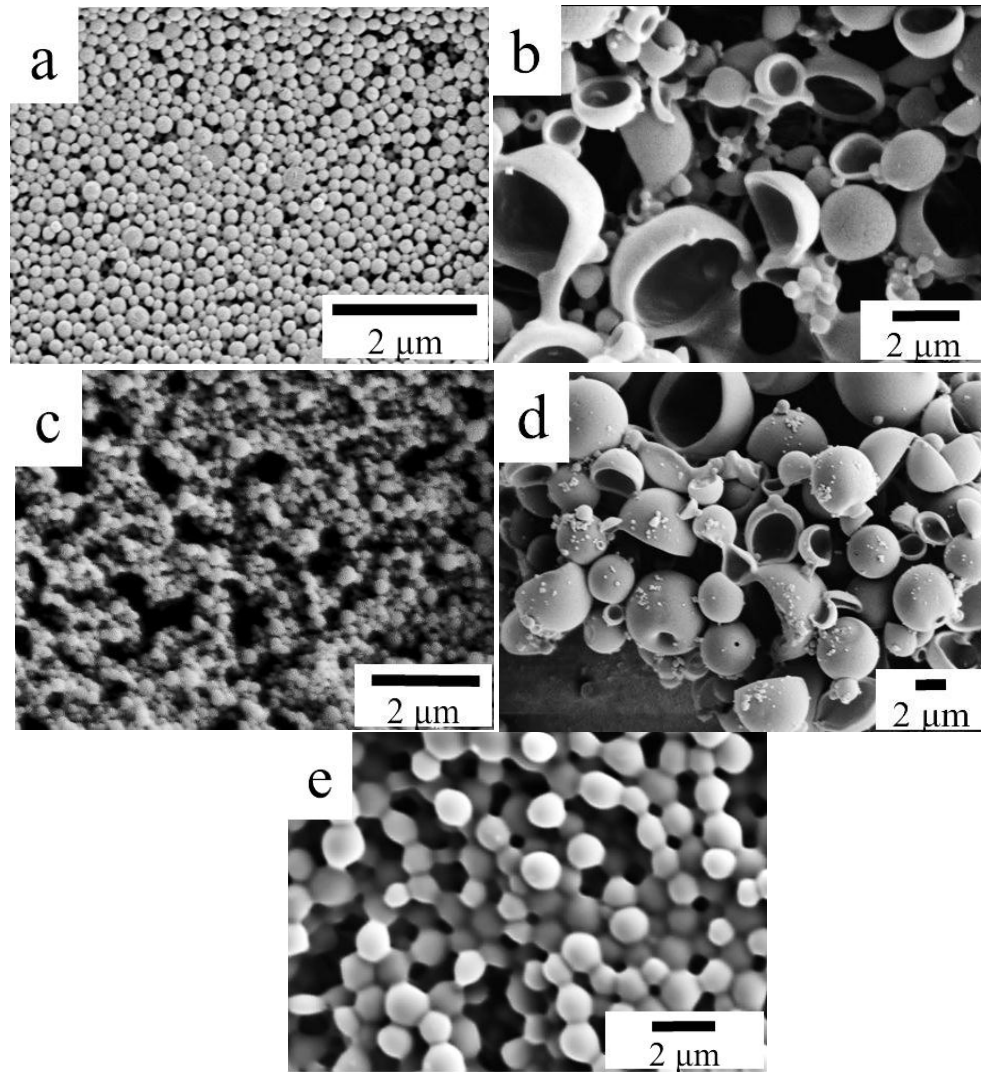


Figure 2. 16 SEM images of PLA particles formed at emulsification temperatures of 25 °C (a), 65 °C (b), 40 °C (c), and 55 °C (d), respectively. SEM image of nanospherical polystyrene particles formed at mixing shear rate of 12500 s^{-1} for 1 minute (e).

Therefore, the transitional changes of particle shape and size in our single emulsion system occurred by the combined influences of i) viscous turbulent regime where the diameter of eddy is greater than that of emulsion droplet and ii) emulsification temperature which is greater than the glass transition temperature of the polymer. As the viscosity is increased, the mixing regime is shifted from inertial turbulent to viscous turbulent flow regime and nano-size droplets are caught inside the larger turbulent eddies.

When the emulsification temperature is above the polymer glass transition temperature, polymers tend to be deformed and elongated which increase the coalescence among multi-body collisions. Higher temperature also results in the dehydration of surfactant hydrophilic chains. The originally entrapped water can be released from the interface into the oil which facilitates the formation of inner water droplets [107]. Unique multiple emulsions-like droplets are formed after emulsification process. Along with the coalescence and escape of inner water droplets, hollow structure is obtained after diffusion.

2.6 Conclusion

A novel one-step fast emulsion process is proposed that utilizes turbulent fluid flow to induce the shape and size change in polymeric particles. The formation mechanism of hollow particles was studied based on earlier theories of emulsification in turbulent fluid flow. Turbulent regime and emulsification temperature have been investigated as controlling factors. The understanding of the process in our system allows the scaling up of the fabrication process and extends applications of these polymeric particles with their unique shape and properties. They could be used in applications that require higher surface area to volume ratio. Loading nanoparticles or other molecules of interest could also be further achieved. Especially due to the particle structure and the fast process, this method can be used to develop novel microencapsulation and delivery systems. Further work is being carried out to extend similar shape formation using other polymers and also tailor specific functions.

Chapter 3

Encapsulation of Hydrophilic Materials into Hydrophobic Polymer by Emulsion Solvent Removal Technique

Papers submitted to peer-reviewed research journals

3.1 INTRODUCTION

Encapsulation process has been widely applied in pharmaceutical and biomedical industry, food systems, printing, cosmetics, and agricultural area [108-110]. Especially in the drug delivery system, encapsulation for controlled release of drug substances can greatly protect drugs from degradation, improve the bioavailability of drugs, minimize drug side effects, reduce dosing frequency, and mask the drug taste and odor [111, 112]. Due to the world wide interest, improvement for efficient encapsulation becomes an area of great importance to extend its applications and meet diverse needs. Numerous encapsulation routes have been developed and selected to achieve the product specifications at the effective and reproducible production as well as high throughput. One of the most promising methods is emulsion solvent removal technique which leads to a versatile incorporation of hydrophilic or hydrophobic compounds [113, 114]. Unlike spray drying, solvent removal technique can be used for highly temperature-sensitive compounds and better control the particle size. There are also no phase separation-inducing agents needed which may be left in the final products as coacervation method [115]. More fundamental details on these processes will be introduced in the next part. A high encapsulation efficiency and low solvent residual content can be achieved by optimizing the encapsulation conditions and formulations.

Polymeric systems are widely employed as carriers due to their biodegradability or biocompatibility. Biodegradable polymers can be gradually degraded into non-toxic small molecules and adsorbed *in vivo* and simultaneously the compound contained is gradually released. In the production of polymeric particles by encapsulation processes, poly(lactic acid) (PLA) is the most commonly used by far owing to its excellent

biocompatibility. PLA has been studied as a controlled release carrier for various drugs since 1970s [116].

Many types of hydrophobic compounds have been formulated into PLA by solvent removal technique. As we have described in the previous chapter, single emulsion can be used. A hydrophobic compound or drug is first dispersed or dissolved in an organic solvent in which PLA is also dissolved. The organic phase is then emulsified into an aqueous phase to form the oil-in-water (O/W) emulsion droplets. The solvent in the emulsion is diffused out and droplets are hardened to solid particles loaded with the targeted compound. However, this method is applicable only to hydrophobic compounds since hydrophilic ones may not be dissolved in the organic solvent.

Alternative methods, such as double emulsion (W/O/W), water-in-oil emulsion (W/O), and solid-in-oil-in-water (S/O/W), have been attempted to incorporate hydrophilic compounds within polymer matrix [117, 118]. Double emulsion method usually requires tedious preparation procedures, rigid control of temperature and viscosity, and easily introduces the third components into the final products. The remaining of organic solvent in the final particles from W/O emulsion is a big problem in terms of safety and environment issues. In the protein encapsulation by S/O/W emulsion, it's difficult to well disperse solid protein nano-/micro-particles in the organic solvent, which greatly limits its applications.

Therefore, there is a need to develop the encapsulation of either hydrophobic or hydrophilic compounds in a simple and effective way. Many studies based on the emulsion solvent removal technique have different modifications and features. However, they included either troublesome preparation procedures or extra additives and solvents

which are disadvantageous in the large-scale production. In addition, these processes are usually suitable for encapsulating one type of compounds, either hydrophobic or hydrophilic, and limited by the selection of polymeric materials and solvents.

In this study, we extend the applications of our controllable emulsion diffusion method to the area of encapsulation. Previous work has shown that our single emulsion method can not only produce O/W type emulsion but also *in situ* dynamic W/O/W type emulsion in seconds which has been mentioned to be suitable for encapsulating hydrophilic compounds. Two hydrophilic materials were tested, nisin which is a small peptide and magnetic nanoparticles (NPs) which are in the size less than 10 nm. Changes in the morphology and structure of the composite particles were observed. Colloidal properties, such as particle size and shape, were also controlled. In addition, the encapsulated content was measured at different operation conditions.

3.2 BACKGROUNDS

Encapsulation is usually referred to a technology of incorporating the active agent or core material surrounded by a shell or embedded in a matrix which can isolate the encapsulated materials from the environment and release them at a controlled rate [119] (see Figure 3.1). In the microencapsulation, different methods and compositions result in either microcapsules or microspheres. Various encapsulation processes have been developed for diverse needs and core materials. They are generally based on physical, chemical or combine phenomena. We list some representative techniques commonly used in the encapsulation production.

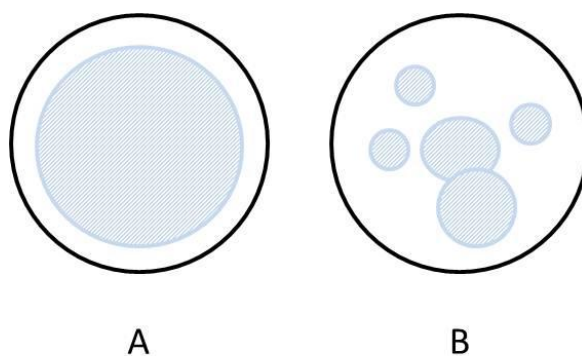


Figure 3. 1 Morphology of microparticles: A) reservoir system; B) matrix system. (Redrawn with permission from Ghosh [120])

3.2.1 Emulsion solvent removal technique

The basic procedures are similar to emulsion processing which has been described in the previous chapter. Hydrophobic compounds have been encapsulated primarily by O/W single emulsion process. The solvent in the emulsion can be removed by evaporation at elevated temperatures or extraction in the plenty of water. This method is not applicable for hydrophilic compounds as they may diffuse out into the aqueous phase, leading to a great loss.

Modifications have been attempted to overcome this defect. Kobayashi et al. have introduced a method to produce microspheres containing water-soluble medicament from O/W emulsions [121]. A solid dispersion was formed by dissolving a water-soluble medicament and a biodegradable polymer in one or two solvents which both can dissolve and following by solvent removal. The solid dispersion was further dissolved in an organic solvent which was emulsified to give O/W emulsions and then removed to form encapsulated microspheres. O/O emulsion has also been successfully applied to encapsulate proteins in the polymer matrix with good stability. Water-miscible organic

solvent, acetonitrile, was employed to dissolve both bovine serum albumin (BSA), PLA, and PEG, while cotton oil was the continuous phase to form the O/O emulsion [122].

Double emulsion has been well known to encapsulate hydrophilic compounds with high encapsulation efficiency [123]. Therefore, this system has been widely used for protein and peptide delivery.

The properties of composite particles are greatly relevant to the polymer (molecular weight, concentration, solubility), formulation (phase volume ratio, loading ratio, solution viscosity), the emulsifier (concentration), processing conditions (temperature, mixing speed, solvent removal rate), etc [124]. The water-immiscible organic solvents may be one or a mixture of two or more solvent, for example, ethyl acetate, methylene chloride, chloroform, carbon tetrachloride, dichloromethane, methyl ethyl ketone, etc. However, the use of solvents, such as methylene chloride and chloroform, is not recommended in the concern of safety challenges and toxicity. Therefore, considering the environmental and human safety issues, ethyl acetate is selected as a dispersing solvent in this study. The biodegradable polymer, which is used as the carrier for encapsulated compounds, may be any polymer which does not show any biological activities and are easily decomposed in the human body. Suitable examples of the biodegradable polymer include poly(lactic acid) (PLA), poly(glycolic acid) (PGA), poly(hydroxybutyric acid) (PHB), poly(caprolactone) (PCL), poly(valerolactone) (PVL), poly(acrylic acid) (PAA), poly(methylmethacrylate) (PMMA), poly(lactide-co-glycolide) (PLGA), or a mixture.

3.2.2 Phase separation and coacervation

Coacervation technique was introduced and investigated by Bungenberg de Jong and Kruyt in 1929 [125]. A homogeneous solution of the core material and the coating material which is usually liquid polymer is formed. The coating is then deposited on the core material, followed by further hardening (see Figure 3.2). No matter the simple or complex coacervation process, they both involve the phase separation of a homogeneous polymer solution by a coacervating agent. The common coacervating agents include silicone oil, light liquid paraffin, and polybutadiene. pH, temperature, the adding rate of the desolvation agent, and the crosslinking agent are important parameters to the characteristics of final microspheres [126]. Hydrophilic coatings such as gelatin and gum acacia can also be used to encapsulate hydrophobic compounds [127]. External environments can be controlled to release the contents. However, not only the introducing of extra solvents, this method also can easily obtain large aggregates before complete phase separation.

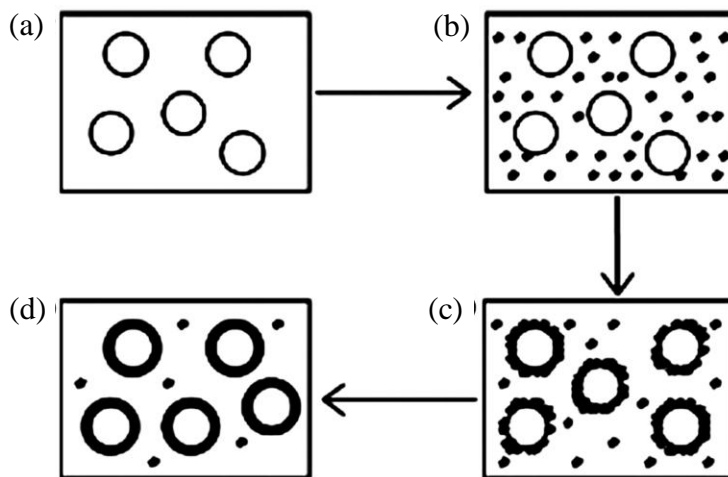


Figure 3. 2 Schematic representation of the coacervation process. a) Core materials are dispersed in the solution of coating materials; b) phase separation of coacervate from solution; c) deposition of coacervate on the core materials; d) coalescence of coacervate to form continuous shell. (Reproduced with permission from [120])

The method of preparing microparticles based on interfacial phase separation has also been developed. Yeo *et al.* reported this technique to produce reservoir-type microcapsules which contain the biodegradable polymer membrane and hydrophilic core [128]. When the water-insoluble polymer droplets were in contact with the aqueous droplets, the polymer film would be formed at the interface. The encapsulated drug could maintain its stability and avoid mechanical stress during fabrication.

3.2.3 Spray drying

Spray drying is one of the most widely used processes in industry due to its good reproducibility, easy control and scale up, and less dependent on the drug and polymer solubility [129]. The core material is dissolved or dispersed in the polymer solution and the resulting solution is sprayed into heated air forming fine droplets, called atomization. The shell material solidifies on the surface of the core material during solvent evaporation. Several factors, properties of the shell materials, the core materials, and the infeed emulsion, drying parameters greatly influence the final encapsulation efficiency [130]. Many anticancer drugs that are toxic, unstable, easily degraded have been encapsulated in the biodegradable polymers, such as PLA and PLGA [131]. Some of the products are stick to the inner wall of equipment causing the production loss. In addition, large aggregates are also frequently found.

3.2.4 Introduction of Nisin

Nisin is one of the small protein antibiotics that contain dehydro residues and dehydrobutryne and thioether cross-linkages. It is effective against gram-positive

bacteria such as *Listeria monocytogenes* and also consumable by humans, allowing its wide applications in the food industry. One proposed mechanism is that as nisin is a cationic antimicrobial, it can bind negatively charged bacteria membrane by electrostatic interactions [132]. Discrete sizes of pores are generated when nisin inserts into the membrane, which leads to the efflux of ions, amino acids, and cellular ATP. Nisin is a low molecular weight peptide and contains 34 amino acids (Figure 3.3). The solubility of nisin is pH-dependent, showing higher solubility at lower pH. It is stable under heat at the dried powder form [133]. When in the solution, nisin can keep the heat stability at around pH 3.0-3.5 after heating at 115 °C and 20 min.

Excessive nisin is required to guarantee the effective inhibition of pathogen growth. Nisin activity can be reduced by compounds in food, such as Ca^{2+} , Mg^{2+} , sodium metabisulfite, or during food consumption by enzymes [134]. Therefore, a delivery system has to be built to improve its antimicrobial activity and long term efficacy. Nisin has been embedded in the packaging materials such as PLA for prolonging the biological activity [135]. However, the film casting is difficult and protein can be inactivated. Modification has also been done on nisin by attaching PEG on the surface [136]. It also altered the peptide structural properties. Efforts have been put on nisin-loaded polymeric nano-/micro-particles due to their stability and easy formulations [137]. However, low peptide loading and fragile protein structure are still the limited problems.

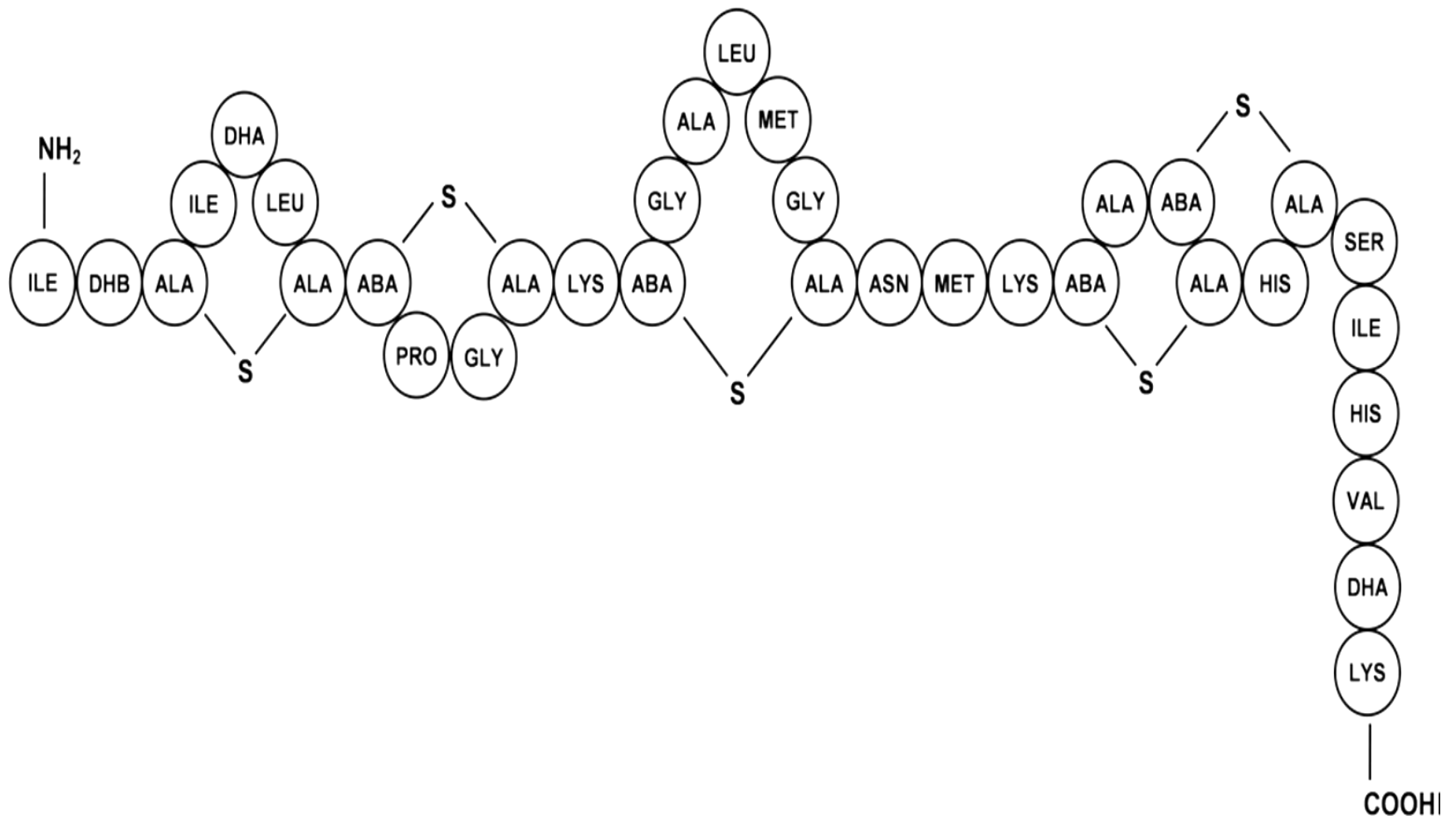


Figure 3. 3 Primary structure of nisin. (Reproduced with permission from [138])

3.2.5 Magnetic NPs

Magnetic NPs have been extensively used in the biomedical field, such as drug targeting, biosensing applications, cell tracking, magnetic resonance imaging (MRI), etc [139-141]. There are different types of magnetic NPs depending on different magnetic characteristics. Iron oxide NPs are the most studied due to their high magnetic susceptibility, stability, and biocompatibility. Magnetic microspheres consist of superparamagnetic cores and the surrounded polymer shell, usually in the sizes of nanometers to micrometers. The polymer coatings can be produced by phase separation, emulsion solvent evaporation, emulsion polymerization, and swelling and penetration [140, 142-144]. These magnetic carriers need to be in the controllable size, carry sufficient loadings of active ingredients, and have minimal toxicity and immunological response [145]. A lot of attention has been given to the incorporation of magnetic NPs in a high extent.

3.3 MATERIAL AND METHODS

3.3.1 Material

Nisin Z powder was provided by Metna Corporation (activity >38,000 IU/mg). Poly(D,L-lactic acid) (PLA, $M_w=51,000$ Da, $T_g= 52.5$ °C) was purchased from LakeShore Biomaterials (California, USA). The poloxamer Pluronic F68 (PF68) (average $M_w=8,400$ Da) was obtained from Sigma Aldrich. It is a low foaming and non-ionic surfactant consisting of block polymers in which central polyoxypropylene oxide (PPO) flanked by two polyoxyethylene oxide (PEO) tails. Ethyl acetate (EtOAc) and glycerol were from J.T. BAKER and used as received. All the chemicals used were analytical

grade without further purification. All aqueous solutions in the processes were prepared with deionized (DI) water supplied by a Barnstead nanopure Diamond-UV purification unit equipped with a UV source and final 0.2 μ m filter at 18.2 M Ω purity.

3.3.2 Preparation of hydrophilic magnetic NPs

Detailed description of preparation of aqueous suspension of magnetic nanoparticles is available elsewhere [146, 147]. Fe³⁺ and Fe²⁺ ions are mixed in the molar ratio of 2:1. 5 ml of ammonium hydroxide is added drop-wise. The mixture is heated to 800C under nitrogen purging for 30 mins. 1 ml of citric acid (2.38 M) is added to the above mixture and the temperature is raised to 950C. Heating is continued for additional 90 minutes. The colloidal solution is then separated by centrifugation (9000 rpm) and washed thrice with a mixture of acetone and water to get a stable dispersion. The nanoparticles are then dispersed in 30 ml of deionized water and stored at room temperature.

3.3.3 PLA/nisin particles production

EtOAc and water were mutually saturated and used as dispersed organic solvent (oil phase) and dispersion aqueous medium (water phase), respectively. PLA solutions were prepared by dissolving PLA into 6 mL water-saturated EtOAc (O). 18 mL EtOAc-saturated aqueous solution (W) was added with PF68 and then mixed with different volume fractions of glycerol to adjust its viscosity. Nisin powders were added into the aqueous solution to reach different concentrations. Well-mixed aqueous solutions were centrifuged at 12,000 rpm for 10 min to remove the insoluble materials before emulsification. A modified high shear Taylor-Couette type T K Filmics nanomixer

(Model 40-40) from the PRIMIX Corporation, Japan was used for experiments to generate the uniform emulsion samples. Both oil phase and water phase solutions were added in the chamber of nanomixer. The oil phase solution was emulsified with the aqueous continuous solution at the mixing speed rate of $12,500 \text{ s}^{-1}$ and temperature of $60 \text{ }^{\circ}\text{C}$ in 1 min to give the emulsions. The emulsion solution was then added to plenty of pure DI water and stirred in a beaker to induce the diffusion of EtOAc from oil phase. After overnight diffusion, the colloidal dispersion was thus transferred to glass vial and stored at $4 \text{ }^{\circ}\text{C}$ for future use.

3.3.4 PLA/magnetic NPs preparation

The same oil and water phase solutions were prepared. Magnetite solution was added into the aqueous solution at the volume ratio of 1 to 50. The same T K Filmics nanomixer (Model 40-40) was used for experiments to generate the uniform emulsion samples. The preparation procedures are the same as those in preparing PLA/nisin particles.

3.3.5 Shear and temperature resistance test on the preformed nisin solution

Nisin solution was obtained by suspending nisin powder in 0.01 N HCl solution (pH=2) to achieve theoretical nisin activity of 400 IU/mL. The nisin suspension was centrifuged at 8500 rpm for 15 min at $4 \text{ }^{\circ}\text{C}$ and the supernatant was recovered. Prepared nisin solution was stored at $4 \text{ }^{\circ}\text{C}$ as a stock solution until use.

The modified high shear Taylor-Couette type nanomixer was used for experiments to generate the uniform high shear stress on samples. Nisin solutions were mixed with speed rates of 20, 30, and 40 m/s at room T ($\sim 25 \text{ }^{\circ}\text{C}$) respectively. Higher

mixing temperature of ~60 °C was also applied on sample solutions mixed at 20 and 40 m/s to evaluate the synergistic effect of shear force and temperature on the nisin activity. Volume of nisin solution used in each trial was 20 mL. Nisin activity test was carried out by Dr. Liu's group in the Department of Biosystem Engineering at Michigan State University. Sample solutions were used as fresh.

3.3.6 Nisin encapsulation quantification

Reverse-phase HPLC was applied to quantify the nisin concentration in the solutions. The amount of the encapsulated nisin in the final particles was determined by the change of nisin amount in the solution before and after the emulsion diffusion process.

3.3.7 Zeta potential analysis for particle surface charge

Zeta potential was measured using 90Plus Brookhaven Instrument. PLA particles were added to 1 mM KCl solution. Zeta potential measured is an average of 10 runs for each sample. The results are shown as means \pm standard deviation.

3.3.8 Particle morphology characterization

Colloidal dispersion after dialysis was dropped on a glass slide and placed on a model FluoView confocal laser scanning microscope (CLSM). Images were made at 633 nm for confocal reflection and at 405/430-470 nm (ex./em.) for autofluorescence at two channels.

Scanning Electron Microscope (SEM) was used to estimate the mean particle size as well as coefficient of variation for particle size. SEM used for high resolution imaging was JEOL 6400 at Center for Advanced Microscopy in Michigan State University, at working distance of 8 mm and accelerating voltage of 6 KV. PLA particles were

collected onto 0.1 μ m filter membrane and washed by plenty of pure DI water under vacuum. Dried particles along with membrane were then covered with gold coating facilitating their conductivity under electron microscope.

Part of the colloidal dispersion was placed in a sealed dialysis membrane and gently stirred in the pure DI water at room temperature overnight. PLA particles were purified by allowing diffusion of glycerol and excess PF68 molecules through the selectively permeable membrane. Transmission electron microscopy (TEM) was done on polymeric composite particles using JEOL 2200FS 60 kV field emission TEM. Copper grids coated with carbon were used to support particles. Microtoming was applied to get a thin cross-sectional slice from the final particle sample for microscopic inspection.

3.4 RESULTS AND DISCUSSION

3.4.1 Preliminary tests on shear and temperature resistance of nisin

In the mixing process of emulsion-diffusion method, the fluid flow inevitably undergoes a breakdown by turbulent eddies. In addition, shear stress and cavitation produce a disruption of microorganisms. In order to study the effect of shear stress on nisin activity in our system, preliminary tests were necessary to ensure the acceptable preparation conditions for PLA/nisin particles. Nisin activities of control and prepared sample solutions were tested by our collaboration group. Data were provided by a collaborator, Zhiguo Liu in Biosystems and Agricultural Engineering at Michigan State University.

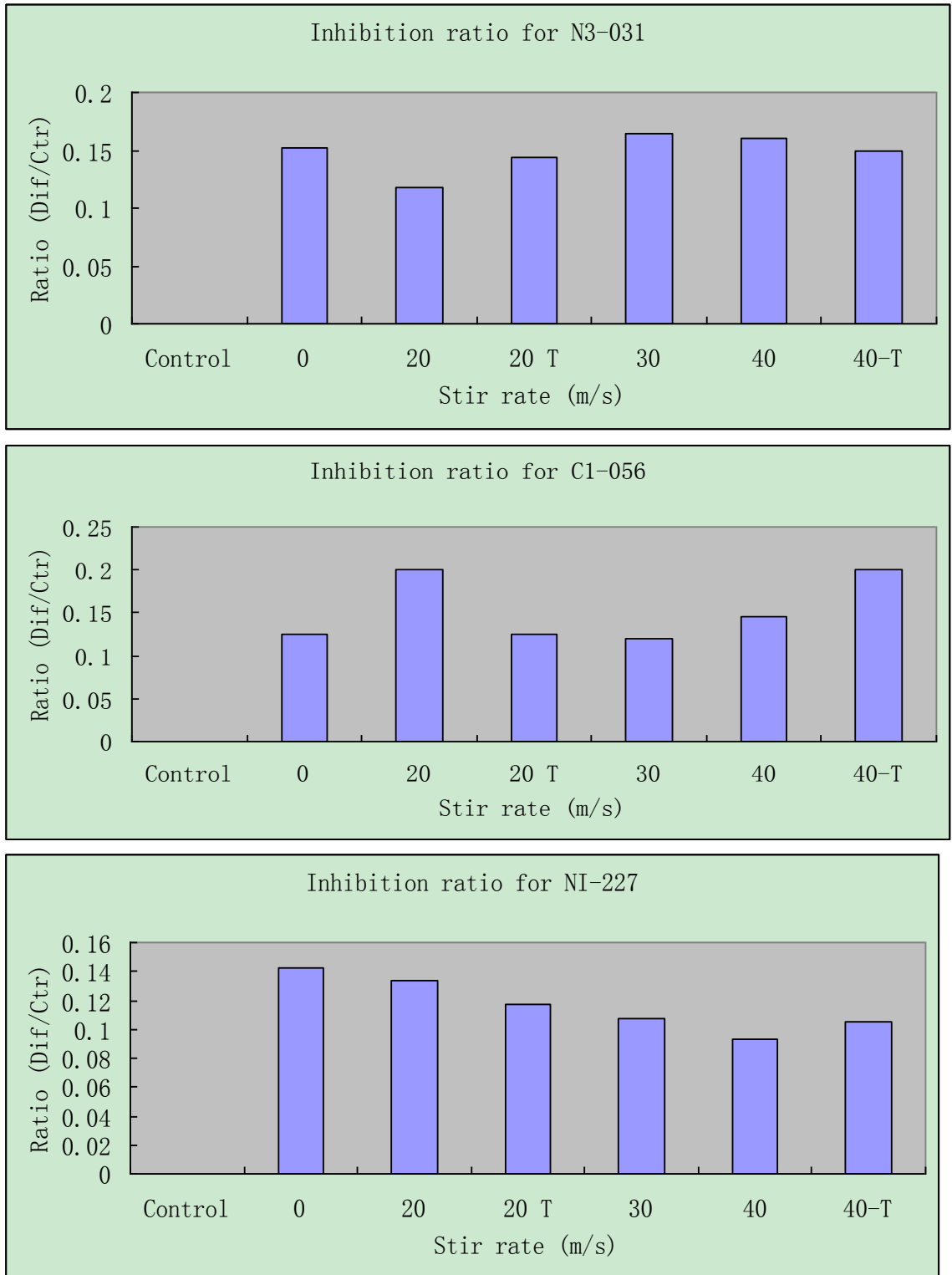
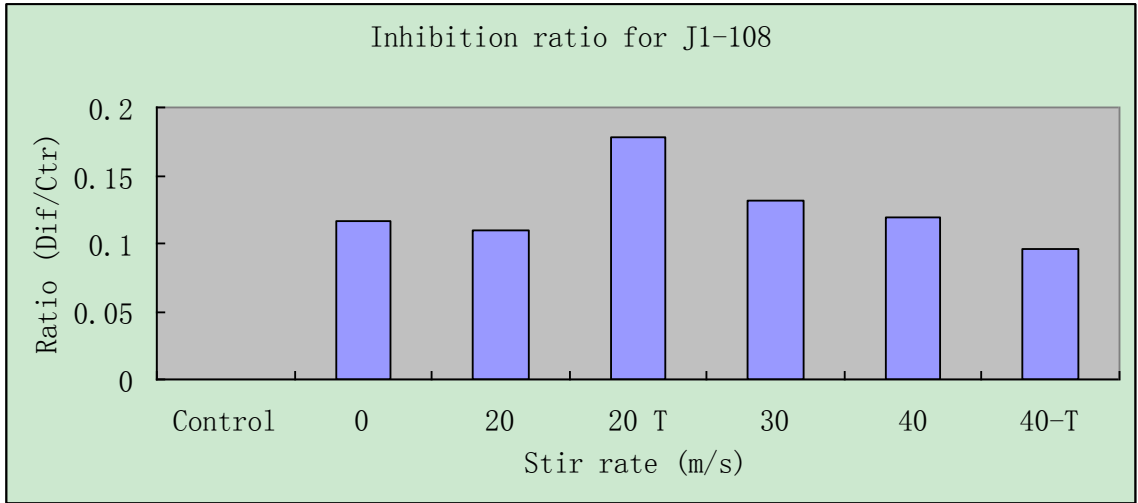


Figure 3. 4 Inhibition ratios of different sample nisin solutions for four subtypes of listeria monocytogenes. The inhibition ratio was defined as (OD630 reading difference from control group) / (OD630 reading of control group).

Figure 3.4 (cont'd)



Nisin activity was indicated by its inhibition capability on different bacteria. No significant change on the inhibition activity of nisin was observed in different sample solutions (shown in the Fig. 3.4). Shear stress and temperature shows little effect on the nisin activity, which allows us to further our research on the nisin encapsulation under certain mixing conditions.

3.4.2 Nisin distribution in the PLA particles

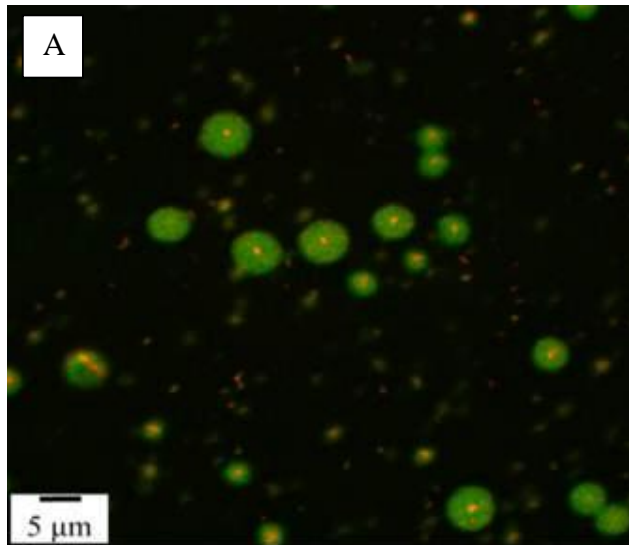
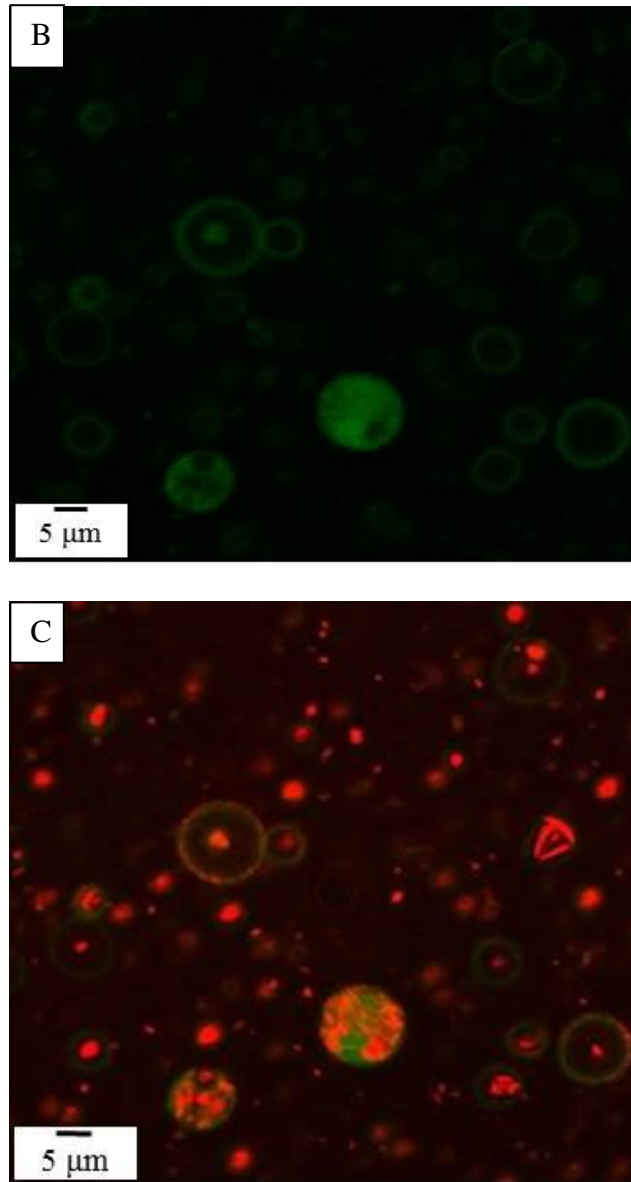


Figure 3. 5 CLSM images of composite particle surface and cross-sectional view.

Figure 3.5 (cont'd)



CLSM can be used to directly observe the distribution of nisin in the particles. In the Fig. 3.5, the red region correlated with PLA reflection and the green region correlated with peptides and proteins which is nisin used in the system. Figure 3.5A shows the nisin distribution on the outer surface of final particles. When applied z-series imaging, the nisin distribution within the particles could be observed (Fig. 3.5B and 3.5C). The green region in the Fig. 3.5C showing the nisin distribution inside the particles mostly

overlapped with the red region which represents the shell wall of hollow polymeric microspheres, indicating the successful encapsulation of nisin not only on the surface of polymeric composite particles but also within their shell walls.

3.4.3 Surface characterization of composite particles

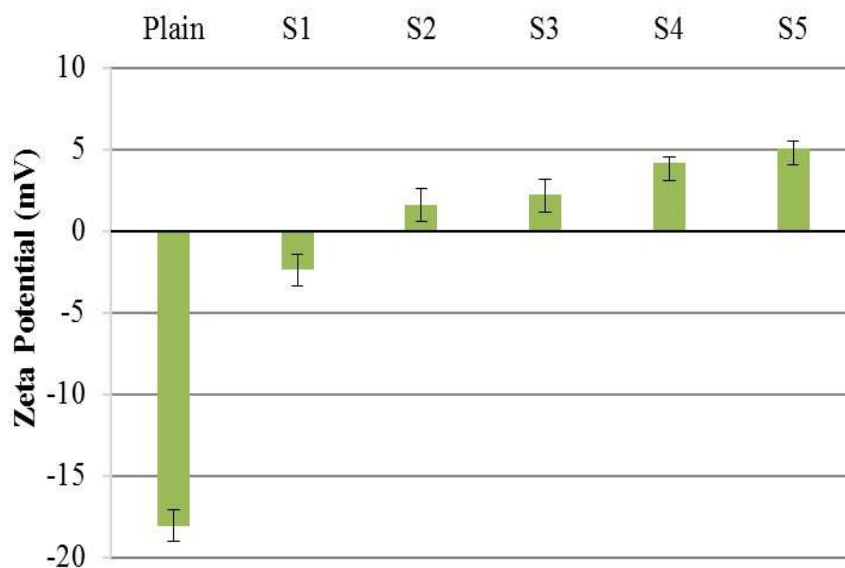


Figure 3. 6 Zeta potential of plain PLA and polymeric composite particles at different nisin loadings of 0.025 (S1), 0.075 (S2), 0.125 (S3), 0.175 (S4), and 0.225 (S5) mg/ml in the water phase solution.

Zeta potential analysis was performed to measure the surface charge of final particles prepared at different nisin loadings. Plain PLA particles have been well known to present negative charges on the surface. This is consistent with the zeta potential measured as -18 mV. And nisin is known to be a cationic peptide. The polymeric composite particles showed slightly positive charged properties on the surface which indicated that the negative surface charge of PLA particles was shielded in the presence of nisin. The surface charge increased with increasing nisin loadings confirming that there was nisin adsorbed on the surface of PLA carriers.

3.4.4 Morphological observation of composite particles

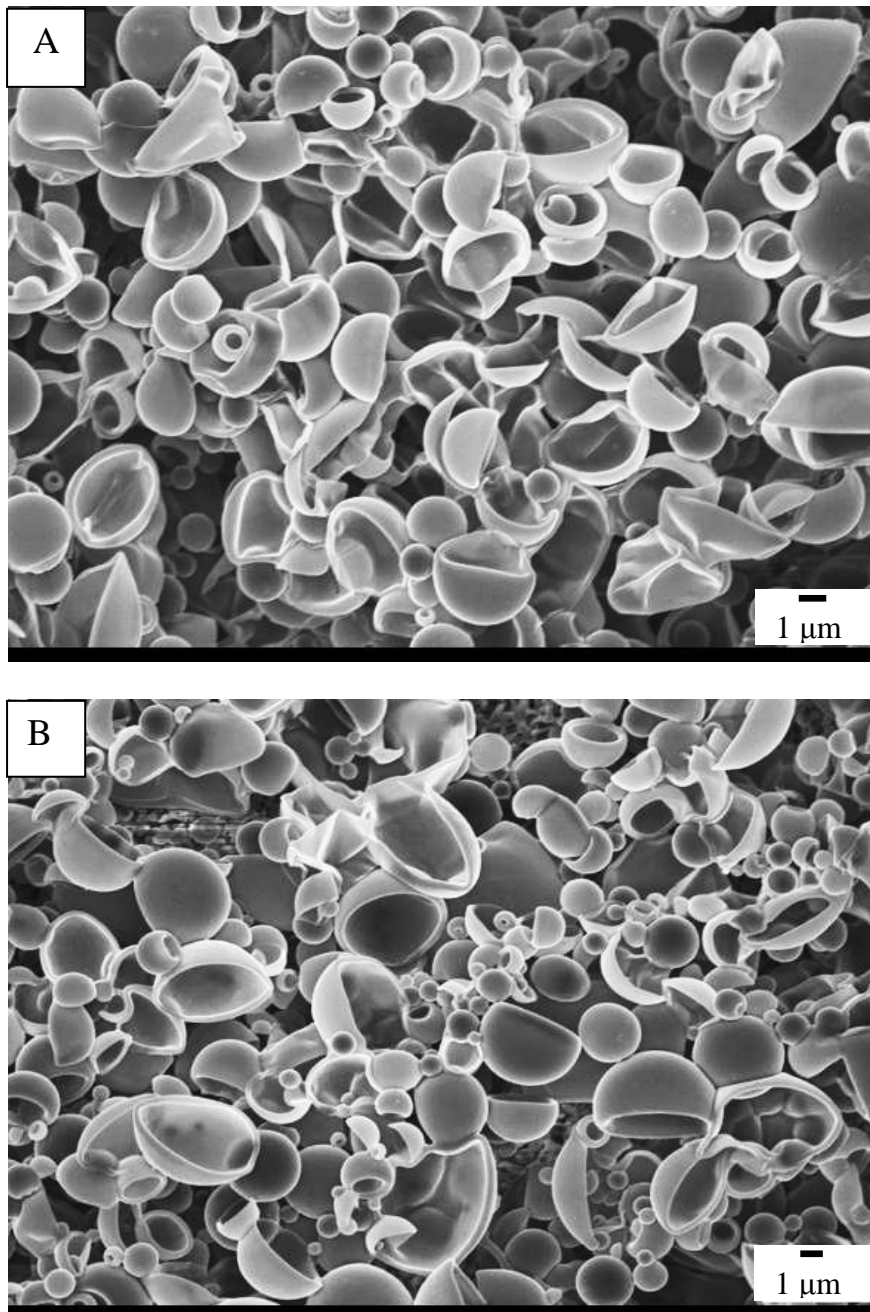
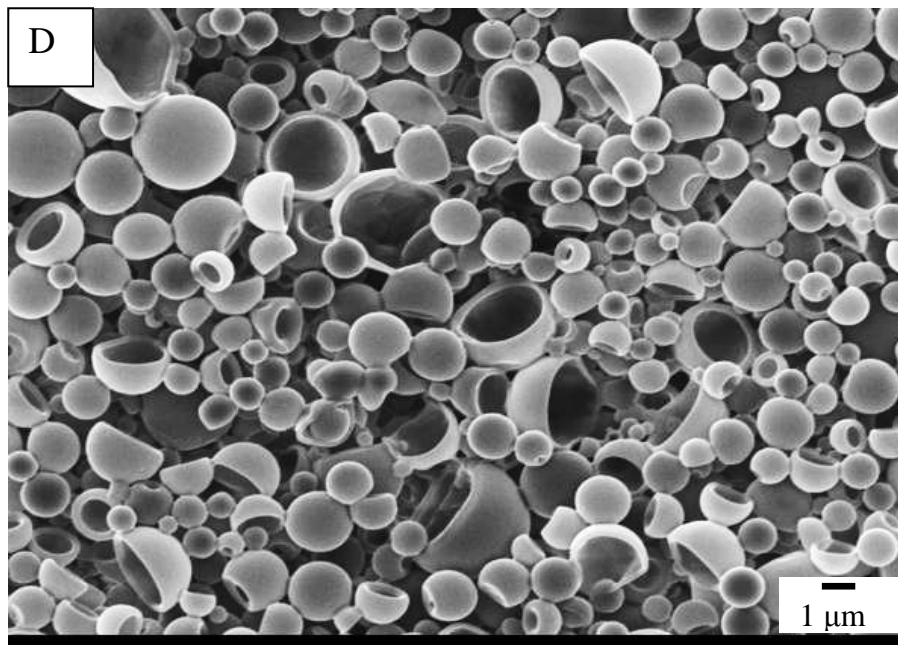
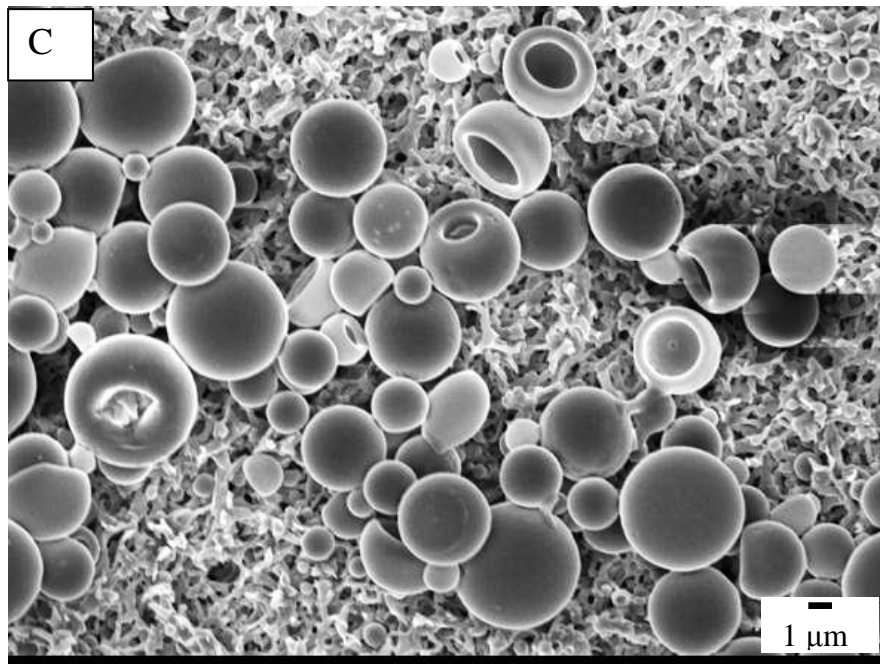


Figure 3. 7 SEM images of final polymeric composite particles with nisin loadings of 0.05 (A), 0.25 (B), 0.5 (C), 0.75 (D) mg/ml in the water phase solution.

Figure 3.7 (cont'd)



We can see that increasing nisin concentration in the water phase has little effect on the particle size and shape. The concept of dynamic control of particle production by our emulsion solvent removal technique is still applicable. The thickness of particle shell

wall was increased with increasing the nisin loading. Supported by previous data that indicated the existence of nisin in the polymeric composite particles, it may be due to the increase of nisin encapsulated within the polymer carriers that generated the thicker shell wall.

3.4.5 Quantification of nisin encapsulation

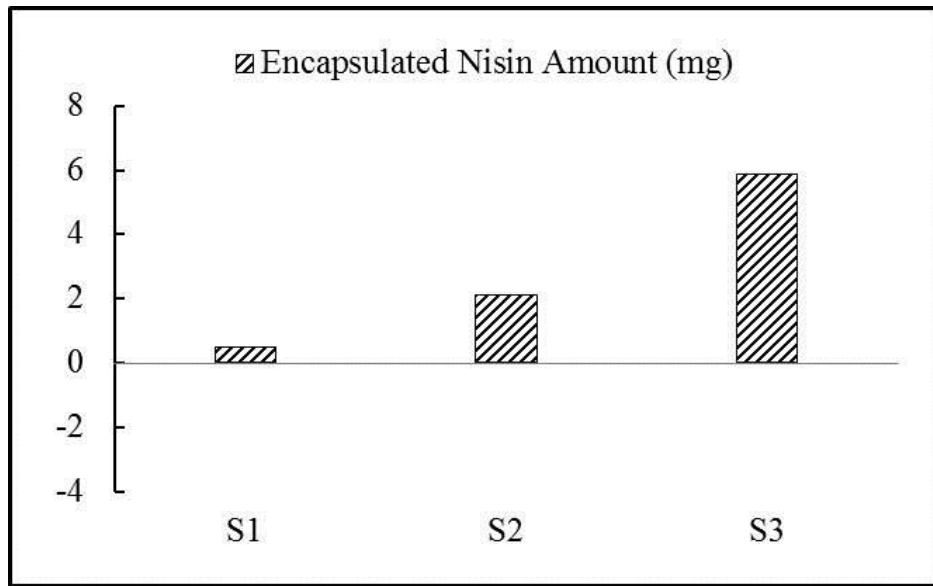


Figure 3. 8 Encapsulated nisin amount of different polymeric composite particles. S1, S2, and S3 represent the particles with nisin loadings of 1.5, 2.0, 3.0 mg/ml.

The amount of nisin encapsulated in the polymeric particles is increased with increasing the nisin loadings in the water phase solution (as shown in the Fig. 3.8). This indicates the possibility of controlling the encapsulation amount by adjusting the formulations. Since all the remaining nisin in the aqueous solution can be recollected and reused, the waste of nisin after the preparation can be avoided.

3.4.6 Dynamic control of nisin encapsulation

The emulsion solvent removal process in our system has been tested as a dynamically reversible control on the particle size and shape, for example solid nanospheres and hollow microspheres, by controlling the key processing parameters. This reversible manipulation can also be used in the encapsulation. The more alternations of temperatures the emulsification process took, the more nisin amount was encapsulated. Therefore, the encapsulation amount as well as particle size and shape can be easily controlled by this process which shows superior advantages of easy operation and scale-up production.

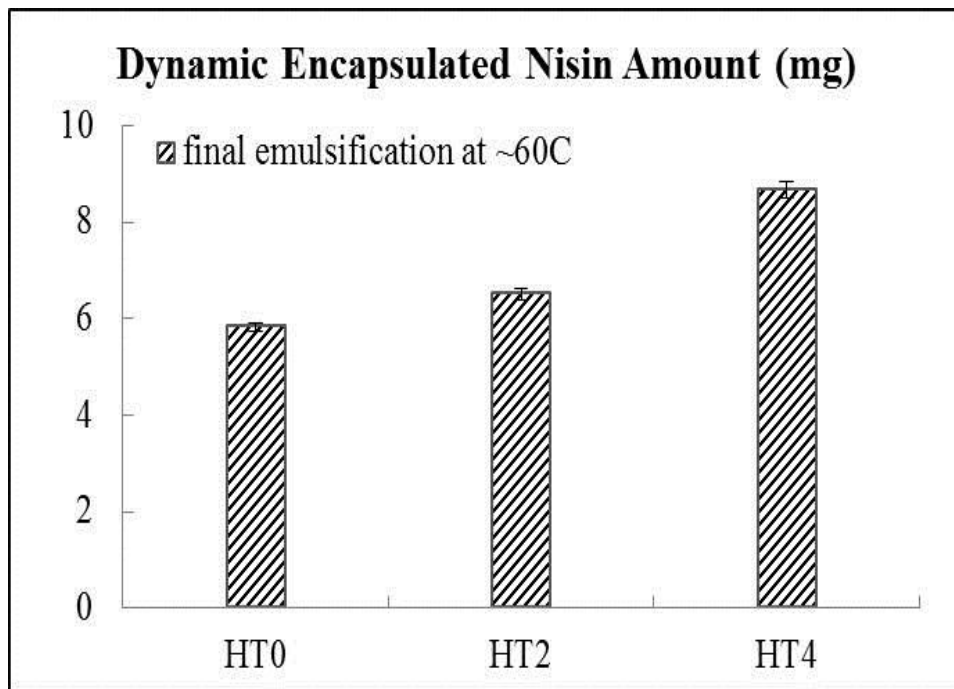
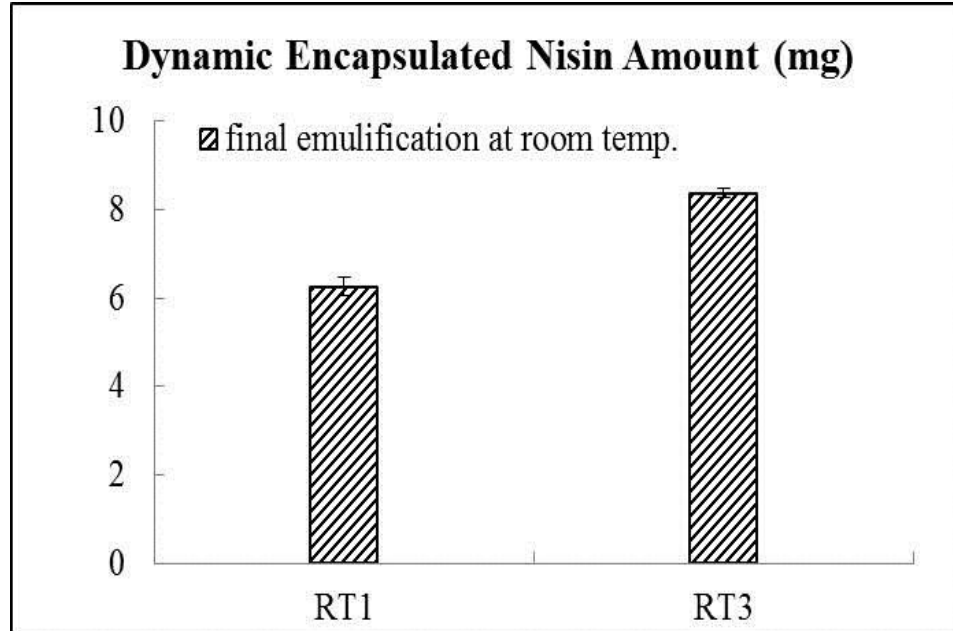


Figure 3. 9 The effect of alternating emulsification temperatures between ~60 °C and room temperature (25 °C) on the encapsulated nisin amount. HT0, HT2, and HT4 represent that the emulsification process was performed by alternating temperatures 0 time, 2 times, and 4 times and the ending emulsification temperatures were at ~60 °C. RT1 and RT3 represent that the emulsification was performed by alternating temperatures 1 time and 3 times, and the ending emulsification temperatures were at room temperature.

Figure 3.9 (cont'd)



3.4.7 Observations of magnetic NPs encapsulation

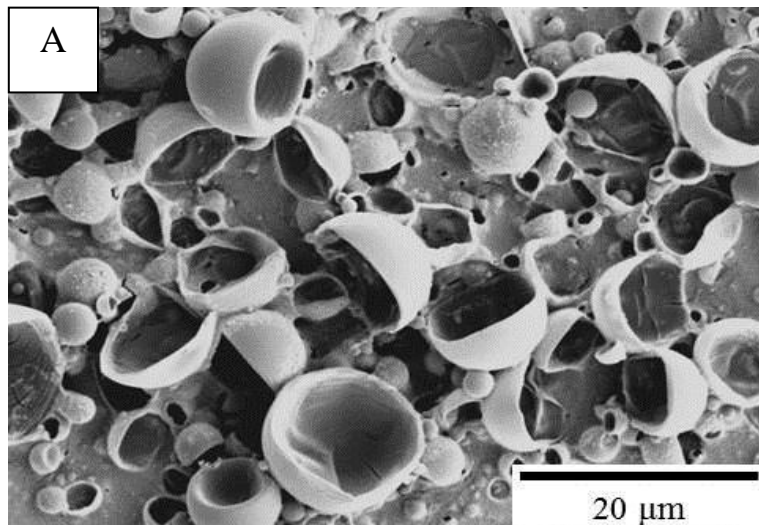
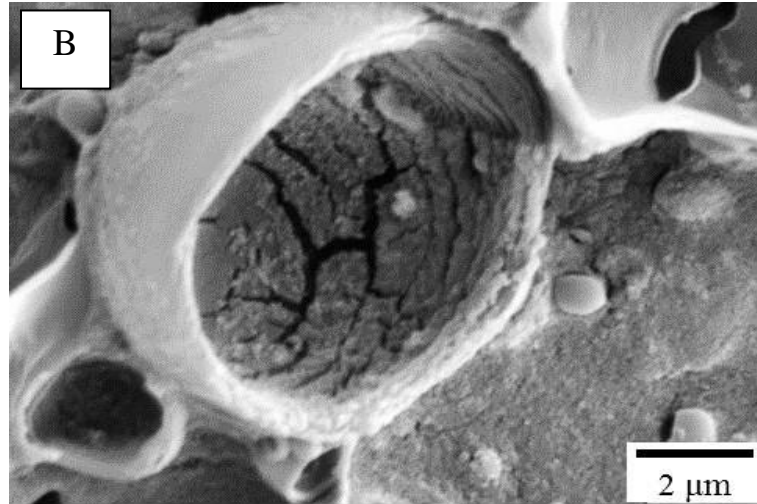


Figure 3. 10 SEM images of PLA/magnetic NPs composite particles at low (A) and high (B) magnification.

Figure 3.10 (cont'd)



These final particles can be collected by the magnet indicating the successful encapsulation of magnetite NPs within polymer carriers. SEM images have shown that the polymeric composite particles kept the hollow structure which suggests that the manipulation of our emulsion solvent removal technique is still applicable for nanoparticle encapsulation system (Fig. 3.10A). High SEM magnification revealed the surface details of individual particles. The shell wall turned to be rough and large amount of nanoparticles were found to be adsorbed or embedded on the inner or outer surface of particles (Fig. 3.10B).

In order to further investigate the distribution of magnetite nanoparticles, TEM was used for observing the sectional view of single composite particle. Consistent with the observation of SEM, hollow structure was clearly seen (Fig. 3.11A). When high magnification was focused on part of the particle shell wall, magnetite NPs were found greatly cumulated within it (Fig. 3.11B). This confirms that magnetite NPs have been

encapsulated in the composite particles and our process is suitable for encapsulating NPs in certain size range.

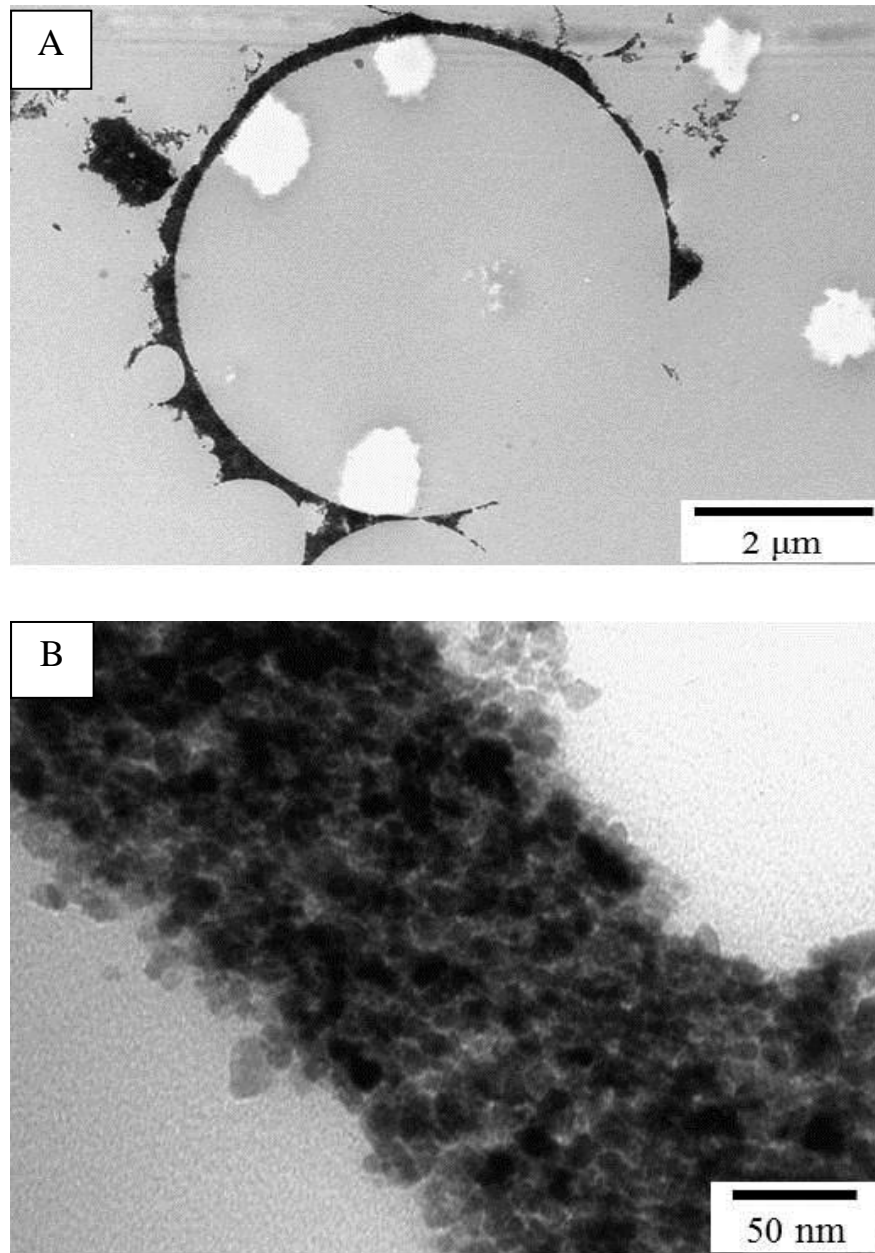


Figure 3. 11 TEM images of PLA/magnetic NPs composite particles at the cross-sectional view. A) a representative hollow structure composite particle; B) part of particle shell wall at high magnification.

3.5 CONCLUSION

The present study shows that our emulsion diffusion method can successfully encapsulate hydrophilic compounds, including small peptides and nanoparticles, into the hydrophobic polymer matrix. Structural studies have indicated that hydrophilic compounds are mostly incorporated in the polymer shell wall. The dynamic control on the size and shape of polymeric composite particles is still applicable. Since the emulsification is performed in a short time and no extra chemicals and steps need to be added, this method can be easily controlled and scaled up, providing a promising means for encapsulating hydrophilic materials of interest with different size and shape for various applications.

Chapter 4

Fractionation of Corn Stover by a Novel Nanoshear Hybrid Alkaline Pretreatment

4.1 INTRODUCTION

The main worldwide energy resources and products are derived from fossil fuels, oil, and natural gas. However, growing concerns in the environmental, renewable, and economic issues have shifted the future energy dependence to other alternative energy, such as biomass, wind, solar, nuclear, etc [148]. The large energy demand is gradually fulfilled by ethanol, biodiesel, and other biofuel products. Displacement of imported petroleum with renewable raw materials and the build-up of bio-based industry are proposed as the strategic goals accepted in the biorefinery development [149]. They can be varied depending on the type of raw materials, the available technologies, the scale-up level of equipment, and the market demands [150-152]. The move toward bio-based economies has been greatly developed in recent years. The efficient use of renewable materials not only meets both resource and energy needs, but make bio-based processes more economically competitive. The integrated concept of biorefinery with the requirement of full utilization of biomass has been widely accepted, in which different fractions of biomass are converted to a wide range of value added products such as fuels, power, materials, and chemicals by series of sustainable treatments and processes [149, 153]. A biorefinery integrating biofuels and their useful by-products offers a high return on investment, which promoted lots of efforts to incorporate coproducts into it, e.g. pulping process.

Lignocellulose is the most abundant renewable biomass produced from photosynthesis, including wood, agricultural residues, and paper wastes. These biomass materials are composite polymer materials mostly composed of cellulose, hemicellulose, and lignin, primary fractionation of which into their major components could allow the

production of cellulose and its derivatives or potentially generating monomeric sugars for further high value added products. Processing these materials to biofuels is more technically challenging than that of corn starch and sugarcane, due to their natural recalcitrance to enzymes or microbes [154, 155]. Pretreatment is required to facilitate the alteration of biomass structure before the first step of conversion, which significantly increases the accessibility of cellulose and hemicellulose to hydrolytic materials and efficient conversion of cellulosic substrates, thus the production of bioenergy and biomaterials [156]. In addition, effective pretreatment technologies also offer the great potential to minimize the degradation polysaccharide products, limit the inhibitors, and lower the operating energy and costs [154, 157]. Despite burned as energy sources, the unconverted lignin fraction is attracting growing interest for value-added applications, such as binder additives, surfactants and aromatic chemicals [158-160]. Therefore, to achieve a complete and profitable utilization of lignocellulose, the efficient and cost-effective fractionation and conversion of constitutive components is a key challenge in the biorefinery system.

In this study, we applied a novel nanoshear hybrid alkaline pretreatment method with the aid of a modified Taylor-Couette reactor to accelerate the breakup of large polymeric structures in the lignocellulosic biomass, corn stover, down to nanoscale biocomposites. This easy set-up process synergizes alkaline pretreatment with high shear flow to remove hemicellulose and lignin in a mild process temperature and short-time operating, leaving a high cellulose fraction in the residues.

4.2 BACKGROUNDS

4.2.1 Lignocellulosic biomass

Lignocellulosic biomass is the natural renewable resource. Besides the major components of polysaccharides and lignin, it also contains a small amount of pectin, protein, extractives, and ash [161]. The composition can be different from woody and non-woody feedstocks. For example, hardwood has higher cellulose content and wheat straw has more hemicellulose. The lignin content in softwoods is usually higher than that in hardwoods, which makes the softwood more challenging in the pulping process.

4.2.1.1 Cellulose

Cellulose, major structural polysaccharide in the cell wall, is a linear polymer chain formed by bonding the anhydroglucose units via β -(1,4)-glycosidic linkages (Fig. 4.1). It is composed of chains of six carbon sugars in the unit form of $(C_6H_{10}O_5)_n$, where n is the number of repeating glucose units also called the degree of polymerization (DP). These chains partially organized in parallel forming crystalline structure. Element fibrils, which are long chain polymers consists of D-glucofuranose monomers, form larger microfibrils with DPs of approximately 250. Hydrogen bonding and van der Waals forces are usually considered as the main strong linkages among long cellulose chains. Cellulose is present in both crystalline and amorphous form, among which the crystalline structure is the majority. Crystalline cellulose is more susceptible to enzymatic degradation than the amorphous one. Despite insoluble either in water or dilute acid solutions, cellulose can be swollen and partially dissolved by alkaline solutions.

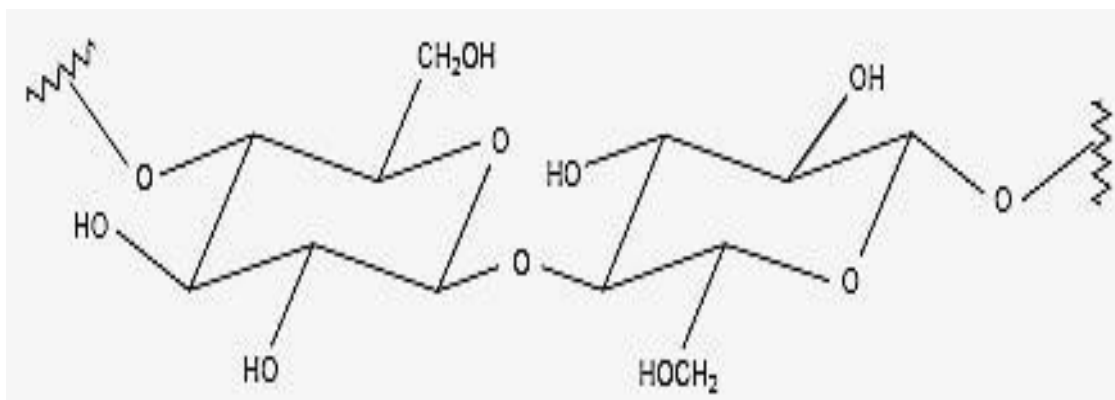


Figure 4. 1 Structure of repeating unit of a cellulose chain in the lignocellulosic biomass.

4.2.1.2 Hemicellulose

Hemicellulose is a collective term representing primarily xylan and other polysaccharides such as mannans, galactans, glucose, and some acids. Hemicellulose serves as a linking between cellulose fibers by hydrogen bonding and direct linkages. The backbone of hemicellulose is homopolymer or heteropolymer with short branches linked by β -(1,4)-glycosidic or β -(1,3)-glycosidic bonds (Fig. 4.2). As highly branched together, it is lack of crystalline structure. Due to its loose structure, hemicellulose is easily hydrolyzed and degraded. It is known that hemicellulose has a lower hydrolysis temperature than that of cellulose[162]. The addition of acid can increase the solubility of hemicellulose in water [156].

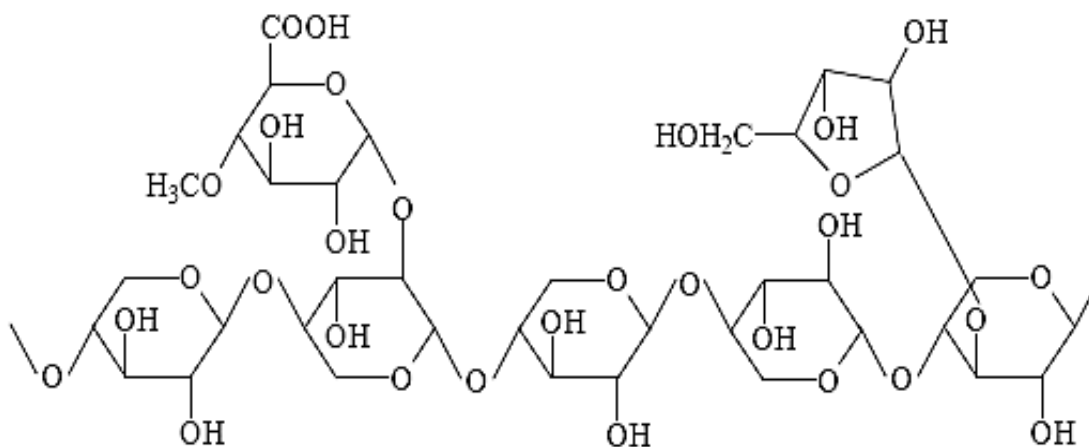


Figure 4. 2 Structure of partial xylans from softwood chain.

4.2.1.3 Lignin

Lignin is a cross-linked macromolecule with amorphous arrangement of phenylpropane units (Fig. 4.3). It serves to bind the cellulose fibers and is resistant to compress and bend, being considered as a formidable barrier against enzymatic attack [163]. Lignin is the most recalcitrant component among the cell wall biopolymers. The stable linkages between lignin and carbohydrates are considered as one of the separation obstacles of biomass components [164]. Donohoe et al. [165] have observed the decompartmentalization and relocation of lignin within and out of the cell wall due to its thermal softening property.

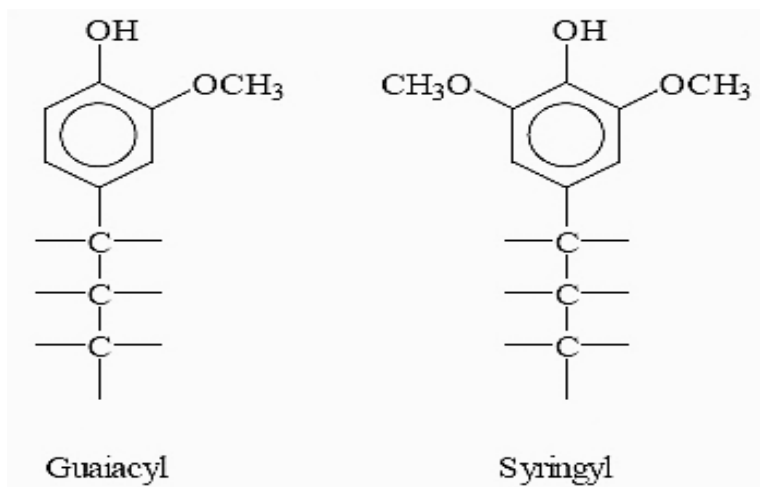


Figure 4. 3 Structure of building units of lignin in the lignocellulosic biomass.

4.2.2 Pretreatment of lignocellulosic biomass

Pretreatment processes are developed to remove lignin and hemicellulose, to disrupt the crystallinity of cellulose, hence improve the digestibility of cellulose and the yield of sugars from lignocellulosic materials [166-168] (Fig. 4.4). Pretreatment can be carried out based on physical, physicochemical, chemical, biological, electrical phenomena, or a combination of them [169-171]. Some basic and representative pretreatment methods have been introduced here.

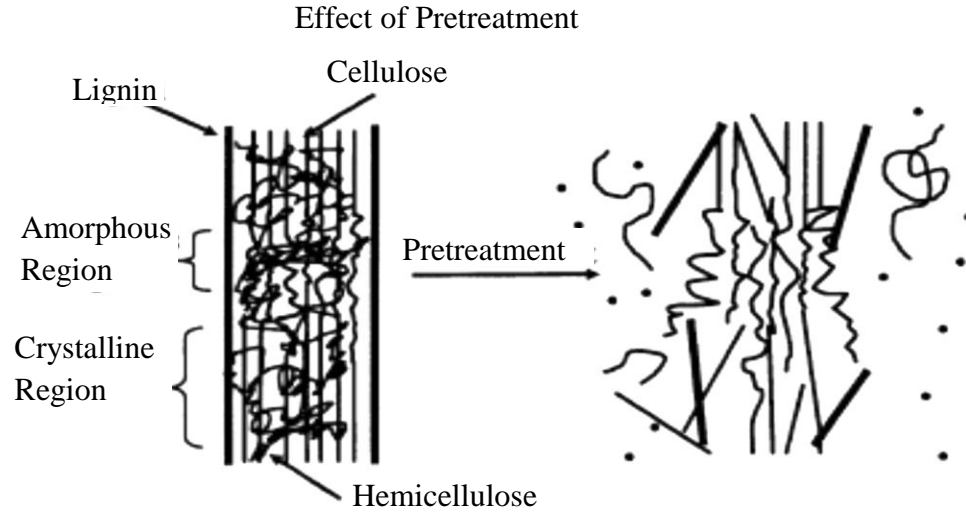


Figure 4. 4 Scheme of pretreatment on lignocellulosic materials. (Reproduced with permission from [169])

4.2.2.1 Alkaline Pretreatment

Alkali such as sodium, potassium, calcium, and ammonium hydroxide, and calcium hydroxide are commonly used as effective pretreatment agents. Alkaline pretreatment has the greatest effect on the lignin where extensive delignification occurs [172]. Lignin removal reduces the nonproductive adsorption sites and exposes the cellulose to enzymes. Lower processing temperatures and pressures are required in alkaline pretreatment compared to other techniques [169]. Not only lignin content, Kong et al. reported that alkalis also removed acetyl groups from hemicellulose, which reduced the hindrance of enzymes and enhanced the carbohydrate digestibility [173]. Lignin and hemicellulose are selectively removed or solubilized during pretreatment, leaving the cellulose relatively unbroken.

The predominantly used delignification method is kraft pulping which can dissolve lignin out from biomass by NaOH and sodium sulfide (Na_2S) at elevated temperature (~160-180 °C) [174, 175]. A mixture of sulfur and salts is retained in the

lignin stream, subsequently recovered in the bleaching process. Partial or total removal of lignin contributes almost pure cellulose fibers in the bleached kraft pulp. Hydroxymethyl group present in side chains of the lignin is partially released as formaldehyde in the kraft cook. Phenolic lignin units can form the quinone methides by eliminating the α -hydroxyl or α -ether group in the alkaline pulping [176].

4.2.2.2 Acid Pretreatment

Acid pretreatment takes the action mostly on the cellulose and hemicellulose. Sulfuric acid (H_2SO_4), hydrochloric acid (HCl), nitric acid (HNO_3), phosphoric acid (H_3PO_4), and their mixture have been commonly used to treat lignocellulosic biomass in the concentrated or diluted form [177, 178]. Hemicellulose is usually hydrolyzed to xylose and other sugars resulting in the cellulose in the residual solids more digestibility. Dilute sulfuric acid pretreatment has been shown to increase the accessible surface for enzymes by removing hemicellulose in combination with the breakdown of cellulose and modifying the lignin structure [179]. Recent studies have reported the formation of lignin droplets deposited on the surface of residues under certain acidic and temperature conditions, showing the impact of diluted acid pretreatment on the morphological changes of lignocellulosic biomass [180].

This pretreatment has been applied in numerous feedstocks from hardwoods to grasses and agricultural residues. Different processing temperatures, solid loadings, and acid loadings have been evaluated. However, it has some limitations of costly materials, corrosion issue, neutralization of hydrolysates before fermentation, and formation of fermentation inhibitors.

4.2.2.3 Ammonia Fiber/Freeze Explosion (AFEX)

AFEX is a physicochemical process where lignocellulosic biomass is exposed to liquid ammonia at elevated temperatures (70-180 °C) and pressures for a period of time, then followed by the sudden reduction of pressure. It is similar to steam explosion. It has been reported that ammonia primarily targets to the degradation of lignin and also breaks up the lignin-carbohydrate linkages [181]. The structure of pretreated residues is changed despite that almost no hemicellulose and lignin are removed. Both micro- and macro-accessibility of the cellulase to cellulose are enhanced. Liquid ammonia also causes cellulose swelling and a phase change from cellulose I to cellulose III. AFEX pretreatment has been used on many lignocellulosic biomass including hardwoods, agricultural residues, and some softwoods. However, it is not a very effective technology for lignocelluloses with relatively high lignin content such as softwoods and nut shells [182, 183]. A lot of research groups have been working on optimizing processing conditions and parameters, such as ammonia loading, moisture content of substrate, temperature, residence time, etc. to achieve economy and effectiveness success.

Many other pretreatment methods have also been thoroughly investigated by many research groups, aiming for different lignocellulosic materials and applications. Mechanical pretreatment, e.g. milling, is usually carried out before the processing to reduce the biomass particle size. Liquid hot water pretreatment contacts water with biomass at high temperature and pressure, in which most of hemicellulose is removed [184, 185]. Organosolv process generally utilizes an organic solvent or mixtures of organic solvents with water, such as ethanol, methanol, acetone, and ethylene glycol, to remove the lignin at high temperature [186]. Low temperature process can be achieved by the addition of catalysts including inorganic or organic acids. The solvent is the inhibitor

for the enzymatic hydrolysis and fermentation so that it has to be removed before the subsequent steps. Oxidative delignification can effectively delignify the lignocellulose by the aid of an oxidizing agent including hydrogen peroxide (H_2O_2), ozone, and oxygen [187]. The aromatic ring in the lignin polymer is reacted with oxidizing chemicals, resulting in the conversion of the lignin to carboxylic acids. Ionic liquids are salts in the liquid phase at certain temperature which are comprised of an inorganic anion and organic cation in the structure [188]. They have been reported to act as selective solvents for lignin or cellulose due to their polarity and unique properties, inducing the separation of lignin and increase of cellulose accessibility. Carbon dioxide explosion method is similar to steam and AFEX where CO_2 is injected with biomass and released by sudden decompression [189]. Supercritical CO_2 has also been introduced as an extraction solvent to facilitate enzymatic hydrolysis of hardwoods and softwoods.

4.3 MATERIAL AND METHODS

4.3.1 Material

Premilled corn stover samples (1-2 mm) were obtained from Technova Corporation (Lansing, MI). The enzyme Accellerase 1000 was a complex of exoglucanase, endoglucanase, hemi-cellulase and beta-glucosidase (Danisco US Inc., Genencor Division, Rochester, NY) with enzyme activity of 46.92 FPU/mL determined by Purdue University. Sodium citrate (Dihydrate, Granular) and citric acid (Monohydrate, Granular) were purchased from J.T. BAKER and used as received. Sodium hydroxide was purchased from Spectrum Chemical MFG. Corp and used as received. All aqueous solutions were prepared with deionized (DI) water supplied by a Barnstead nanopure

Diamond-UV purification unit equipped with a UV source and final 0.2 μ m filter. MILLEX syringe driven filter unit (0.22 μ m) and BD 1mL syringe with tuberculin slip tip were ordered from Biochemistry Research Store at Michigan State University. Glass microanalysis filter holder assembly was used for filtration (Fisher scientific, PA) with filter paper (Grade 1, 11 μ m , D70 mm) from Whatman. Aminex HPX-87H column (Bio-Rad Laboratories, Hercules, CA) and a refractive index detector were employed in the HPLC system for sugar analysis.

4.3.2 Corn stover pretreatment

2g corn stover raw materials were mixed in the TK Filmics nanomixer (model 56-50, Primix Corporation, Japan) with 50 mL 0.4%, 2%, 4%, 8%, 12%, and 20% w/v NaOH solutions at shear rate of 12500 s⁻¹ for two minutes, respectively. Another one sample of 2g corn stover was mixed in 50 mL DI water at the same operating conditions for comparison. After mixing, the pretreated samples were washed to neutrality with DI water, followed by filtration to remove most of water. Washed solids were spread evenly on the aluminum foil and air-dried for 2 days. Moisture content was measured based on oven-dried method.

4.3.3 Enzymatic hydrolysis

The pretreated samples were enzymatically hydrolyzed using Accellerase 1000 (Danisco US Inc. Genencor Div., NY). Pretreated corn stover samples were immersed in pH 4.8 citrate buffer solution, and then incubated in water bath shaker at 150 rpm, 50 °C up to 168 h. The procedure and calculations were performed as NREL Laboratory

Analytical Procedure (LAP) 013 [190]. At least triplicate tests were performed to produce one data point.

4.3.4 Composition analysis

Compositions of each sample were determined according to NREL LAP 002 [191]. A 0.1 g air-dried sample was weighed into the pressure tube. Each sample was analyzed in duplicate, at minimum. 1 mL of 72% sulfuric acid solution was added to each tube which was then placed in a water bath set at $30 \pm 3^\circ\text{C}$ for 1 hr. The solution was diluted to the concentration of 4 wt% and performed a 1 hr autoclaving at 121°C . After autoclaving, the samples were slowly cooled down to near room temperature and 5mL of them were transferred out to get neutralized to pH 5-6 by calcium carbonate. All the decanted liquid was filtered through 0.22 μm filter before high performance liquid chromatography (HPLC) analysis. For acid soluble lignin analysis, UV-spectrometer was used at wavelength 320nm in the appropriate dilution. The autoclaved hydrolysis solids were centrifuged at 12,000 rpm for 25 min and rinsed by DI water to determine the acid insoluble lignin. The solids were oven-dried at 105°C until a constant weight.

4.3.5 Sugar analysis

Calibration sugar standards and samples were analyzed by HPLC (Agilent Technologies Inc., CA). The concentrations of monomeric glucose and xylose were calculated based on the calibration sugar standard curve.

4.3.6 Microscope observation by Scanning Electron Microscope (SEM)

To keep cell wall structure of pretreated samples from collapsing, critical point drying was applied to remove the rest of water from neutralized slurry samples.

Completely dried samples were coated by gold film and scanned at low accelerating voltage 10KV.

4.4 RESULTS AND DISCUSSION

4.4.1 Analysis of compositional change

Not only the low and moderate NaOH concentrations were tested, but the high alkaline concentration range was also studied. The single effects of mechanical force and chemicals were also evaluated by involving only mechanical shearing or alkali in the pretreatment process. Polysaccharides and lignin content were measured for untreated and different pretreated corn stover (shown in Fig. 4.5). Compared to the untreated corn stover, all these three components were slightly increased in the compositional fractions in residues pretreated only with water. This indicates the positive effect of mechanical shearing on the partial removal of extractives, especially the water-soluble ones, in the bulk material. Total content of cellulose, hemicellulose, and lignin was increased from ~ 75% to about 90%. Mechanical pretreatment has also been reported to reduce the fiber size and crystallinity, leading to high surface accessibility [192, 193].

With the addition of NaOH, cellulose turned to be enriched whereas lignin and hemicellulose content were decreased in residues. The higher NaOH in the pretreatment, the higher cellulose content but lower lignin and hemicellulose contents were found, resulting in more effective fractionation of corn stover solids. The cellulose content was increased from 46% to 82.7% while approximately up to 75% and 70% of hemicellulose and lignin were dissolved. No further increase of cellulose content was obtained when corn stover was pretreated with NaOH concentration above 20% (w/v). The rate of cellulose content increased with the increase of alkali loading became lower in the range

of NaOH concentration from 8% to 20% (w/v), with which the cellulose content only increased from 80% to 82%. The solubilization of hemicellulose and lignin into liquid phase was accelerated by alkali, effectively condensing cellulose in the bulk material. J. Konn et al.[194] have demonstrated the dissolution of fiber material under alkaline conditions, involving releasing acetic acid and methanol via deesterification reactions and diffusion-limited release of xylan and lignin. Compared to compositional fractions from other conventional pretreatment processes, the cellulose content from our method is still significant showing above 80% condensed in residues.

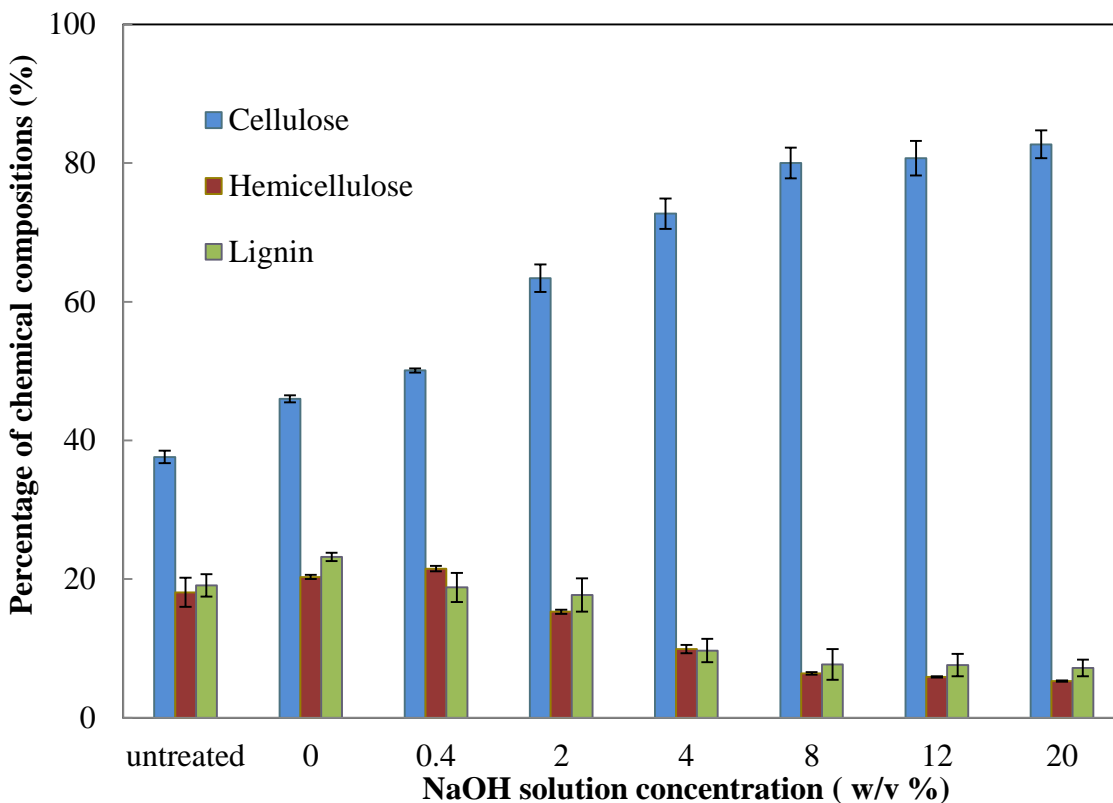


Figure 4. 5 Major chemical components of untreated and pretreated corn stover at different NaOH concentrations. All samples were analyzed at least triplicates with standard deviation (\pm SD) calculated.

4.4.2 Proposed mechanism

Our system is similar to kraft pulping process. However, it is operated at a reduced temperature (~ 100 °C) and much shorter processing time (2 min or less), still showing comparable cellulose content and pretreatment efficiency. The kinetic study of delignification can be referred to from kraft pulping. A large amount of empirical models have been developed to correlate the rate of delignification with process variables [152, 195-197]. It has been described by Vanchinathan et al. that the bulk phase kraft delignification is related to reaction temperature, rate coefficient, effective alkali concentration [196]. The rate coefficient of reaction is a function of flow condition and temperature as well. Despite low reaction temperature compared with that of conventional kraft pulping, high mixing intensity may boost the reaction rate based on our experimental results [198].

As the short reaction time and large bulk material size, mass diffusion between bulk solution and biomass material may be considered as a limiting step in our pretreatment. Gustafson et al. have derived a mass balance model for kraft pulping process which pointed out the importance of diffusivity of species [197]. In our system, high shear rate can be provided to facilitate the diffusion of alkali into the biomass and transfer degraded lignin and hemicellulose out. It may explain that despite the low reaction temperature and short reaction time, large amount of hemicellulose and lignin were removed efficiently.

With our unique mixing condition, separation of major components from biomass could be greatly improved. This method not only shows great potential in the biofuel

production with highly cellulose-enriched products, but also directs the promising application on pulping or related industries.

4.4.3 Microscopy observations on morphological changes

To investigate the morphological changes of pretreated corn stover, SEM images of pretreated corn stover were taken and representative images at NaOH concentrations of 8% and 20% (w/v) were shown in Fig. 4.6. After our nanoshear hybrid alkaline pretreatment, cellulose fibers were twisted with fine disintegrated cellulose microfibrils and mini-pores exposed on the surface. Corn stover structure was greatly disrupted when relatively high NaOH concentration was applied.

The diffusion of alkali into cell wall matrix was significantly enhanced with the help of high shear stress on eliminating the diffusion boundary between solid and liquid phases. The fast penetration of alkali contributes to the removal of hemicellulose and lignin in a very short processing time. Due to high shearing on the bulk materials, corn stover was twisted in the perpendicular axis to fibers by strong mechanical force. In addition, as mentioned in the background, cellulose can be decrystallized in the alkaline solution. Thus, the loosened and open-up structure can highly improve the cellulose accessibility to enzymes in subsequent steps. It indicates that our hybrid pretreatment is beneficial not only to the separation of cell wall components but also to the change of cellulose fiber structure.

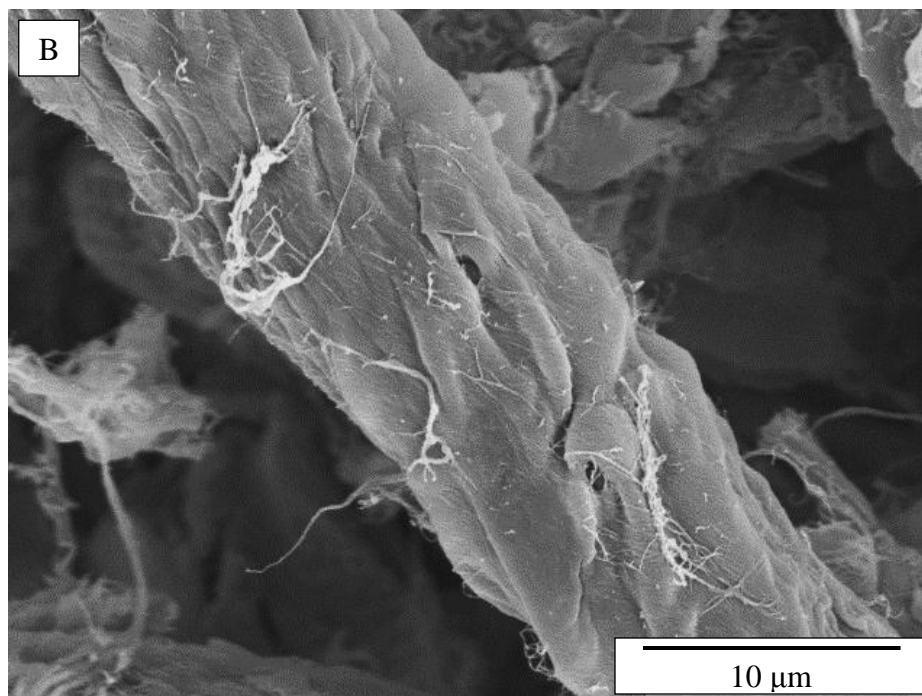
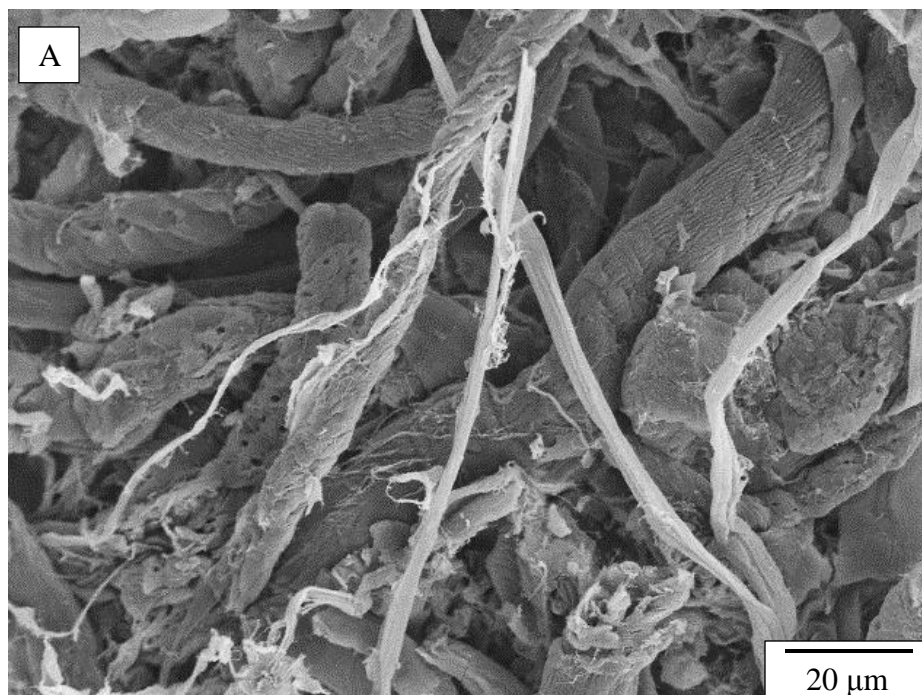
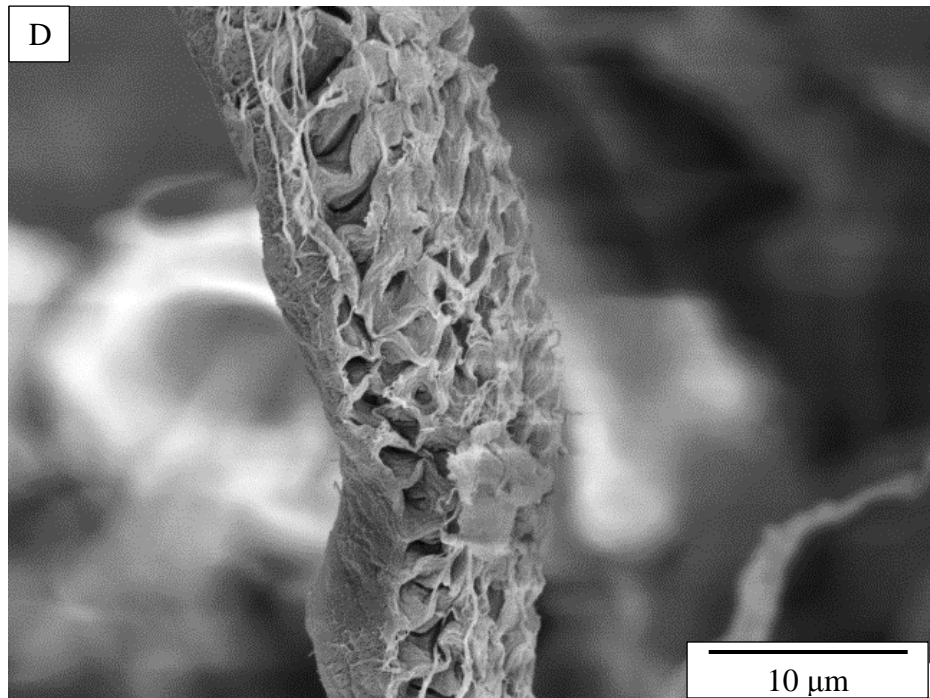
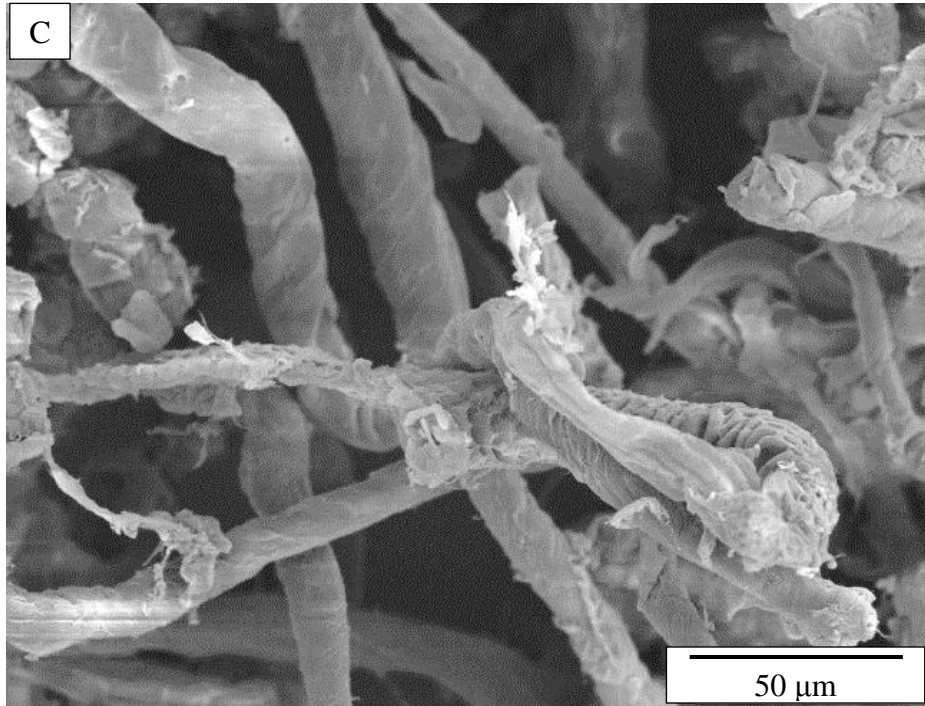


Figure 4. 6 SEM images of corn stover pretreated at 8% (A and B) and 20% (C and D) (w/v) NaOH solutions and shear rate of 12500 s^{-1} in 2 min. A) and C) are taken at low magnification; B) and D) are at relatively high magnification.

Figure 4.6 (cont'd)



4.4.4 Hybrid pretreatment effect on enzymatic hydrolysis

The separation of lignocellulosic carbohydrates and lignin has been reported to enhance the accessibility of enzymes to cellulose and hemicellulose, achieving high sugar yields in the hydrolysis. Our pretreated corn stover samples have enriched cellulose and greatly disrupted fiber structure, both of which are beneficial to the efficiency of the subsequent enzymatic hydrolysis.

Figure 4.7 shows the cellulose and hemicellulose conversion of pretreated corn stover after the two minutes hybrid pretreatment. Cellulose in the 4% (w/v) NaOH pretreated corn stover was 92% converted to glucose in one day and almost completely converted after three days. At the same time, hemicellulose in the same residues achieved 88% conversion in one day. When alkali concentration in the pretreatment was reduced to 0.4% (w/v), the hydrolysis of both components was still efficient compared to untreated corn stover (not shown here), with approximately 65% cellulose conversion and 51% hemicellulose conversion in three days.

As mentioned before, disrupted cell wall structure by the combination of shear and alkali effect renders the corn stover vulnerable to enzymes, resulting in efficient hydrolysis. In addition, the removal of lignin also facilitates the adsorption of enzymes to pretreated corn stover. Our hybrid pretreatment greatly enhances the enzymatic hydrolysis of corn stover in a short processing time and reduced temperature, possibly reducing both the pretreatment and hydrolysis costs.

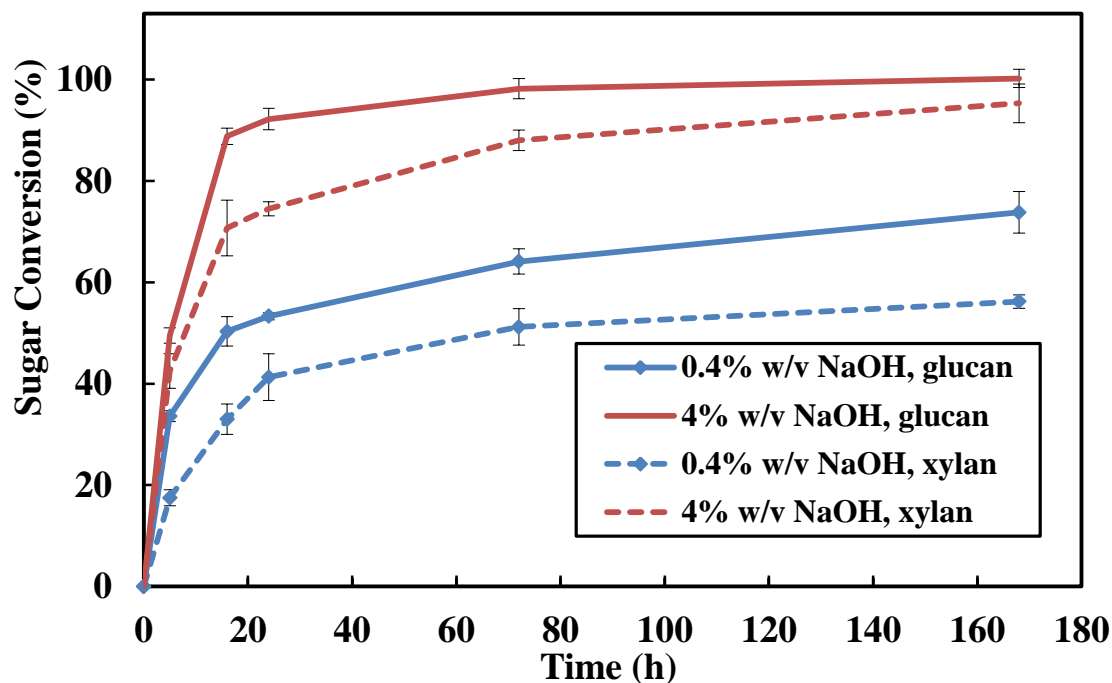


Figure 4. 7 Cellulose and hemicellulose conversion of corn stover pretreated with 0.4% and 4% (w/v) NaOH. The enzyme loading is 20 FPU/g cellulose and incubation temperature is 50 ± 1 °C.

4.5 CONCLUSION

A novel and fast nanoshear hybrid alkaline pretreatment method was demonstrated. Efficient fractionation of lignocellulosic components can be achieved at a reduced temperature and short processing time. Large portion of hemicellulose and lignin can be removed from the bulk corn stover. Pretreated residues were enriched in cellulose. The microstructural changes were revealed by SEM study, indicating the disruption of cell wall matrix and disintegration of cellulose fibers. Enzymatic hydrolysis of cellulose and hemicellulose was greatly enhanced. This process enables the environmental friendly and efficient separation method of biorenewable materials. Further improvement and optimization can be continued to meet diverse needs and commercialized purpose.

Chapter 5

Impact of Cationic Polyelectrolyte on the Nanoshear Hybrid Alkaline Pretreatment of Corn Stover: Morphology and Saccharification Study

Paper accepted in *Bioresource Technology*, vol 133, p 45-50, 2013

5.1 INTRODUCTION

The need for alternative renewable fuel is urgent because of the increasing supply concerns and problem of CO₂ emissions. The production of ethanol as biofuel from lignocellulosic biomass is one of the most feasible options in terms of production scale and market value [199-201]. Enzymatic hydrolysis is considered the most promising and also extensively studied technology in bioenergy processes, because of its mild and specific characteristics. However, currently a rapid and effective conversion of lignocellulosic materials to fermentable sugars by enzymatic hydrolysis is still hard to obtain [202, 203]. Additionally lignocellulosic biomass is inherently recalcitrant to enzymes due to its complex and robust cell wall structure [204]. Therefore, the pretreatment process needs to be performed to fractionate lignocellulosic components into a digestible form and also to integrate the production of high-value added co-products into the bio-refinable fuel and power output [169, 171, 205]. Since the pretreatment and the enzymatic hydrolysis are key processes for successful production of cellulosic ethanol, major concern is put on the large consumption of enzymes and costly pretreatment needed to maximize ethanol yields.

Pretreatments such as biological, chemical, physical, and thermal processes aim to disrupt the naturally resistant shield of lignin and increase the accessibility of enzymes to cellulose and hemicellulose [169]. One of the promising approaches is the utilization of chemical additives, such as inorganic salts and surfactants, to improve the efficiency of enzymatic hydrolysis [206]. For example, surfactants, especially non-ionic surfactants, have been applied after the biomass pretreatments to enhance the cellulose hydrolysis as well as to decrease the enzyme loadings [207]. The positive effects of the addition of

surfactants have been proposed to be to increase the availability of enzymatic reaction sites, to reduce the enzyme denaturation, to remove the recalcitrant lignin, etc [208]. Attempts have also been made by investigating the effect of surfactants on the pretreatment processes which showed the prevention of unproductive bindings of enzymes to lignin and thus increased enzymatic hydrolysis yields [209]. Several studies have reported the utilization of inorganic salts in the biomass pretreatments as it successfully accelerates the degradation of cellulose and hemicellulose and improves sugar yields [210, 211].

Cationic polyelectrolytes, as good strength additives and retention agents, have attracted a considerable interest in the paper industry [212, 213]. The cationic polyelectrolytes have good adsorption properties onto cellulosic fibers contributed by electrostatic interactions [214]. The use of cationic polyelectrolytes in the kraft pulping process as flocculation agents was based on the study of interactions between these polymers and lignin under various solution conditions [213]. Recent studies in terms of the saccharification rate and pulp washing are advancing their potential as efficient additives for lignocellulosic ethanol production [215]. Li and Pelton have shown the successful removal of kraft lignins with poly(diallyldimethylammonium chloride) (PDAC) at high pH where carboxyl groups in the lignin chains were dissociated and formed the macroscopic complexes with PDAC [212]. However, as far as we know, there is no study applying polyelectrolytes as additives for biomass pretreatment.

In this regard, the main purpose of this study is to evaluate the effectiveness of polyelectrolytes on the pretreatment process with alkali in the nanoshear hybrid pretreatment process which was recently developed by our group [216]. The pretreatment

based on our high shear flow nanomixing reactor has been reported to greatly fractionate lignocellulosic components from cell wall matrix. PDAC was selected as a strong, positively charged polyelectrolyte, which has been commonly used to modify the cellulose surface and stabilize the lignin. The investigation of biomass changes in composition and structure was studied and the effect on enzymatic conversion efficiency was also reported.

5.2 BACKGROUNDS

5.2.1 Effect of surfactants on the pretreatment of lignocellulosic biomass

Few reports are available on the pretreatment of lignocellulosic biomass assisted by surfactants. The utilization of surfactants in the pretreatment may be firstly reported by Ladisch that pre-wetting the cellulosic materials with the nonionic surfactant, such as 1% Triton X-100, enhanced the cadoxen solvolysis of cellulose [217]. Lignin is widely recognized as a negative influence on the efficient enzymatic hydrolysis. Therefore, more straightforward application of surfactants in the pretreatment process was introduced to increase the solubility of lignin to water, making the pretreatment more effective. Kurakake et al. added the nonionic surfactant, Tween 20 (polyoxyethylene sorbitan monolaurate), into the UCT-solvent pretreatment of lignocellulosic material bagasse to improve the extraction of hydrophobic degradation products by forming micelles and further enhance the subsequent enzymatic hydrolysis [218].

In the view of this idea, dilute acid pretreatment has also been attempted to combine with surfactants due to the expectation of dual removal of hemicellulose and lignin to promote the cellulose accessibility, therefore, substantial enhancement of the enzymatic hydrolysis. Qi et al. have shown the promising effect of Tween 20 assisted

sulfuric acid pretreatment on the enzymatic hydrolysis and simultaneous saccharification and fermentation (SSF), resulting from the extraction of hydrophobic degradation products and modification of the surface of lignin by the added surfactant [219]. Qing et al. tested with different surfactants, Tween 80, dodecylbenzene sulfonic acid, and polyethylene glycol 4000 (PEG), on the diluted sulfuric acid pretreatment and reported that the addition of surfactants increased the lignin removal and the changes in the lignin that reduced its non-productive binding to enzymes [209]. The similar work has also been done with Triton X-100 in the mild acid pretreatment of sugarcane tops [220]. Not only a variety of nonionic surfactants but also ionic ones have been investigated in the pretreatment. Xin et al. have applied the anionic surfactant, sodium dodecyl sulphate (SDS), in the waste newspaper pretreatment to efficiently help the detachment of ink particles and other components from the surface which therefore enhance its enzymatic digestibility [221].

Most work has shown the positive effect of surfactants as additives on enzymatic hydrolysis [208, 222]. Tween 80 has been proven to lead to higher cellulose conversions and enzyme recoveries, in the hypothesis that the surfactant hindered the immobilization of enzymes [223]. Different mechanisms have been proposed for the enhanced enzymatic hydrolysis by surfactant addition. Kaar and Holzapple have showed from kinetic analyses that the addition of Tween resulted in a higher effective hydrolysis rate and stabilized enzymes from the denaturation during the hydrolysis [224]. Surfactant has also been shown to alter the substrate structure and facilitate the desorption of enzymes from substrate, which thus increased the accessible sites of substrate and prolong the enzyme life [225].

5.2.2 Effect of inorganic salts on the pretreatment of lignocellulosic biomass

The inorganic salts, also called as metal salts, have been found to make a great contribution to the decomposition of cellulose and hemicellulose in biomass, especially in the acid or hot water pretreatment. These inorganic salts existing in the form of sulfate, phosphate, and chloride are considered to be good alternatives providing milder conditions for lignocellulosic materials and reducing the process cost as well as toxic byproducts due to their strong catalytic effect on the hydrolysis process and less corrosive than acid. The catalyst concentration and type as well as pretreatment temperature and time are widely investigated to optimize the removal of hemicellulose and cellulose, enhance the sugar recovery, and reduce the inhibitor concentration. Yan et al. utilized Fe^{3+} on HCl hydrolysis of peat which contains a high content of hemicellulose and obtained a high yield of sugars after pretreatment [226]. In the patent demonstrated by Nguyen and Tucker, the addition of ferrous sulfate (FeSO_4) in an aqueous acid solution resulted in higher overall fermentable sugar yields than those using dilute acid alone, and thus allowed the reduction of process severity [227]. They indicated that it was due to the lower activation energy of cellulose hydrolysis. The effect of different inorganic salts, such as KCl, NaCl, CaCl_2 , MgCl_2 , and FeCl_3 , on the primary hydrolysis products of hemicellulose, xylose and xylotriose, was also studied in the hot water pretreatment [228]. Significant increases of xylose monomer and xylotriose degradation were found in the treatment, especially treated by FeCl_3 , compared to that with only pressurized hot water at the same temperature.

In addition, the single effect of various types of inorganic salts has been investigated on the pretreatment of lignocellulosic biomass. Liu et al. have applied inorganic salts alone, such as NaCl, KCl, CaCl₂, MgCl₂, FeCl₂, FeSO₄, FeCl₃, and Fe₂(SO₄)₃, on pretreating corn stover without the addition of other chemicals [211]. They found that the amount of hemicellulose removed was greatly increased while the cellulose degradation was kept as low as possible when corn stover was treated with FeCl₃ at lower temperature. Most of monomeric and oligomeric sugars in liquor could be recovered. The pretreated corn stover turned to be softer and more digestible.

To study the degradation mechanism of hemicellulose catalyzed by metal salts, Yu et al. have tested three types of metal salts and revealed that compared to alkaline metal chlorides and alkaline earth metal chlorides, transition metal chlorides significantly accelerated the degradation of hemicellulose contributing to their stable formation of saccharide-metal cation intermediate complex[229]. Not only hemicellulose that can be greatly influenced but also the lignin was altered in the pretreatment. They found that most lignin remained but deposited on the surface of residues as droplets and small amount of lignin-derived products were in the hydrolyzate.

5.2.3 Effect of cationic polyelectrolytes on the enzymatic hydrolysis of lignocellulosic biomass

As we mentioned, the cost of the enzyme is a very significant portion of the cost of the hydrolysis process. Therefore, compositions, equipment, and processes that can increase the enzyme efficiency and reduce the usage will be beneficial to increasing the commercial viability of the production of biofuels. Feng et al. first used cationic

polyelectrolytes, poly(N,N)-dimethyl aminopropylene bromide and poly(2-hydroxyl 1-3-dimethylamino propylene chloride), and anionic polyelectrolytes, poly(methyl acrylic acid) and poly(benzethylene sulfonate), on the saccharification of cellulase [230]. They demonstrated that polyelectrolytes could increase the adsorption of one cellulase component C_x on the substrate and change the activity ratio of different cellulase components, resulting in the enhancement of the saccharification.

Recent years, polyelectrolytes, cationic polyacrylamides (c-PAM), have been studied in the hydrolysis of fiber and starch. Hydrolysis rate was shown to increase by more than 50% [231, 232]. The binding of cellulase to fiber was also enhanced in the presence of c-PAM which served as a linking material to tether the enzyme to the substrate. Reye et al. proposed a patching mechanism that c-PAMs attached to the fibers and minimized the charge repulsion between the substrate and enzymes, which promoted the binding and thus increased the hydrolysis rate [233]. Further investigation on the mechanism by Mora et al. found that c-PAMs mostly increased the rate of endoglucanase hydrolysis and associated more with the amorphous region of the fibers than with the crystalline [215].

5.3 MATERIAL AND METHODS

5.3.1 Material

The premilled Michigan grown corn stover (CS) samples (1-2 mm) were obtained from Metna Corporation (Lansing, MI). The enzyme Accellerase 1000 was a complex of exoglucanase, endoglucanase, hemi-cellulase and beta-glucosidase (Danisco US Inc., Genencor Division, Rochester, NY) with enzyme activity of 46.92 FPU/mL determined

by Purdue University. Sodium citrate (Dihydrate, Granular) and citric acid (Monohydrate, Granular) were purchased from J.T. BAKER and used as received. Sodium hydroxide was purchased from Spectrum Chemical MFG. Corp and used as received. Cationic polyelectrolyte, poly(dimethyldiallylammonium chloride) (PDAC), (M_w 100,000~200,000), was purchased from Aldrich Chemistry with 20% wt in water. All aqueous solutions in the processes were prepared with deionized (DI) water supplied by a Barnstead nanopure Diamond-UV purification unit equipped with a UV source and a final 0.2 μ m filter. T K Filmics nanomixer (Model 56-50, PRIMIX Corporation, Japan) was used to perform the pretreatment. MILLEX syringe driven filter unit (0.22 μ m) and Becton, Dickinson and Company BD 1mL syringe with tuberculin slip tip were ordered from Fisher scientific. Glass microanalysis filter holder assembly was used for the filtration (Fisher scientific, PA) with filter papers (Grade 1, 11 μ m, D70 mm) from Whatman. Aminex HPX-87H column (Bio-Rad Laboratories, Hercules, CA) and a refractive index detector were employed in the high performance liquid chromatography (HPLC) system for sugar analysis.

5.3.2 Sample pretreatment

The corn stover samples were pretreated by the T K Filmics nanomixing reactor. The corn stover samples, 2g of each, were mixed with 50 mL 0.4% and 4% w/v NaOH solutions at the mixing shear rate of 12500 s⁻¹ for 2 min with and without 10 mM and 60 mM PDAC based on the molecular weight of the polymer repeat unit (0.081g and 0.485g in the mass weight), respectively. No external removal or addition of heat to the system was provided. The mixing temperature could reach up to 100 °C under ambient pressure

without the addition of extra heating. After the 2 min mixing, cooling water was introduced until the system temperature was brought down to 25 °C. After the mixing, the pretreated samples were washed to neutrality with deionized water (DI) water, followed by filtration to get rid of most of water. Washed solids were spread evenly on the aluminum foil and air-dried for 2 days. Moisture content was measured based on oven-dried method.

5.3.3 Enzymatic hydrolysis

The pretreated samples were enzymatically hydrolyzed using Accellerase 1000 (Danisco US Inc. Genencor Div., NY). Pretreated corn stover samples were immersed in pH 4.8 citrate buffer solution, and then incubated in water bath shaker at 150 rpm, 50 °C up to 168 h. The procedure and calculations were performed as NREL Laboratory Analytical Procedure (LAP) 013 [190]. At least triplicate tests were performed to produce one data point.

5.3.4 Composition analysis

The compositions of each sample were determined according to the NREL LAP 002 [191]. A 0.1 g air-dried sample was weighed into the pressure tube. Each sample was analyzed in duplicate, at minimum. 1 mL of 72% sulfuric acid solution was added to each tube which was then placed in a water bath set at $30 \pm 3^\circ\text{C}$ for 1 hr. The solution was diluted to the concentration of 4 wt % and performed a 1 hr autoclaving at 121 °C. After autoclaving, the samples were slowly cooled down to near room temperature and 5mL of them were transferred out to get neutralized to pH 5-6 by calcium carbonate. All the decanted liquid was filtered through 0.22 μm filter before the HPLC analysis. For the acid soluble lignin analysis, UV-spectrometer was used at wavelength 320 nm in the

appropriate dilution. The autoclaved hydrolysis solids were centrifuged at 12,000 rpm for 25 min and then rinsed with DI water at least three times to determine the acid insoluble lignin. The solids were oven-dried at 105°C until a constant weight was achieved.

5.3.5 Sugar analysis

Calibration sugar standards and samples were analyzed by HPLC (Agilent Technologies Inc., CA). The concentrations of monomeric glucose and xylose were calculated based on the calibration sugar standard curve.

5.3.6 Surface morphology of pretreated samples

To study the morphology of the pretreated sample surfaces, scanning electron microscope (SEM) measurements were performed. The samples were gold coated and scanned at low accelerating voltage of 10KV with JEOL 6400 SEM at Center for Advanced Microscopy in Michigan State University. In order to maintain the structure of pretreated samples for SEM, critical point drying method was used instead of air drying.

5.3.7 Inner structure of pretreated samples

Transmission electron microscopy (TEM) was used to observe the inner or intra cell wall structure of untreated and pretreated samples by JEOL100 CXII at Center for Advanced Microscopy in Michigan State University. The samples were dehydrated in 30%, 50%, and 100% (w/v) acetone/aqueous solutions for 20 min respectively. In order to fix the sample for microtoming which is done by a Power Tome XL (RMC, Boekeler Instruments, Tucson, AZ), different volume ratios of acetone-resin mixture, 3:1, 2:1, 1:1, and pure resin were used to embed samples for 1 day, respectively. Ultrathin sections

were cut with a diamond knife on an ultramicrotome and then examined with TEM. Sections were stained with potassium permanganate (KMnO₄) before observation.

5.3.8 Confocal Laser Scanning Microscope (CLSM)

Olympus FluoView 1000 LSM was used, which can detect Lignin auto-fluorescence by exciting the sample at $\lambda=488\text{nm}$ and collecting emission data using filter of $\lambda=505\text{-}525\text{nm}$. All samples were scanned under the same laser power.

5.3.9 X-ray photoelectron spectroscopy (XPS)

A Perkin Elmer Phi 5600 ESCA system was used for the XPS analysis with magnesium K α X-ray source at a take-off angle of 45°. The samples were tested by Composite Materials & Structures Center at Michigan State University.

5.4 RESULTS AND DISCUSSION

5.4.1 Chemical compositions change

The chemical compositions of untreated and pretreated samples are listed in Figure 5.1. All the pretreated samples have higher cellulose and lower lignin contents than the untreated one (shown in Fig. 5.1A), which is similar to the previous studies on the alkaline pretreated residues [234]. Alkaline chemicals such as sodium hydroxide (NaOH) have been known to remove lignin from biomass cell wall matrix by reacting with carboxylic acid and phenolic groups of lignin, making them more alkali-soluble [235]. When PDAC was added into the pretreatment process with 0.4% and 4% (w/v) NaOH, both lignin content increased in the residues indicating the possibility of lignin retention (Fig. 5.1B and 5.1C). Higher lignin content as well as lower cellulose and hemicellulose contents were obtained with higher PDAC addition. When NaOH

concentration of 4% (w/v) was applied in the pretreatment, lignin contents in the pretreated corn stover all decreased and more cellulose was retained compared to those in the corn stover pretreated with 0.4% (w/v) NaOH. However, a comparison between Figures 5.1B and 5.1C shows that the relative lignin retention was higher from the pretreatment with higher NaOH concentration. Total of the carbohydrates and lignin recovery decreased to approximately 80% along with the presence of PDAC. It is suggested that PDAC maintains lignin in the residues according to data of composition changes.

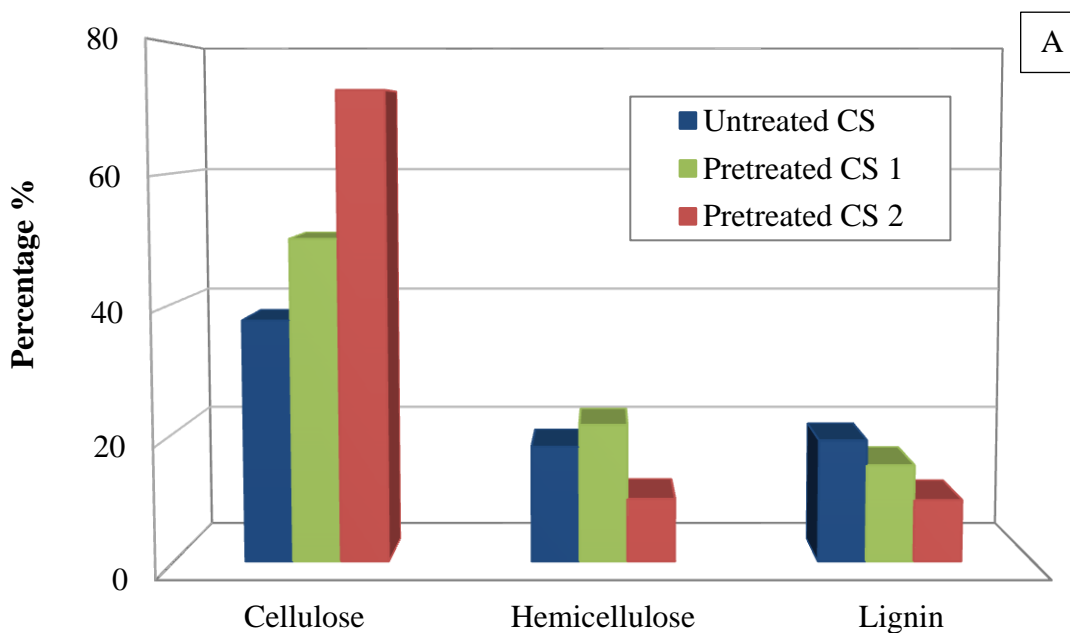
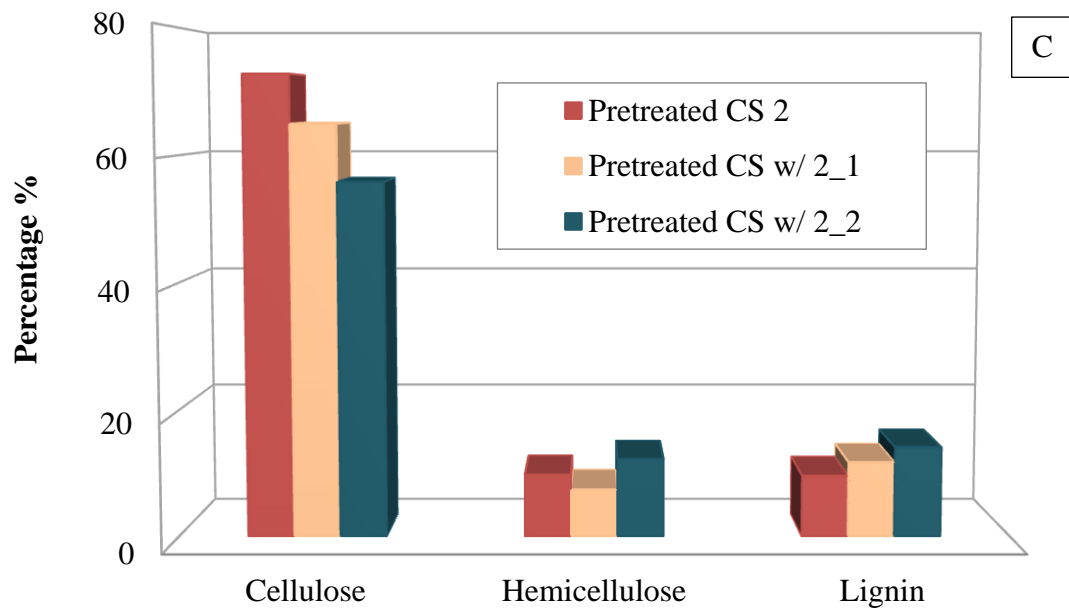
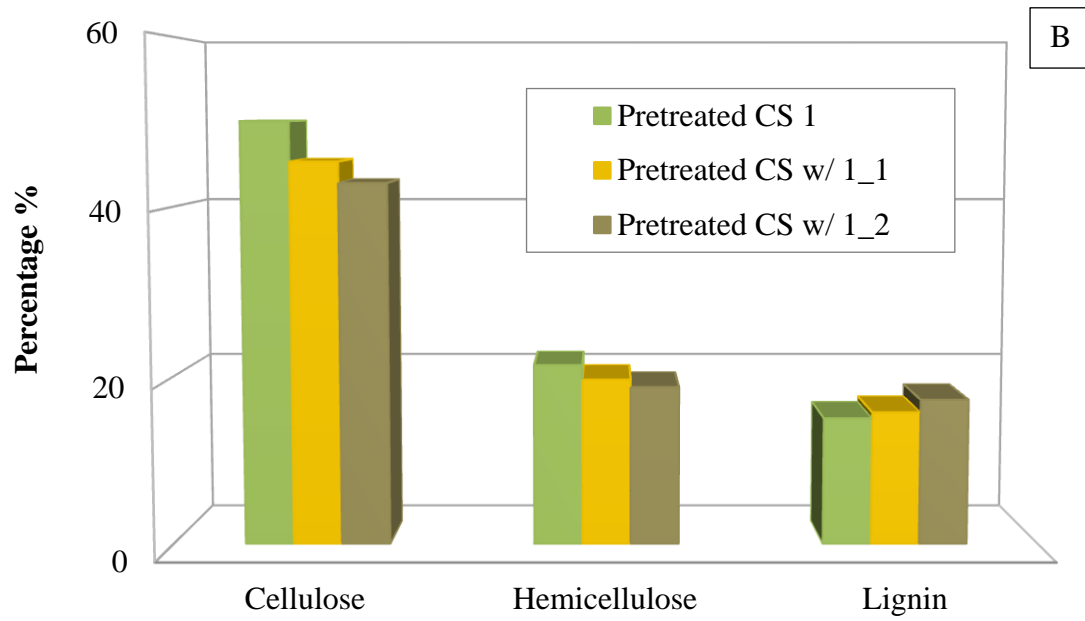


Figure 5. 1 Percentage of major chemical components in untreated and pretreated corn stover. A) Untreated CS: Corn Stover without pretreatment; Pretreated CS 1: Corn Stover pretreated with 0.4% (w/v) NaOH; Pretreated CS 2: Corn Stover pretreated with 4% (w/v) NaOH. B) Pretreated CS w/ 1_1: Corn Stover pretreated with 0.4% (w/v) NaOH and 10mM PDAC; Pretreated CS w/ 1_2: Corn Stover pretreated with 0.4% (w/v) NaOH and 60mM PDAC; Pretreated CS w/ 2_1: Corn Stover pretreated with 4% (w/v) NaOH and 10mM PDAC; Pretreated CS w/ 2_2: Corn Stover pretreated with 4% (w/v) NaOH and 60mM PDAC.

Figure 5.1 (cont'd)



5.4.2 Microscopic morphology observation of pretreated corn stover

To evaluate the effect of PDAC on the structural changes of pretreated corn stover, a qualitative assessment of their morphologies was firstly conducted with SEM images at different polyelectrolyte concentrations, as seen in Figure 5.2. The untreated corn stover had uneven and intact surface which is known as inherent recalcitrance for enzymatic hydrolysis. After the pretreatment, the cell walls of corn stover were altered and boundaries were clearly defined (Fig. 5.2B). The separated individual fibers with size of 10 μm to 20 μm were revealed from all pretreated samples. As we can see in Fig. 5.2C and 5.2D, the addition of PDAC in the pretreatment led to more microfibril bundles partially separated and expanded from the rough surface with considerable cracks and pores on it. Smaller fibril bundles in nano-scale were also observed in those samples which may be considered as further fibrillation of fiber surface layers. These structural changes are believed to be associated with increasing the available surface area and thus leading to higher enzyme accessibility to cellulose [236].

Additionally, it is interesting to find that nano-scale droplets which appear more or less spherical were covered on the fiber surface. More droplets as a thin layer of deposits were found on the surface of corn stover pretreated with higher PDAC concentration, giving dramatic changes in the morphology of the pretreated corn stover samples. This indicates that the surface of pretreated corn stover was getting textured possibly not only because of mechanical disruption as well as ridges and folds along the fiber surface but also interactions with the polyelectrolytes (Fig. 5.2D).

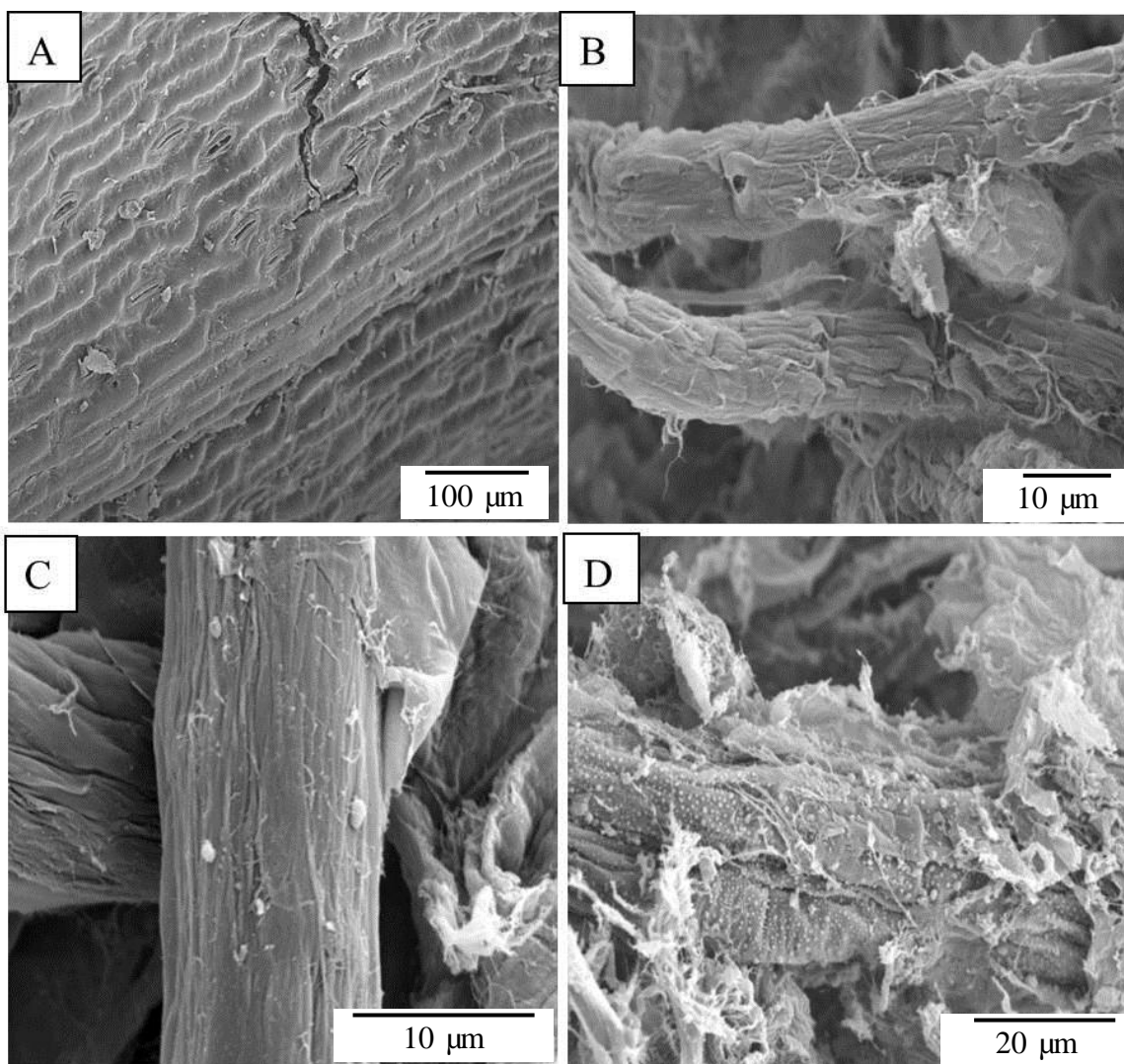


Figure 5. 2 SEM image of untreated and pretreated corn stover. A) Untreated corn stover; B) Corn stover pretreated with 4% (w/v) NaOH; C) Corn stover pretreated with 4% (w/v) NaOH and 10 mM PDAC; D) Corn stover pretreated with 4% (w/v) NaOH and 60 mM PDAC.

5.4.3 Verification of droplets deposited on the surface

CLSM has been used to facilitate the structural or morphological studies on lignin distribution, fiber surface, and cell wall transverse dimensions, mainly attributed to its detection of laser-induced autofluorescence from lignified plants and nondestructive optical sections in thick translucent specimens [237, 238]. When the samples were scanned at the same laser power, the emission intensity of autofluorescence could be

considered proportional to the lignin concentration on the sample surface. The lignin on the untreated corn stover surface was uniformly distributed with bright autofluorescence, as shown in Fig. 5.3A. The pretreated corn stover without PDAC showed low level of autofluorescence indicating high delignification on the surface area (Fig. 5.3B), whereas the corn stover subjected to PDAC treatment exhibited the increase in autofluorescence intensity (Fig. 5.3C). This was followed by an additional increase in intensity with the increase of PDAC concentration (Fig. 5.3D).

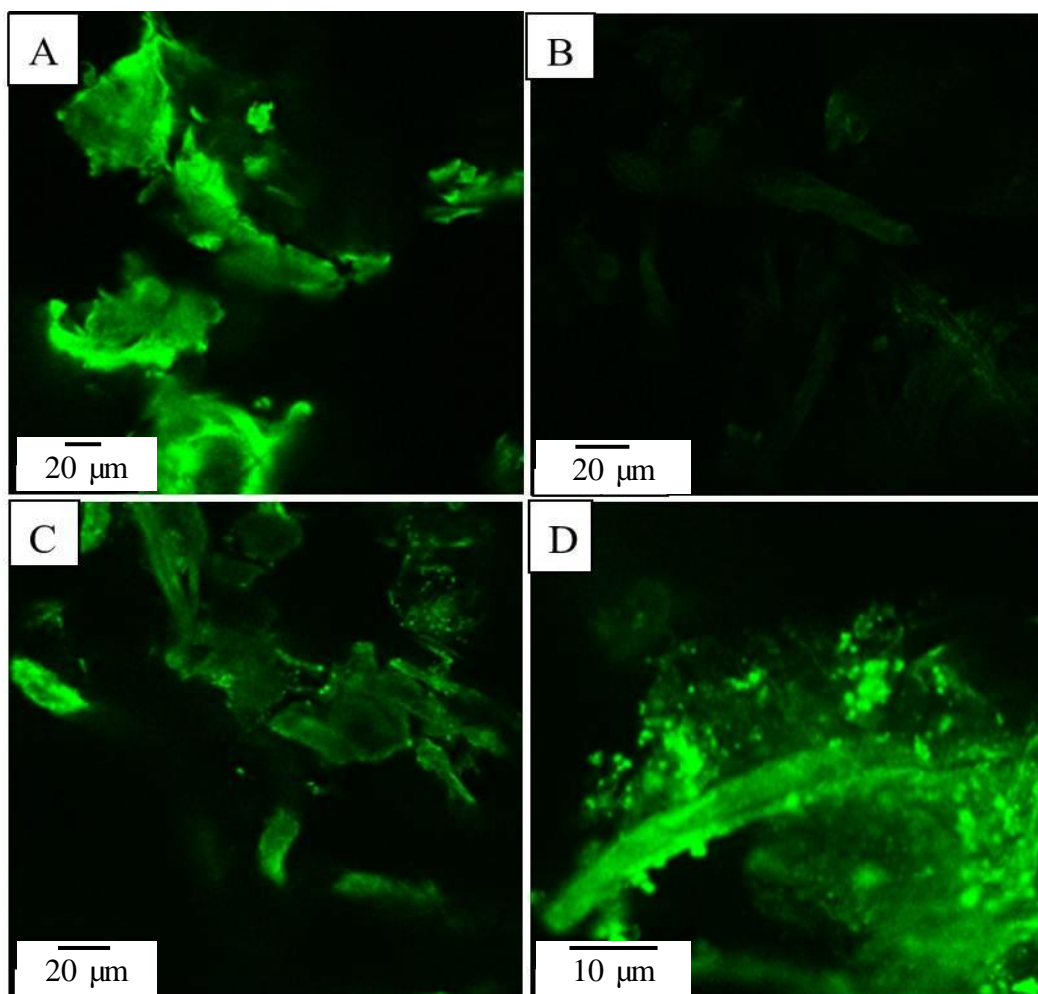


Figure 5. 3 CLSM image of untreated and pretreated corn stover. A) Untreated corn stover; B) Corn stover pretreated with 4% (w/v) NaOH; C) Corn stover pretreated with 4% (w/v) NaOH and 10 mM PDAC; D) Corn stover pretreated with 4% (w/v) NaOH and 60 mM PDAC.

In Fig. 5.3C and 5.3D, a large amount of fluorescent globular droplets or aggregates were clearly shown, which is in accordance with the SEM observation on surface morphology of the corresponding pretreated samples. The similar formation of lignin droplets on the fiber surface have been reported in other pretreatment processes, such as diluted acid, hot water, steam explosion, and organosolv [180, 185, 239, 240]. They demonstrated the phenomenon of lignin agglomeration into droplets by the treatment that lignin is transformed to a high elastic state at the temperature above the lignin phase transition of at least 130 °C and migrates away from cell wall matrix. It is believed that lignin redistribution dramatically opens up the cell wall structure and improves the swelling of fibers [180, 241]. However, our method is carried out at a reduced temperature, from room temperature up to 100 °C, which is much less than the transition point of lignin. The retention and redistribution of lignin at this temperature have not been reported yet.

5.4.4 Surface content analysis by X-ray photoelectron spectroscopy (XPS)

As surface morphological changes were observed with SEM and CLSM, XPS also known as electron spectroscopy for chemical analysis (ESCA) has also been applied to quantify the surface composition of the lignocellulosic materials [242, 243] . As mentioned elsewhere that pure cellulose contains no C-C (C1) carbon and pure wood lignin contains 49% C1 carbon, the surface coverage of lignin can be estimated by the equation,

$$\phi \text{ lignin} = \frac{C1-(4 \times N1)}{49\%} \times 100\% \quad (5.1)$$

Where C1 is the area of the C1 peak divided by the total area of the C1s peak and N1 is the area of N1s peak coming from PDAC. Since PDAC contains four C1 carbons per each nitrogen atom, coefficient constant used here was four.

The surface coverages by lignin from XPS analysis of different pretreated samples are listed in Table 5.1. A comparison between results of pretreated corn stover with and without the addition of cationic PDAC indicated that lignin was enriched on the surface in the presence of the polyelectrolytes during the pretreatment process. The significant increase of lignin and nitrogen contents were seen from the pretreated corn stover with 60 mM PDAC loading, which indicated the enriched deposition of lignin and polyelectrolyte on the surface. These results from microscopic observation and surface characterization verified that isolated droplets deposited on the surface of pretreated samples were lignin or lignin-polyelectrolyte complex. Lignin can be solubilised from cell wall matrix with negative charges by the alkali [235]. Maximova et al. have reported that when the extracted lignin concentration was higher than the polyelectrolyte concentration, lignin-polyelectrolyte complexes may show net negative charges and be repulsive to the slightly negatively charged cellulose surface [242]. It may explain that little increase of lignin content has been obtained on the surface when 10 mM PDAC was used.

Table 5. 1 Lignin surface coverage of pretreated corn stover analyzed by XPS

Sample	C1s	N1s	O1s	C1 area percentage %	Lignin surface coverage %
4% NaOH pretreated	67.3	0.5	32.1	36.5	46.0
4% NaOH w/ 10mM PDAC pretreated	68.2	0.5	31.1	37.2	48.0
4% NaOH w/ 60mM PDAC pretreated	76.6	2.3	21.1	56.0	68.8

5.4.5 Visualization of cell wall by TEM

The TEM observations confirmed those with CLSM and further provided details on the structural changes within cell walls. The cross-sectional images of untreated and pretreated corn stover were taken with the aid of KMnO_4 allowing the emphasis of lignin location [244]. The best representative examples for each sample were presented here, as shown in Fig. 5.4. The untreated corn stover has dark staining evenly distributed throughout the compound middle lamellar (CML) indicating that it is strongly lignified (Fig. 5.4A). The alkaline pretreated corn stover showed collapsed CML and kinked texture as it was studied in our previous patent application (Fig. 5.4B) [216]. Staining with KMnO_4 which forms complex with lignin confirmed the presence of lignin as discrete dark particles or agglomerates in the presence of PDAC (Fig. 5.4C and 5.4D) [245]. Those randomly distributed and irregularly shaped dense droplets existed within the cellulose microfibrils matrix or on the outer surfaces of the cell walls of pretreated corn stover with PDAC supporting our previous observations. In the presence of PDAC in the pretreatment process, solubilised lignin tended to form the complex with the oppositely charged PDAC at the alkaline condition and then redeposited between

cellulosic fibrils as droplets. Cellulose undergoes swelling when treated with alkali [235]. Swollen cellulose can be more easily penetrated by the treatment fluid as well as polyelectrolytes. It has also been shown that cationic polyelectrolytes can diffuse into cellulosic fibers driven by electrostatic interactions within the porous fiber wall [246]. The diffusion of PDAC into the cell wall matrix may aid to the formation of lignin enriched droplets embedded within, which was seen in the TEM images as shown in Fig. 5.4C and 5.4D. In addition, disrupted cell wall structure became more kinking and pores were found within the CML and secondary walls.

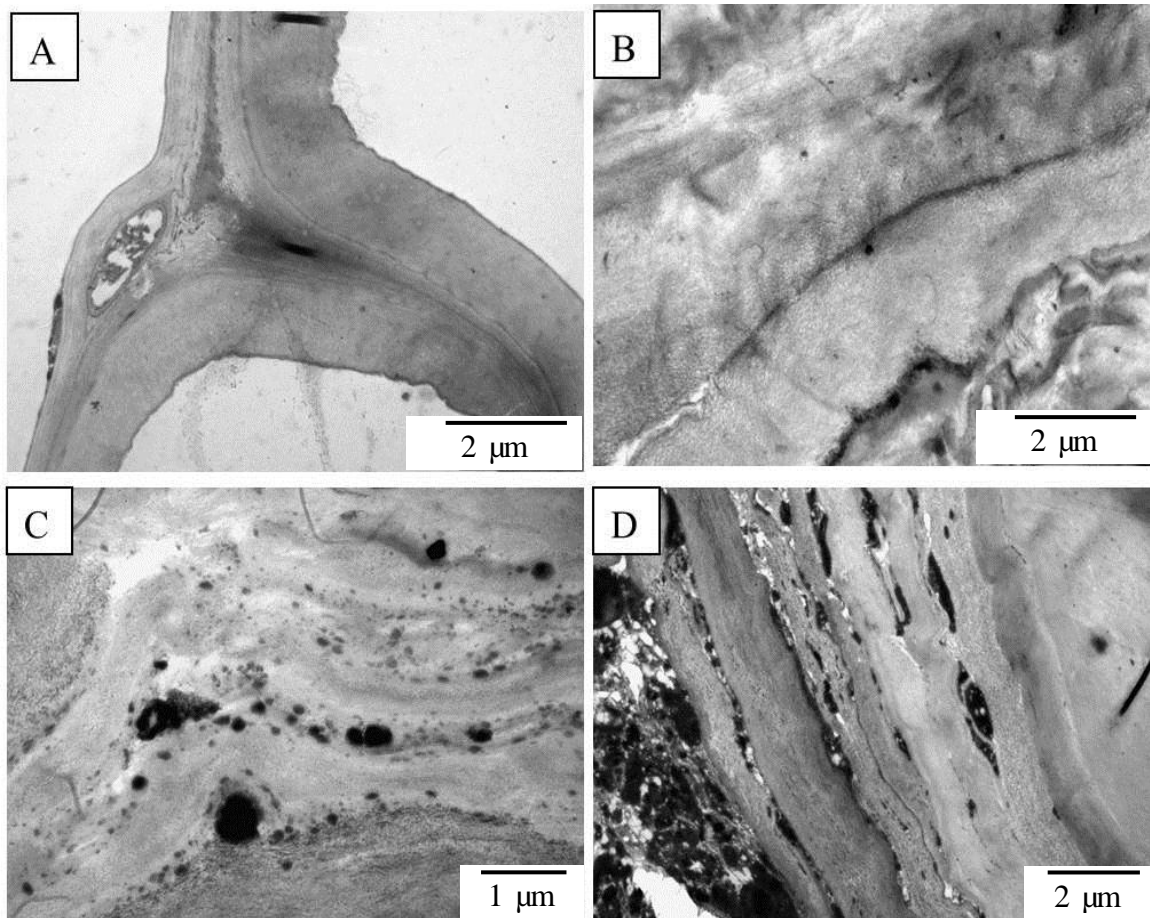


Figure 5. 4 TEM images of sectional view of untreated and pretreated corn stover which were stained with KMnO_4 . A) Untreated corn stover; B) Corn stover pretreated with 4% (w/v) NaOH; C) Corn stover pretreated with 4% (w/v) NaOH and 10 mM PDAC; D) Corn stover pretreated with 4% (w/v) NaOH and 60 mM PDAC.

5.4.6 Effect of the polyelectrolyte on sugar yields

The recent findings indicate that altering lignin structure and location can also limit the inhibitory effect and possibly increase the cellulose accessibility [180, 241, 247, 248]. Kumar and Wyman reported that the acid pretreated lignin had the lower cellulase affinity than base pretreated one, despite of the relatively higher lignin content [249]. In our system, lignin after the pretreatment formed clusters similar to those in the dilute acid pretreatment, which may cause negligible inhibition of enzymatic hydrolysis as mentioned.

It has been shown that in our unique nanoshear hybrid alkaline pretreatment, PDAC could be used to facilitate the cellulose disruption and lignin redistribution, which significantly affects the change of biomass morphological properties. Increased porosity, improved accessibility of cellulose surface, and enhanced removal of hemicellulose have been suggested to be related to lignin redistribution [241]. Another importance is that lignin can be moved away from these cellulose microfibrils without being removed from the biomass with intensive separations. It attracts the interest on modifying mechanical properties of pulp sheets in papermaking industry in a simple and efficient way [214].

Cellulose and hemicellulose are the major sugar sources for fermentation to biofuel. To understand the effect of polyelectrolyte PDAC on sugar release, enzymatic hydrolysis was performed at enzyme loading of 20 FPU/g glucan as used in our previous studies [216]. The nanoshear hybrid alkaline pretreated corn stover was compared as a control sample to better evaluate the single effect of PDAC as a new additive. The enzymatic hydrolysis slightly increased when 10mM PDADMAC was applied and the enhancement increased with higher PDADMAC loading (60 mM). With the addition of

60mM PDADMAC, the cellulose conversion of pretreated corn stover was achieved approximately 7% higher than the one pretreated without polyelectrolyte after 24h (shown in Fig. 5.5A). Enhancement of 6% could also be obtained in the hemicellulose conversion for the pretreated corn stover with PDAC (shown in Fig. 5.5B).

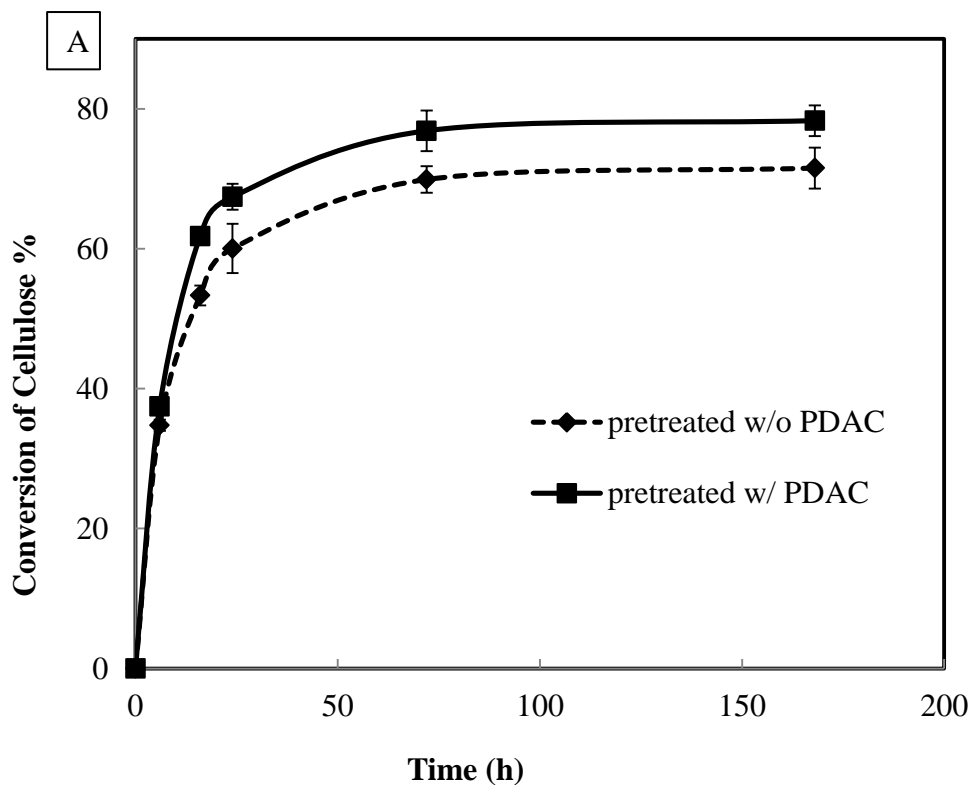
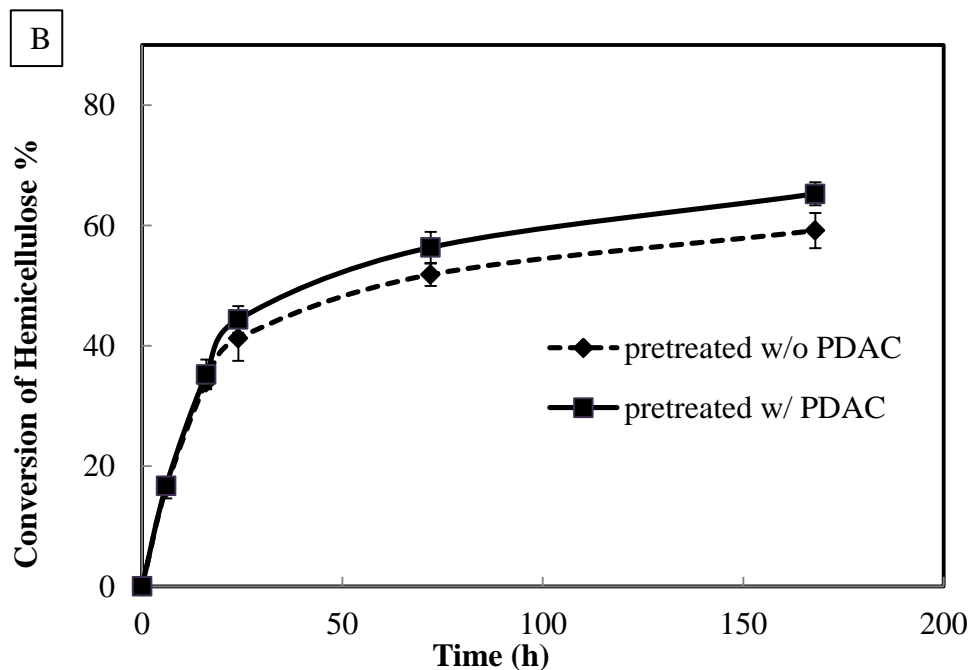


Figure 5. 5 Sugar conversions of 0.4% (w/v) NaOH and 10 mM PDADMAC pretreated corn stover. The substrate loading is 2% (w/v) and enzyme loading is 20 FPU/g glucan.

Figure 5.5 (cont'd)



However, it has been noted that the presence of lignin hinders the enzymatic hydrolysis not only as a physical barrier but also by forming unproductive binding with enzymes [208, 250]. Therefore, this contradiction suggests that the addition of PDAC could change either the lignin structure or the interaction between lignin and enzymes. Many research work has shown the increased sugar conversion led by structural changes in lignin during the pretreatment processes, where lignin was isolated, migrated, and redistributed as droplets onto the fiber surface [180, 185, 239, 248]. This has been suggested to increase the pore volume and surface area of pretreated biomass and improved their hydrolysis. It is similar to the structural changes in our system resulting from the destruction and redistribution of lignin as droplets with polyelectrolyte and kinked or curled cellulose fibrils from the surface. Lignin is also likely shielded from interacting with enzymes by the formation of complex with polyelectrolytes [209]. In

addition, cationic polyelectrolytes have been reported to increase the rate of enzymatic conversion of cellulose fiber to glucose via eliminating the repulsion and increasing the binding between enzymes and the substrate [215, 231]. Enhancements of cellulose and hemicellulose conversions by PDAC shed the light on the possibilities of reducing the amount of enzyme usage and increasing the economic efficiency of hydrolysis process. This is a promising alternative to reduce the dosage of high price enzymes with low cost polyelectrolytes. Together with our short-time and low temperature pretreatment processing (2 min or less and room temperature), this operation is beneficial to achieve both effective pretreatment and enzymatic hydrolysis.

5.5 CONCLUSION

Polyelectrolyte shows its potential as a pretreatment additive that facilitates the lignin redistribution and increases both cellulose and hemicellulose conversions in the subsequent enzymatic hydrolysis. Instead of migrating away from cell wall matrix, the lignin formed globular complex with cationic polyelectrolytes and redeposited on the surface or in the microfibril matrix of pretreated corn stover. Cell wall layers experienced significantly morphological changes with retained lignin drops and fibrillated cellulose compared to the pretreatment without the polyelectrolyte addition. These changes contribute to greater accessibility and less inhibitory action of lignocellulosic carbohydrates to enzymes. The polyelectrolyte addition appears to be an effective means to enhance the hydrolysis efficiency with no need for large fractionation of lignocellulosic components. The modification of cellulose surface can also be easily achieved.

Chapter 6

Future Work

Transitional behavior of polymeric hollow microsphere formation by emulsion

diffusion method

- We have found that the viscosity of the aqueous continuous phase and the emulsification temperature are two key processing parameters to obtain the open-hollow structure PLA particles by single emulsion method. The formation of multiple emulsions is greatly related to the droplet interactions during emulsification, including breakup and coalescence. Therefore, besides the mixing conditions, the solution conditions can also affect the interactions between droplets, such as pH and salt concentration in the aqueous phase solution. The fabrication process needs to be optimized to better control the particle size and size distribution.
- More different types of polymers can be tried with emulsion polymerization by this method. Polymer monomers are dissolved in the oil phase solution. The control of those processing parameters can still be applied to manipulate the formation of final polymers in different particle shapes and sizes.
- Instead of using surfactants, solid particles can be added in the aqueous phase solution to stabilize the emulsion droplets, which is named as pickering emulsion. The addition of solid particles may create new materials with interesting properties and geometries.

Encapsulation of hydrophilic materials into hydrophobic polymer by emulsion solvent removal technique

- Iron oxide nanoparticles and nisin peptides have been successfully encapsulated into the polymer matrix, forming hollow structure composite particles. The optimal encapsulation conditions need to be further determined. Release properties, such as degradation rate and stability can be explored to better understand the properties of composite particles.
- The range of new materials that can be incorporated can be increased, achieving more value-added products. The dynamic control of encapsulated particles in the nano-size can be investigated to open up new product attributes.

Fractionation of corn stover by a novel nanoshear hybrid alkaline pretreatment

- Our hybrid pretreatment has been shown to efficiently facilitate the removal of lignin and hemicellulose from bulk materials. Due to this advantage, other feedstocks with high lignin or hemicellulose content can be also tested. Other pretreatment conditions, such as alkaline to substrate ratio and temperature, can be examined to build up the pretreatment profile.
- Alkaline pretreatment has been reported as an effective process even at reduced temperatures. Besides sodium hydroxide, other chemicals such as calcium hydroxide, aqueous ammonia, alkaline hydrogen peroxide, and the combination of any of them can be investigated to achieve the effective pretreatment and reduced cost.

- Based on the experimental data, simulation of the bulk material-to-sugar conversion can be conducted to evaluate the overall effectiveness and economy.

Impact of cationic polyelectrolyte on the nanoshear hybrid alkaline pretreatment of corn stover

- The addition of cationic polyelectrolyte has shown its positive effect on the modification of biomass surface and improvement of enzymatic hydrolysis. Experimental conditions, such as polyelectrolyte loading and polyelectrolyte to alkali ratio, can be further studied to optimize the process effectiveness. The quantification of polyelectrolyte in the residues needs to be conducted to better understand the interaction between polyelectrolyte and biomass materials.
- Further verification of proposed mechanism on the enzyme attachment test can be also studied to allow a better understanding of the additive effect. Lower alkaline concentration and enzyme loading can be tested to evaluate its application on the reduced alkali and enzyme loading.
- The isolation of lignin drops can be carried out before and after enzymatic hydrolysis to better understand the effect of polyelectrolyte on the lignin structure.
- Besides PDAC, other types of cationic polyelectrolytes such as c-PAM and cationic starch, can be also tested by this method.

REFERENCES

REFERENCES

1. Asa, T., *Method of and apparatus for agitating treatment liquid*, 1996: US.
2. Daniel P. Lathrop, J.F., Harry L. Swinney, *Transition to shear-driven turbulence in Couette-Taylor flow*. *Physical Review A*, 1992. **46**(10): p. 6390-6405.
3. Hinze, J.O., *Fundamentals of the hydrodynamic mechanism of splitting in dispersion processes*. *AIChE Journal*, 1955. **1**(3): p. 289-295.
4. Kolmogorov, A.N., *On the breaking of drops in turbulent flow*. *Doklady Akademii Nauk URSS*, 1949. **66**(5): p. 825-828.
5. C Medina, M.S.-M., A Radomski, OI Corrigan, MW Radomski, *Nanoparticles: pharmacological and toxicological significance*. *British Journal of Pharmacology*, 2007. **150**: p. 552-558.
6. Minchao Zhang, Y.L., Da Wang, Rui Yan, Shengnan Wang, Li Yang, Wangqing Zhang, *Synthesis of polymeric yolk-shell microspheres by seed emulsion polymerization*. *Macromolecules*, 2011. **44**: p. 842-847.
7. Laura Ann Bauer, N.S.B., Gerald J. Meyer, *Biological applications of high aspect ratio nanoparticles*. *Journal of Materials Chemistry*, 2004. **14**: p. 517-526.
8. Nan Li, G.Y., Yaning He, Xiaogong Wang, *Hollow microspheres of amphiphilic azo homopolymers: self-assembly and photoinduced deformation behavior*. *Chemical Communications*, 2011. **47**(16): p. 4757-4759.
9. Guohe Hu, D.Y., Jing Zhang, Honglu Liang, *Optical detection of the morphology of hollow polymer particles prepared from seeded emulsions in the presence of n-octanol*. *Colloids and Surfaces A: Physicochemical and Engineering Aspects*, 2010. **356**(1-3): p. 78-83.
10. Michael J. Heslinga, E.M.M., Omolola Eniola-Adefeso, *Fabrication of biodegradable spheroidal microparticles for drug delivery applications*. *Journal of Controlled Release*, 2009. **138**: p. 235-242.
11. Guo-Dong Fu, G.L.L., K.G. Neoh, E.T. Kang, *Hollow polymeric nanostructures-Synthesis, morphology and function*. *Progress in Polymer Science*, 2011. **36**: p. 127-167.
12. Xiong Wen Lou, L.A.A., Zichao Yang, *Hollow Micro-/Nanostructures: Synthesis and applications*. *Advanced Materials*, 2008. **20**(21): p. 3987-4019.
13. Wei Bin, W.S., Song Hongguang, Liu Hongyan, Li Jie, Liu Ning, *A review of recent progress in preparation of hollow polymer microspheres*. *Petroleum Science*, 2009. **6**(3): p. 306-312.

14. Milad Al Helou, N.A., Marie-Alice Guedeau-Boudeville, Michael Rosticher, Ahmed Mourchid, *Structure and mechanical properties of polylactide copolymer microspheres and capsules*. *Polymer*, 2010. **51**(23): p. 5440-5447.
15. Yichen Cao, B.Y., Limin Wu, *Facile fabrication of hollow polymer microspheres through the phase-inversion method*. *Langmuir*, 2010. **26**(9): p. 6115-6118.
16. Guoliang Li, X.Y., Bin Wang, Junyou Wang, Xinlin Yang, *Monodisperse temperature-responsive hollow polymer microspheres: Synthesis, characterization and biological application*. *Polymer*, 2008. **49**: p. 3436-3443.
17. Shiding Miao, C.Z., Zhimin Liu, Buxing Han, Yun Xie, Sujiang Ding, Zhenzhong Yang, *Highly efficient nanocatalysts supported on hollow polymer nanospheres: Synthesis, characterization, and applications*. *Journal of Physical Chemistry*, 2008. **112**(3): p. 774-780.
18. Hassan Sawalha, K.S., Remko Boom, *Biodegradable polymeric microcapsules: Preparation and properties*. *Chemical Engineering Journal*, 2011. **169**: p. 1-10.
19. Xiaoying Yang, L.C., Bin Han, Xinlin Yang, Hongquan Duan, *Preparation of magnetite and tumor dual-targeting hollow polymer microspheres with pH-sensitivity for anticancer drug-carriers*. *Polymer*, 2010. **51**(12): p. 2533-2539.
20. K. Bouchemal, S.B., E. Perrier, H. Fessi, *Nano-emulsion formulation using spontaneous emulsification: solvent, oil and surfactant optimisation*. *International Journal of Pharmaceutics*, 2004. **280**: p. 241-251.
21. Capek, I., *Preparation of metal nanoparticles in water-in-oil (w/o) microemulsions*. *Advances in Colloid and Interface Science*, 2004. **110**: p. 49-74.
22. Dong-Hwang Chen, S.-H.W., *Synthesis of Nickel nanoparticles in water-in-oil microemulsions*. *Chemistry of Materials*, 2000. **12**(5): p. 1354-1360.
23. D.Y. Han, H.Y.Y., C.B. Shen, X. Zhou, F.H. Wang, *Synthesis and size control of NiO nanoparticles by water-in-oil microemulsion*. *Powder Technology*, 2004. **147**: p. 113-116.
24. Christian Zimmermann, C.F., Matthias Wanner, Dagmar Gerthsen, *Nanoscale gold hollow spheres through a microemulsion approach*. *Small*, 2007. **3**(8): p. 1347-1349.
25. Sang Jyuk Im, U.J., Younan Xia, *Polymer hollow particles with controllable holes in their surfaces*. *Nature Materials*, 2005. **4**(9): p. 671-675.
26. Tanaka, T., et al., *A Novel Approach for Preparation of Micrometer-sized, Monodisperse Dimple and Hemispherical Polystyrene Particles*. *Langmuir*, 2010. **26**(6): p. 3848-3853.
27. Meng Li, J.X., *Facile route to synthesize polyurethane hollow microspheres with size-tunable single holes*. *Langmuir*, 2011. **27**: p. 3229-3232.

28. Rosler, A., G.W.M. Vandermeulen, and H.A. Klok, *Advanced drug delivery devices via self-assembly of amphiphilic block copolymers*. *Adv Drug Delivery Reviews*, 2001. **53**: p. 95-108.
29. Fu, G.-D., et al., *Hollow polymeric nanostructures—Synthesis, morphology and function*. *Progress in Polymer Science*, 2011. **36**(1): p. 127-167.
30. Narayan, P., D. Marchant, and M.A. Wheatley, *Optimization of spray drying by factorial design for production of hollow microspheres for ultrasound imaging*. *J Biomed Mater Res*, 2001. **56**(3): p. 333-41.
31. McDonald, C.J. and M.J. Devon, *Hollow latex particles: Synthesis and applications*. *Adv Colloid Interface Sci*, 2002. **99**: p. 181-213.
32. Mu, B., R. Shen, and P. Liu, *Crosslinked polymeric nanocapsules from polymer brushes grafted silica nanoparticles via surface-initiated atom transfer radical polymerization*. *Colloids Surf B Biointerfaces*, 2009. **74**(2): p. 511-5.
33. Okubo, M. and T. Nakagawa, *Formation of multihollow structures in crosslinked composite polymer particles*. *Colloid Polym Sci*, 1994. **272**: p. 530-35.
34. Quintanar-Guerrero, D., et al., *A mechanistic study of the formation of polymer nanoparticles by the emulsification-diffusion technique*. *Colloid Polym Sci*, 1997. **275**: p. 640-47.
35. Rosca, I.D., F. Watari, and M. Uo, *Microparticle formation and its mechanism in single and double emulsion solvent evaporation*. *J Control Release*, 2004. **99**(2): p. 271-80.
36. Gao, F., et al., *Double emulsion templated microcapsules with single hollow cavities and thickness-controllable shells*. *Langmuir*, 2009. **25**(6): p. 3832-8.
37. Sawalha, H., K. Schroën, and R. Boom, *Biodegradable polymeric microcapsules: Preparation and properties*. *Chemical Engineering Journal*, 2011. **169**(1-3): p. 1-10.
38. Guinebretiere, S., et al., *Study of the emulsion-diffusion of solvent: preparation and characterization of nanocapsules*. *Drug Development Research*, 2002. **57**(1): p. 18-33.
39. Moinard-Checot, D., et al., *Mechanism of nanocapsules formation by the emulsion-diffusion process*. *J Colloid Interface Sci*, 2008. **317**(2): p. 458-68.
40. Ji, S.W., et al., *Transitional behavior of polymeric microsphere formation in turbulent shear flow by emulsion diffusion method*. *Polymer*, 2012. **53**: p. 205-12.
41. Kumar, S., *On phase inversion characteristics of stirred dispersions*. *Chem Eng Sci*, 1996. **51**(5): p. 831-34.
42. Cao, Y., B. You, and L. Wu, *Facile fabrication of hollow polymer microspheres through the phase-inversion method*. *Langmuir*, 2010. **26**(9): p. 6115-8.

43. Sawalha, H., et al., *Poly lactide microspheres prepared by premix membrane emulsification—Effects of solvent removal rate*. Journal of Membrane Science, 2008. **310**(1-2): p. 484-493.
44. Sawalha, H., et al., *Preparation of hollow poly lactide microcapsules through premix membrane emulsification—Effects of nonsolvent properties*. Journal of Membrane Science, 2008. **325**(2): p. 665-671.
45. Asua, J.M., *Emulsion polymerization: From fundamental mechanisms to process developments*. J Polym Sci Part A, 2004. **42**: p. 1025-41.
46. Kowalski, A., M. Vogel, and R.M. Blankenship, *Sequential heteropolymer dispersion and a particulate material obtainable therefrom, useful in coating compositions as a thickening and/or opacifying agent*, 1984: US Patent.
47. McDonald, C.J., K.J. Bouck, and A.B. Chaput, *Emulsion polymerization of voided particles by encapsulation of a nonsolvent*. Macromolecules, 2000. **33**: p. 1593-1605.
48. Wang, H.G., P. Chen, and X.M. Zheng, *Hollow permeable polysiloxane capsules: a novel approach for fabrication, guest encapsulation and morphology studies*. J Mater Chem, 2004. **14**: p. 1648-51.
49. Yang, X., et al., *Synthesis of pH-sensitive hollow polymer microspheres and their application as drug carriers*. Polymer, 2009. **50**(15): p. 3556-3563.
50. Chen, Y., et al., *Preparation of polymeric nanocapsules by radiation induced miniemulsion polymerization*. European Polymer Journal, 2007. **43**(7): p. 2848-2855.
51. Shirin-Abadi, A.R., A.R. Mahdavian, and S. Khoei, *New Approach for the Elucidation of PCM Nanocapsules through Miniemulsion Polymerization with an Acrylic Shell*. Macromolecules, 2011: p. 110902093317070.
52. Zhang, L.F. and A. Eisenberg, *Multiple morphologies of Crew Cut aggregates of Polystyrene-*b*-Poly(acrylic acid) block copolymers*. Science, 1995. **268**(5218): p. 1728-31.
53. Antonietti, M. and F. S., *Vesicles and liposomes: A self assembly principle beyond lipids*. Adv Mater, 2003. **15**(16): p. 1323-33.
54. Petrov, P.D., M. Drechsler, and A.H.E. Muller, *Self-assembly of asymmetric poly(ethylene oxide)-block-poly(*n*-butyl acrylate) diblock copolymers in aqueous media to unexpected morphologies*. J Phys Chem B, 2009. **113**: p. 4218-25.
55. Qian, J. and F.P. Wu, *Vesicles prepared from supramolecular block copolymers*. Macromolecules, 2008. **41**: p. 8921-26.
56. Yu, Y., L.F. Zhang, and A. Eisenberg, *Morphogenic effect of solvent on crew-cut aggregates of amphiphilic diblock copolymers*. Macromolecules, 1998. **31**: p. 1144-1154.

57. Shen, H.W., L.F. Zhang, and A. Eisenberg, *Multiple pH-induced morphological changes in aggregates of polystyrene-block-poly(4-vinylpyridine) in DMF/H₂O mixtures*. *J Am Chem Soc*, 1999. **121**: p. 2728-40.
58. Discher, B.M., et al., *Polymersomes: Tough Vesicles Made from Diblock Copolymers*. *Science*, 1999. **284**(5417): p. 1143-1146.
59. Maskos, M. and J.R. Harris, *Double-shell vesicles, strings of vesicles and filaments found in crosslinked micellar solutions of poly(1,2-butadiene)-block-poly(ethylene oxide) diblock copolymers*. *Macromol Rapid Commun*, 2001. **22**: p. 271-73.
60. Ahmed, F., et al., *Block copolymer assemblies with cross-link stabilization: from single-component monolayers to bilayer blends with PEO-PLA*. *Langmuir*, 2003. **19**: p. 6505-11.
61. Stoenescu, R. and W. Meier, *Vesicles with asymmetric membranes from amphiphilic ABC triblock copolymers*. *Chemical Communications*, 2002(24): p. 3016-3017.
62. Holder, S.J., et al., *The first example of a poly(ethylene oxide)-poly(methylphenylsilane) amphiphilic block copolymer: vesicle formation in water*. *Chemical Communications*, 1998(14): p. 1445-1446.
63. Jenekhe, S.A., *Self-Assembled Aggregates of Rod-Coil Block Copolymers and Their Solubilization and Encapsulation of Fullerenes*. *Science*, 1998. **279**(5358): p. 1903-1907.
64. Yang, J., et al., *Formation of polymer vesicles by liquid crystal amphiphilic block copolymers*. *Langmuir*, 2006. **22**: p. 7907-11.
65. Duan, H.W., et al., *Self-assembly of unlike homopolymers into hollow spheres in nonselective solvent*. *J Am Chem Soc*, 2001. **123**: p. 12097-098.
66. Kuang, M., et al., *A novel approach to polymeric hollow nanospheres with stabilized structure* *Electronic supplementary information (ESI) available: experimental details*. See <http://www.rsc.org/suppdata/cc/b2/b210851h>. *Chemical Communications*, 2003(4): p. 496-497.
67. Caruso, F., *Hollow capsule processing through colloidal templating and self assembly*. *Chemistry-A European Journal*, 2000. **6**(3): p. 413.
68. Okubo, M., K. Ichikawa, and M. Fujimura, *Production of multi-hollow polymer microspheres by stepwise alkali/acid method II. Alkali treatment process*. *Colloid Polym Sci*, 1991. **269**: p. 1257-62.
69. Okubo, M., A. Ito, and T. Kanenobu, *Production of submicron-sized multihollow polymer particles by alkali/cooling method*. *Colloid Polym Sci*, 1996. **274**: p. 801-04.
70. Okubo, M., A. Ito, and A. Hashiba, *Production of submicron-sized multihollow polymer particles having high transition temperatures by the stepwise alkali/acid method*. *Colloid Polym Sci*, 1996. **274**: p. 428-32.

71. Deng, W., et al., *Influences of MAA on the porous morphology of P(St-MAA) latex particles produced by batch soap-free emulsion polymerization followed by stepwise alkali/acid post-treatment*. J Colloid Interface Sci, 2010. **349**(1): p. 122-6.
72. Yuan, Q., et al., *The mechanism of the formation of multihollow polymer spheres through sulfonated polystyrene particles*. Langmuir, 2009. **25**: p. 2729-35.
73. Okubo, M., et al., *Preparation of micron-size monodisperse polymer particles by seeded polymerization utilizing the dynamic monomer swelling method*. Colloid Polym Sci, 1991. **269**: p. 222-26.
74. Okubo, M. and H. Minami, *Formation mechanism of micron-sized monodispersed polymer particles having a hollow structure*. Colloid Polym Sci, 1997. **275**(992-97): p. 992.
75. Kobayashi, H., et al., *Preparation of multihollow polystyrene particles by seeded emulsion polymerization using seed particles with incorporated nonionic emulsifier: Effect of temperature*. Colloid Polym Sci, 2009. **287**(3): p. 251-57.
76. Srisopa, A., A.M. Imroz Ali, and A.G. Mayes, *Understanding and preventing the formation of deformed polymer particles during synthesis by a seeded polymerization method*. Journal of Polymer Science Part A: Polymer Chemistry, 2011. **49**(9): p. 2070-2080.
77. Hyuk Im, S., U. Jeong, and Y. Xia, *Polymer hollow particles with controllable holes in their surfaces*. Nat Mater, 2005. **4**(9): p. 671-5.
78. Decher, G., *Fuzzy Nanoassemblies: Toward Layered Polymeric Multicomposites*. Science, 1997. **277**(5330): p. 1232-1237.
79. Sukhorukov, G.B., et al., *Stepwise polyelectrolyte assembly on particle surfaces: a novel approach to colloid design*. Polym Adv Technol, 1998. **9**: p. 759-67.
80. Sukhorukov, G.B., et al., *Layer-by-layer self assembly of polyelectrolytes on colloidal particles*. Colloids Surf A: Physicochem Eng Aspects, 1998. **137**: p. 253-66.
81. Caruso, F., *Nanoengineering of Inorganic and Hybrid Hollow Spheres by Colloidal Templating*. Science, 1998. **282**(5391): p. 1111-1114.
82. Yuan, W., Z. Lu, and C.M. Li, *Controllably layer-by-layer self-assembled polyelectrolytes/nanoparticle blend hollow capsules and their unique properties*. Journal of Materials Chemistry, 2011. **21**(13): p. 5148.
83. Dejugnat, C. and G.B. Sukhorukov, *pH-responsive properties of hollow polyelectrolyte microcapsules templated on various cores*. Langmuir, 2004. **20**: p. 7265-69.
84. Donath, E., et al., *Hollow polymer shells from biological templates: fabrication and potential applications*. Chem Eur J, 2002. **8**(23): p. 5481-85.
85. Kaul, S., *Myocardial contrast echocardiography*. Circulation, 1997. **96**: p. 3745-60.

86. Shchukin, D.G., et al., *Gas-filled polyelectrolyte capsules*. *Angew Chem Int Ed Engl*, 2005. **44**(21): p. 3310-4.
87. Winterhalter, M. and A.F. Sonnen, *Stable air bubbles--catch them if you can!* *Angew Chem Int Ed Engl*, 2006. **45**(16): p. 2500-2.
88. Daiguji, H., E. Matsuoka, and S. Muto, *Fabrication of hollow poly-allylamine hydrochloride/poly-sodium styrene sulfonate microcapsules from microbubble templates*. *Soft Matter*, 2010. **6**(9): p. 1892.
89. Wang, A.-J., Y.-P. Lu, and R.-X. Sun, *Recent progress on the fabrication of hollow microspheres*. *Materials Science and Engineering: A*, 2007. **460-461**: p. 1-6.
90. Xu, Q., et al., *Preparation of monodisperse biodegradable polymer microparticles using a microfluidic flow-focusing device for controlled drug delivery*. *Small*, 2009. **5**(13): p. 1575-81.
91. Lensen, D., et al., *Preparation of biodegradable liquid core PLLA microcapsules and hollow PLLA microcapsules using microfluidics*. *Macromol Biosci*, 2010. **10**(5): p. 475-80.
92. Ganan-Calvo, A.M., J. Davila, and A. Barrero, *Current and droplet size in the electrospraying of liquid. Scaling laws*. *J Aerosol Sci*, 1997. **28**(2): p. 249-75.
93. Chang, M.W., E. Stride, and M. Edirisinghe, *Controlling the thickness of hollow polymeric microspheres prepared by electrohydrodynamic atomization*. *J R Soc Interface*, 2010. **7 Suppl 4**: p. S451-60.
94. Slavka Tcholakova, N.V., Nikolai D. Denkov, Thomas Danner, *Emulsification in turbulent flow: 3. Dayghter drop-size distribution*. *Journal of Colloid and Interface Science*, 2007. **310**: p. 570-589.
95. Nina Vankova, S.T., Nikolai D. Denkov, Ivan B. Ivanov, Vassil D. Vulchev, Thomas Danner, *Emulsification in turbulent flow: 1. Mean and maximum drop diameters in inertial and viscous regimes*. *Journal of Colloid and Interface Science*, 2007. **312**: p. 363-380.
96. Nina Vankova, S.T., Nikolai D. Denkov, Vassil D. Vulchev, Thomas Danner, *Emulsification in turbulent flow: 2. Breakage rate constants*. *Journal of Colloid and Interface Science*, 2007. **313**: p. 612-629.
97. Daniel P. Lathrop, J.F., Harry L. Swinney, *Turbulent flow between concentric rotating cylinders at large Reynolds number*. *Physical Review Letters*, 1992. **68**(10): p. 1515-1518.
98. F. Bouchama, G.A.v.A., A.J.E. Autin, G.J.M. Koper, *On the mechanism of catastrophic phase inversion in emulsions*. *Colloids and Surfaces A: Physicochemical and Engineering Aspects*, 2003. **231**: p. 11-17.
99. Shahriar Sajjadi, F.J., Brian W. Brooks, *Phase inversion in abnormal O/W/O emulsions: I. Effect of surfactant concentration*. *Industrial and Engineering Chemistry Research*, 2002. **41**(24): p. 6033-6041.

100. Kumar, S., *On phase inversion characteristics of stirred dispersions*. Chemical Engineering Science, 1996. **51**(5): p. 831-834.
101. F. Groeneweg, W.G.M.A., P. Jaeger, J.J.M. Janssen, J.A. Wieringa, J.K. Klahn, *On the mechanism of the inversion of emulsions*. Chemical Engineering Research and Design, 1998. **76**(A1): p. 55-63.
102. K.S. Soppimath, T.M.A., *Ethyl acetate as a dispersing solvent in the production of poly(DL-lactide-co-glycolide) microspheres: effect of process parameters and polymer type*. Journal of Microencapsulation, 2002. **19**(3): p. 281-292.
103. Delphine Moinard-Checot, Y.C., Stephanie Briancon, Laurent Beney, Hatem Fessi, *Mechanism of nanocapsules formation by the emulsion-diffusion process*. Journal of Colloid and Interface Science, 2008. **317**: p. 458-468.
104. L.A. Girifalco, R.J.G., *A theory for the estimation of surface and interfacial energies. I. Derivation and application to interfacial tension*. Journal of Physical Chemistry, 1957. **61**(7): p. 904-909.
105. Davar Khossravi, K.A.C., *Solvent effects on chemical processes. 3. Surface tension of binary aqueous organic solvents*. Journal of Solution Chemistry, 1993. **22**(4): p. 321-330.
106. Cheng, N.-S., *Formula for the viscosity of a glycerol-water mixture*. Industrial and Engineering Chemistry Research, 2008. **47**: p. 3285-3288.
107. Sherman, P., *Emulsion Science*. 1968: Academic Press.
108. Park, J.H., M.L. Ye, and K. Park, *Biodegradable polymers for microencapsulation of drugs*. Molecules, 2005. **10**: p. 146.
109. Anal, A.K. and H. Singh, *Recent advances in microencapsulation of probiotics for industrial applications and targeted delivery*. Trends in Food Science & Technology, 2007. **18**(5): p. 240-251.
110. Kuang, S.S., J.C. Oliveira, and A.M. Crean, *Microencapsulation as a tool for incorporating bioactive ingredients into food*. Crit Rev Food Sci Nutr, 2010. **50**(10): p. 951-68.
111. Nakano, M., *Places of emulsions in drug delivery*. Advanced Drug Delivery Reviews, 2000. **45**: p. 1.
112. Freiberg, S. and X.X. Zhu, *Polymer microspheres for controlled drug release*. International Journal of Pharmaceutics, 2004. **282**: p. 1.
113. Li, M., O. Rouaud, and D. Poncet, *Microencapsulation by solvent evaporation: State of the art for process engineering approaches*. International Journal of Pharmaceutics, 2008. **363**: p. 26.

114. Yang, Y.Y., T.S. Chung, and N.P. Ng, *Morphology, drug distribution, and in vitro release profiles of biodegradable polymeric microspheres containing protein fabricated by double-emulsion solvent extraction/evaporation method*. *Biomaterials*, 2001. **22**: p. 231.
115. de Kruijff, C.G., F. Weinbreck, and R. de Vries, *Complex coacervation of proteins and anionic polysaccharides*. *Current Opinion in Colloid & Interface Science*, 2004. **9**(5): p. 340-349.
116. Tobio, M., et al., *Stealth PLA-PEG Nanoparticles as Protein Carriers for Nasal Administration*. *Pharmaceutical Research*, 1998. **15**: p. 270.
117. Blanco, M.D. and M.J. Alonso, *Development and characterization of protein-loaded poly(lactide-co-glycolide) nanospheres*. *European Journal of Pharmaceutics and Biopharmaceutics*, 1997. **43**: p. 287.
118. Morita, T., et al., *Protein encapsulation into biodegradable microspheres by a novel S/O/W emulsion method using poly(ethylene glycol) as a protein micronization adjuvant*. *Journal of Controlled Release*, 2000. **69**: p. 435.
119. Huang, Q.R., P. Given, and M. Qian, *Micro/Nanoencapsulation of active food ingredients*. ACS symposium series. Vol. 1007. 2009, Washington, DC: American Chemical Society.
120. Ghosh, S.K., *Functional Coatings: by polymer microencapsulation*. *Functional coatings and microencapsulation: A general perspective*. 2006, Germany: Wiley-VCH.
121. Masao Kohayashi, K., et al., *Method for producing sustained release microsphere preparation*, in *US Patent* 1996.
122. Jiang, W.L. and S.P. Schwendeman, *Stabilization and controlled release of Bovine Serum Albumin encapsulated in poly(D,L-lactide) and poly(ethylene glycol) microsphere blends*. *Pharmaceutical Research*, 2001. **18**: p. 878.
123. Lemoine, D. and V. Preat, *Polymeric nanoparticles as delivery system for influenza virus glycoproteins*. *Journal of Controlled Release*, 1998. **54**: p. 15.
124. Ito, F., H. Fujimori, and K. Makino, *Incorporation of water-soluble drugs in PLGA microspheres*. *Colloids Surf B Biointerfaces*, 2007. **54**(2): p. 173-8.
125. De Jong, B. and H. Kruyt, *P K Akad Wet-Amsterd*, 1929. **32**(849).
126. Thomasin, C., H.P. Merkle, and B.A. Gander, *Physico-chemical parameters governing protein microencapsulation into biodegradable polyesters by coacervation*. *International Journal of Pharmaceutics*, 1997. **147**: p. 173.
127. Huang, Y.I., et al., *Microencapsulation of extract containing shikonin using gelatin-acacia coacervation method: a formaldehyde-free approach*. *Colloids Surf B Biointerfaces*, 2007. **58**(2): p. 290-7.

128. Yeo, Y., *A new process for making reservoir-type microcapsules using ink-jet technology and interfacial phase separation*. Journal of Controlled Release, 2003. **93**(2): p. 161-173.
129. Stefanescu, E.A., C. Stefanescu, and Negulescu, Il, *Biodegradable polymeric capsules obtained via room temperature spray drying: preparation and characterization*. J Biomater Appl, 2011. **25**(8): p. 825-49.
130. Jafari, S.M., et al., *Encapsulation Efficiency of Food Flavours and Oils during Spray Drying*. Drying Technology, 2008. **26**(7): p. 816-835.
131. Fu, Y.J., et al., *Characteristic and controlled release of anticancer drug loaded poly(D,L-lactide) microparticles prepared by spra drying technique*. Journal of Microencapsulation, 2001. **18**(6): p. 733.
132. Garcera, M.J.G., et al., *In vitro pore-forming activity of the lantibiotic nisin Role of protonmotive force and lipid composition*. European Journal of Biochemistry, 1993. **212**: p. 417.
133. Davies, E.A., et al., *Research note: The effect of pH on the stability of nisin solution during autoclaving*. Letters in Applied Microbiology, 1998. **27**: p. 186.
134. Abee, T., et al., *Mode of action of nisin Z against Listeria monocytogenes Scott A grown at high and low temperatures*. Applied and Environmental Microbiology, 1994. **60**: p. 1962.
135. Jin, T. and H. Zhang, *Biodegradable polylactic acid polymer with nisin for use in antimicrobial food packaging*. J Food Sci, 2008. **73**(3): p. M127-34.
136. Guiotto, A., et al., *PEGylation of the antimicrobial peptide nisin A: problems and perspectives*. Il Farmaco, 2003. **58**: p. 4.
137. Allemann, E., J.C. Leroux, and R. Gurny, *Polymeric nano- and microparticles for the oral delivery of peptides and peptidomimetics*. Advanced Drug Delivery Reviews, 1998. **34**: p. 171.
138. Scaffaro, R., L. Botta, and G. Gallo, *Photo-oxidative degradation of poly(ethylene-co-vinyl acetate)/nisin antimicrobial films*. Polymer Degradation and Stability, 2012. **97**(4): p. 653-660.
139. Ahmed, N., et al., *Modified double emulsion process as a new route to prepare submicron biodegradable magnetic/polycaprolactone particles for in vivo theranostics*. Soft Matter, 2012. **8**(8): p. 2554.
140. Yang, S. and H. Liu, *A novel approach to hollow superparamagnetic magnetite/polystyrene nanocomposite microspheres via interfacial polymerization*. Journal of Materials Chemistry, 2006. **16**(46): p. 4480.

141. Wang, Y., et al., *Formulation of Superparamagnetic Iron Oxides by Nanoparticles of Biodegradable Polymers for Magnetic Resonance Imaging*. *Advanced Functional Materials*, 2008. **18**(2): p. 308-318.
142. Zhao, H., K. Saatchi, and U.O. Häfeli, *Preparation of biodegradable magnetic microspheres with poly(lactic acid)-coated magnetite*. *Journal of Magnetism and Magnetic Materials*, 2009. **321**(10): p. 1356-1363.
143. Chen, A.Z., et al., *Development of Fe₃O₄-poly(L-lactide) magnetic microparticles in supercritical CO₂*. *J Colloid Interface Sci*, 2009. **330**(2): p. 317-22.
144. Chung, T.-H. and W.-C. Lee, *Preparation of styrene-based, magnetic polymer microspheres by a swelling and penetration process*. *Reactive and Functional Polymers*, 2008. **68**(10): p. 1441-1447.
145. Arias, J.T., et al., *Synthesis and characterization of poly(ethyl-2-cyanoacrylate) nanoparticles with a magnetic core*. *Journal of Controlled Release*, 2001. **77**: p. 309.
146. Liu, Z.L., et al., *Synthesis and characterization of ultrafine well-dispersed magnetic nanoparticles*. *Journal of Magnetism and Magnetic Materials*, 2004. **283**(2-3): p. 258-262.
147. Massart, R., *Preparation of Aqueous Magnetic Liquids in Alkaline and Acidic Media*. *IEEE Transactions on Magnetics*, 1981. **17**(2): p. 1247-1248.
148. Wellisch, M., et al., *Biorefinery systems-Potential contributors to sustainable innovation*. *Biofuels, Bioproducts and Biorefining*, 2010. **4**: p. 275.
149. Bozell, J.J. and G.R. Petersen, *Technology development for the production of biobased products from biorefinery carbohydrates—the US Department of Energy's "Top 10" revisited*. *Green Chemistry*, 2010. **12**: p. 539.
150. Budarin, V.S., PS; Dodson, JR, et al., *Use of green chemical technologies in an integrated biorefinery*. *Energy & Environmental Science*, 2011. **4**(2): p. 471-479.
151. Takara, D.K., SK, *Green processing of tropical banagrass into biofuel and biobased products: An innovation biorefinery approach*. *Bioresource Technology*, 2011. **102**(2): p. 1587-1592.
152. Cherubini, F.J., G; Wellisch, M, et al., *Toward a common classification approach for biorefinery systems*. *Biofuels Bioproducts & Biorefining-Biofpr*, 2009. **3**(5): p. 534-546.
153. FitzPatrick, M., et al., *A biorefinery processing perspective: treatment of lignocellulosic materials for the production of value-added products*. *Bioresour Technol*, 2010. **101**(23): p. 8915-22.
154. Singh, P.N.R., T.; Dalel Singh, *Pretreatment of lignocellulosic substrates*. *Concise Encyclopedia of Bioresource Technology*, 2004: p. 663-670.

155. Galbe, M. and G. Zacchi, *A review of the production of ethanol from softwood*. Appl Microbiol Biotechnol, 2002. **59**: p. 618.
156. Mosier, N.W., C; Dale, B, et al., *Features of promising technologies for pretreatment of lignocellulosic biomass*. Bioresource Technology, 2005. **96**(6): p. 673-686.
157. Yang, B.W., CE, *Pretreatment: the key to unlocking low-cost cellulosic ethanol*. Biofuels Bioproducts & Biorefining-Biofpr, 2008. **2**(1): p. 26-40.
158. Gargulak, J.L., SE, *Commercial use of lignin-based materials*. Lignin: Historical, Biological, and Materials Perspectives, 2000. **742**: p. 304-320.
159. El Mansouri, N.E.S., J., *Structural characterization of technical lignins for the production of adhesives: Application to lignosulfonate, kraft, soda-anthraquinone, organosolv and ethanol process lignins*. Industrial Crops and Products, 2006. **24**(1): p. 8-16.
160. Nadji, H., et al., *Value-added derivatives of soda lignin from alfa grass (Stipa tenacissima). I. Modification and characterization*. Journal of Applied Polymer Science, 2010. **115**: p. 1546.
161. Jorgensen, H., J.B. Kristensen, and C. Felby, *Enzymatic conversion of lignocellulose into fermentable sugars: Challenges and opportunities*. Biofuels, Bioproducts and Biorefining, 2007. **1**: p. 119.
162. Galbe, M.Z., G, *A review of the production of ethanol from softwood*. Applied Microbiology and Biotechnology, 2002. **59**(6): p. 618-628.
163. Taherzadeh, M.K., K, *Pretreatment of lignocellulosic wastes to improve ethanol and biogas production: A review*. International Journal of Molecular Sciences, 2008. **9**(9): p. 1621-1651.
164. Lawoko, M.H., G; Gellerstedt, G, *Structural differences between the lignin-carbohydrate complexes present in wood and in chemical pulps*. Biomacromolecules, 2005. **6**(6): p. 3467-3473.
165. Donohoe, B.D., SR; Tucker, MP, et al., *Visualizing lignin coalescence and migration through Maize cell walls following thermochemical pretreatment*. Biotechnology and Bioengineering, 2008. **101**(5): p. 913-925.
166. Wyman, C.E., *Handbook on bioethanol: production and utilization*, ed. T. Francis. 1996, Washington DC.
167. Fan, L.L., YH; Beardmore, DH, *Mechanism of the enzymatic-hydrolysis of cellulose-Effects of major structural features of cellulose on enzymatic-hydrolysis*. Biotechnology and Bioengineering, 1980. **22**(1): p. 177-199.
168. Berlin, A.B., M; Gilkes, N, et al., *Inhibition of cellulose, xylanase and beta-glucosidase activities by softwood lignin preparations*. Journal of Biotechnology, 2006. **125**(2): p. 198-209.

169. Mosier, N., et al., *Features of promising technologies for pretreatment of lignocellulosic biomass*. *Bioresour Technol*, 2005. **96**(6): p. 673-86.
170. Eggeman, T. and R.T. Elander, *Process and economic analysis of pretreatment technologies*. *Bioresour Technol*, 2005. **96**(18): p. 2019-25.
171. Taherzadeh, M.J. and K. Karimi, *Pretreatment of lignocellulosic wastes to improve ethanol and biogas production: a review*. *Int J Mol Sci*, 2008. **9**(9): p. 1621-51.
172. Harun, R., et al., *Exploring alkaline pre-treatment of microalgal biomass for bioethanol production*. *Applied Energy*, 2011. **88**(10): p. 3464-3467.
173. Kong, F., C.R. Engler, and E.J. Soltes, *Effects of cell-wall acetate, xylan backbone, and lignin on enzymatic hydrolysis of aspen wood*. *Applied Biochemistry and Biotechnology*, 1992. **34/35**: p. 23.
174. Gierer, J., *Chemistry of delignification. 1. General concept and reactions during pulping*. *Wood Science and Technology*, 1985. **19**(4): p. 289-312.
175. Chakar, F.R., AJ, *Review of current and future softwood kraft lignin process chemistry*. *Industrial Crops and Products*, 2004. **20**(2): p. 131-141.
176. Gierer, J., F. Imsgard, and I. Pettersson, *Possible condensation and polymerization reactions of lignin fragments during alkaline pulping processes*. *Appl Polym Symp*, 1976. **28**: p. 1195.
177. Brink, D.L., *Method of treating biomass materials*, in *US Patent*1993.
178. Harmer, M.A., et al., *A new route to high yield sugars from biomass: phosphoric-sulfuric acid*. *Chem Commun*, 2009: p. 6610.
179. Um, B.H., M.N. Karim, and L.L. Henk, *Effect of sulfuric and phosphoric acid pretreatments on enzymatic hydrolysis of corn stover*. *Applied Biochemistry and Biotechnology*, 2003. **105-108**: p. 115.
180. Donohoe, B.S., et al., *Visualizing lignin coalescence and migration through maize cell walls following thermochemical pretreatment*. *Biotechnol Bioeng*, 2008. **101**(5): p. 913-25.
181. Foster, B.L., B.E. Dale, and J.B. Doran-Peterson, *Enzymatic hydrolysis of ammonia-treated sugar beet pulp*. *Applied Biochemistry and Biotechnology*, 2001. **91**: p. 269.
182. Iyer, P.V., et al., *Ammonia recycled percolation process for pretreatment of herbaceous biomass*. *Applied Biochemistry and Biotechnology*, 1996. **57/58**: p. 121.
183. Kim, J.S., Y.Y. Lee, and S.C. Park, *Pretreatment of wastepaper and pulp mill sludge by aqueous ammonia and hydrogen peroxide*. *Applied Biochemistry and Biotechnology*, 2000. **84/86**: p. 129.

184. Xiao, L.P., et al., *Impact of hot compressed water pretreatment on the structural changes of woody biomass for bioethanol production*. *Bioresources*, 2011. **6**: p. 1576.
185. Zeng, M., et al., *Microscopic examination of changes of plant cell structure in corn stover due to hot water pretreatment and enzymatic hydrolysis*. *Biotechnol Bioeng*, 2007. **97**(2): p. 265-78.
186. Zhao, X., K. Cheng, and D. Liu, *Organosolv pretreatment of lignocellulosic biomass for enzymatic hydrolysis*. *Appl Microbiol Biotechnol*, 2009. **82**(5): p. 815-27.
187. McGinnis, G.D., W.W. Wilson, and C.E. Mullen, *Biomass pretreatment with water and high-pressure oxygen. The wet-oxidation process*. *Ind Eng Chem Prod Res Dev*, 1983. **22**: p. 352.
188. Cheng, G., et al., *Transition of cellulose crystalline structure and surface morphology of biomass as a function of ionic liquid pretreatment and its relation to enzymatic hydrolysis*. *Biomacromolecules*, 2011. **12**(4): p. 933-41.
189. Zheng, Y.Z., H.M. Lin, and G.T. Tsao, *Pretreatment for cellulose hydrolysis by carbon dioxide explosion*. *Biotechnol Prog*, 1998. **14**: p. 890.
190. Selig, M., N. Weiss, and Y. Ji, *Enzymatic saccharification of lignocellulosic biomass*, 2008, National Renewable Energy Laboratory: Golden, Colorado.
191. Sluiter, A., et al., *Determination of structural carbohydrates and lignin in biomass*, 2008, National Renewable Energy Laboratory: Golden, Colorado.
192. Palmowski, L.M., JA, *Influence of the size reduction of organic waste on their anaerobic digestion*. *Water Science and Technology*, 2000. **41**(3): p. 155-162.
193. Muller, C.A.-O., M; Novak, JT, *Application of mechanical shear in an internal-recycle for the enhancement of mesophilic anaerobic digestion*. *Water Environment Research*, 2007. **79**(3): p. 297-304.
194. Konn, J.P., A; Holmbom, B, *Dissolution of fibre material in alkaline pre-treatment and refining of spruce CTMP*. *Holzforschung*, 2006. **60**(1): p. 32-39.
195. Sanjay Naithani; Singh, S.V., *Kinetics of delignification in kraft pulping of tropical hardwoods. Effects of species/lignin variation*. *Journal of Indian Academy of Wood Science*, 1989. **20**(1): p. 49-56.
196. Vanchinathan, S.K., GA, *Kraft delignification kinetics based on liquor analysis*. *Tappi Journal*, 1995. **78**(3): p. 127-132.
197. Gustafson, R.S., CA; Mchean, WT, et al., *Theoretical-model of the kraft pulping process*. *Industrial & Engineering Chemistry Process Design and Development*, 1983. **22**(1): p. 87-96.

198. Edward L. Paul, V.A.A.-O., Suzanne M. Kresta, *Handbook of industrial mixing: science and practice*. 2004: Wiley-Interscience.
199. Bozell, J.J. and G.R. Petersen, *Technology development for the production of biobased products from biorefinery carbohydrates*. Green Chemistry, 2010. **12**: p. 539.
200. Duff, S.J.B. and W.D. Murray, *Bioconversion of forest products industry waste cellulose to fuel ethanol: A review*. Bioresour Technol, 1996. **55**: p. 1.
201. Galbe, M. and G. Zacchi, *A review of the production of ethanol from softwood*. Appl Microbiol Biotechnol, 2002. **59**(6): p. 618-28.
202. Wyman, C.E., *What is (and is not) vital to advancing cellulosic ethanol*. Trends Biotechnol, 2007. **25**(4): p. 153-7.
203. Banerjee, S., et al., *Commercializing lignocellulosic bioethanol: technology bottlenecks and possible remedies*. Biofuels, Bioproducts and Biorefining, 2010. **4**(1): p. 77-93.
204. Grabber, J.H., *How Do Lignin Composition, Structure, and Cross-Linking Affect Degradability? A Review of Cell Wall Model Studies*. Crop Science, 2005. **45**(3): p. 820.
205. Yang, B. and C.E. Wyman, *Pretreatment: the key to unlocking low-cost cellulosic ethanol*. Biofuels, Bioproducts and Biorefining, 2008. **2**(1): p. 26-40.
206. Kumar, R. and C.E. Wyman, *Effect of additives on the digestibility of corn stover solids following pretreatment by leading technologies*. Biotechnol Bioeng, 2009. **102**(6): p. 1544-57.
207. Kim, H.J., S.B. Kim, and C.J. Kim, *The effects of nonionic surfactants on the pretreatment and enzymatic hydrolysis of recycled newspaper*. Biotechnology and Bioprocess Engineering, 2007. **12**: p. 147.
208. Eriksson, T., J. Borjesson, and F. Tjerneld, *Mechanism of surfactant effect in enzymatic hydrolysis of lignocellulose*. Enzyme and Microbial Technology, 2002. **31**: p. 353.
209. Qing, Q., B. Yang, and C.E. Wyman, *Impact of surfactants on pretreatment of corn stover*. Bioresour Technol, 2010. **101**(15): p. 5941-51.
210. Monavari, S., M. Galbe, and G. Zacchi, *The influence of ferrous sulfate utilization on the sugar yields from dilute-acid pretreatment of softwood for bioethanol production*. Bioresour Technol, 2011. **102**(2): p. 1103.
211. Liu, L., et al., *Corn stover pretreatment by inorganic salts and its effects on hemicellulose and cellulose degradation*. Bioresour Technol, 2009. **100**(23): p. 5865-71.
212. Li, P. and R. Pelton, *Wood pulp washing 1. Complex formation between kraft lignin and cationic polymers*. Colloids and Surfaces, 1992. **64**: p. 217.

213. Burke, D.R., et al., *Enhanced solid–liquid clarification of lignocellulosic slurries using polyelectrolyte flocculating agents*. *Biomass and Bioenergy*, 2011. **35**(1): p. 391-401.
214. Wagberg, L., *Polyelectrolyte adsorption onto cellulose fibers-A review*. *Nordic Pulp and Paper Research Journal*, 2000. **15**(5): p. 586.
215. Mora, S., J. Lu, and S. Banerjee, *Mechanism of rate enhancement of wood fiber saccharification by cationic polyelectrolytes*. *Biotechnol Lett*, 2011. **33**(9): p. 1805-8.
216. Lee, I., W. Wang, and S. Ji, *Device and Method for Pretreatment of Biomass*, in *US Patent*2012.
217. Ladisch, C.M., *Cadoxen solvolysis of cellulose*. *Methods in Enzymology*, 1988. **160**: p. 11.
218. Kurakake, M., et al., *Pretreatment of Bagasse by nonionic surfactant for the enzymatic hydrolysis*. *Bioresour Technol*, 1994. **49**: p. 247.
219. Qi, B., X. Chen, and Y. Wan, *Pretreatment of wheat straw by nonionic surfactant-assisted dilute acid for enhancing enzymatic hydrolysis and ethanol production*. *Bioresour Technol*, 2010. **101**(13): p. 4875-83.
220. Sindhu, R., et al., *Surfactant-assisted acid pretreatment of sugarcane tops for bioethanol production*. *Appl Biochem Biotechnol*, 2012. **167**(6): p. 1513-26.
221. Xin, F., et al., *Enzymatic hydrolysis of sodium dodecyl sulphate (SDS)-pretreated newspaper for cellulosic ethanol production by *Saccharomyces cerevisiae* and *Pichia stipitis**. *Appl Biochem Biotechnol*, 2010. **162**(4): p. 1052-64.
222. Kim, S.B. and J.W. Chun, *Enhancement of enzymatic digestibility of recycled newspaper by addition of surfactant in ammonia-hydrogen peroxide pretreatment*. *Applied Biochemistry and Biotechnology*, 2004. **113-116**: p. 1023.
223. Castanon, M. and C.R. Wilke, *Effects of the surfactant Tween 80 on enzymatic hydrolysis of newspaper*. *Biotechnol Bioeng*, 1981. **XXIII**: p. 1365.
224. Kaar, W.E. and M.T. Holtzapple, *Benefits from tween during enzymatic hydrolysis of corn stover*. *Biotechnol Bioeng*, 1998. **59**: p. 419.
225. Helle, S.S., S.J.B. Duff, and D.G. Cooper, *Effect of surfactants on cellulose hydrolysis*. *Biotechnol Bioeng*, 1993. **42**: p. 611.
226. Yan, Y.J., et al., *A study on catalytic hydrolysis of peat*. *Bioresour Technol*, 1996. **57**: p. 269.
227. Nguyen, Q.A. and M.P. Tucker, *Dilute acid/metal salt hydrolysis of lignocellulosics*, in *US Patent*2002.

228. Liu, C.G. and C.E. Wyman, *The enhancement of xylose monomer and xylotriose degradation by inorganic salts in aqueous solutions at 180 degrees C*. Carbohydrate Research, 2006. **341**(15): p. 2550.
229. Yu, Q., et al., *The effect of metal salts on the decomposition of sweet sorghum bagasse in flow-through liquid hot water*. Bioresour Technol, 2011. **102**(3): p. 3445-50.
230. Feng, Y., et al., *The effect of polyelectrolyte additives on the saccharification of cellulase*. Annals of the New York Academy of Sciences, 1992. **672**: p. 603.
231. Reye, J.T., et al., *Cationic polyacrylamides enhance rates of starch and cellulose saccharification*. Biotechnol Lett, 2009. **31**(10): p. 1613-6.
232. Banerjee, S. and J.T. Reye, *Systems and methods for altering rates of enzymatic processes*, in *US Patent* 2011.
233. Reye, J.T., K.E. Maxwell, and S. Banerjee, *Cationic polyacrylamides promote binding of cellulase and amylase*. J Biotechnol, 2011. **154**(4): p. 269-73.
234. He, X., et al., *Enhancing the enzymatic hydrolysis of corn stover by an integrated wet-milling and alkali pretreatment*. Appl Biochem Biotechnol, 2010. **160**(8): p. 2449-57.
235. Jackson, M.G., *Review Article: The alkali treatment of straws*. Animal Feed Science and Technology, 1977. **2**: p. 105.
236. Arantes, V. and J.N. Saddler, *Access to cellulose limits the efficiency of enzymatic hydrolysis: the role of amorphogenesis*. Biotechnol Biofuels, 2010. **3**: p. 4.
237. Jang, H.F., A.G. Robertson, and R.S. Seth, *Transverse dimensions of wood pulp fibres by confocal laser scanning microscopy and image analysis*. Journal of Materials Science, 1992. **27**: p. 6391.
238. Barsberg, S. and K.A. Nielsen, *Oxidative quenching of spruce thermomechanical pulp fiber autofluorescence monitored in real time by confocal laser scanning microscopy- Implications for lignin autofluorescence*. Biomacromolecules, 2003. **4**: p. 64.
239. Koo, B.-W., et al., *Structural changes in lignin during organosolv pretreatment of Liriodendron tulipifera and the effect on enzymatic hydrolysis*. Biomass and Bioenergy, 2012. **42**: p. 24-32.
240. Kallavus, U. and J. Gravitis, *A comparative investigation of the ultrastructure of steam exploded wood with light, scanning and transmission electron microscopy*. Holzforschung, 1995. **49**(2): p. 182.
241. Chundawat, S.P.S., et al., *Multi-scale visualization and characterization of lignocellulosic plant cell wall deconstruction during thermochemical pretreatment*. Energy & Environmental Science, 2011. **4**: p. 973.

242. Maximova, N., et al., *Lignin adsorption on cellulose fibre surfaces: Effect on surface chemistry surface morphology and paper strength*. Cellulose, 2001. **8**: p. 113.
243. Kazayawoko, M., et al., *X-ray photoelectron spectroscopy of lignocellulosic materials treated with maleated polypropylenes*. Journal of Wood Chemistry and Technology, 1998. **18**(1): p. 1.
244. Fromm, J., et al., *Lignin distribution in wood cell walls determined by TEM and backscattered SEM techniques*. Journal of Structural Biology, 2003. **143**(1): p. 77-84.
245. LA, D., *Lignin Distribution During Latewood Formation in Pinus Radiata*. IAWA Bulletin, 1992. **13**(4): p. 381-387.
246. Horvath, A.T., et al., *Diffusion of cationic polyelectrolytes into cellulosic fibers*. Langmuir, 2008. **24**: p. 10797.
247. Rollin, J.A., et al., *Increasing cellulose accessibility is more important than removing lignin: a comparison of cellulose solvent-based lignocellulose fractionation and soaking in aqueous ammonia*. Biotechnol Bioeng, 2011. **108**(1): p. 22-30.
248. Kristensen, J.B., et al., *Cell-wall structural changes in wheat straw pretreated for bioethanol production*. Biotechnol Biofuels, 2008. **1**(1): p. 5.
249. Kumar, R. and C.E. Wyman, *Access of cellulase to cellulose and lignin for poplar solids produced by leading pretreatment technologies*. Biotechnol Prog, 2009. **25**: p. 807.
250. Rahikainen, J., et al., *Inhibition of enzymatic hydrolysis by residual lignins from softwood- study of enzyme binding and inactivation on lignin-rich surface*. Biotechnol Bioeng, 2011. **108**(12): p. 2823-34.